Experimental Analysis of Interactions between Biomolecules and Inorganic Surfaces

Vom Fachbereich Produktionstechnik

der

Universität Bremen

zur Erlangung des Grades

Doktor-Ingenieur

genehmigte

Dissertation

von

M.Sc. Sascha Steckbeck

Gutachter:

Prof. Dr. Lucio Colombi Ciacchi (Universität Bremen)

Prof. Dr. Monika Fritz (Universität Bremen)

Tag der mündlichen Prüfung: 1.7.2014

Dedicated to

my grandfather Helmut

- who always reminded me of staying curious

and

my son Sebastian

- who teached me that sleep is overrated

Contents

List of tables

List of figures

Abstract / Zusammenfassung

Die Adsorption von Biomolekülen, bzw. Proteinen und Peptiden im speziellen, stellt ein Phänomen dar, welches sowohl in technischen, als auch (bio-)medizinischen Bereich eine große Rolle spielt. Durch die Adhäsion von Biomolekülen kann es zu der Anbindung von Zellen oder anderen Organismen kommen, die letztendlich Biofilme ausbilden. Diese können mechanische, optische oder medizinische Eigenschaften so verändern, dass die ursprüngliche Funktion einer Oberfläche nicht mehr gegeben ist. Daher wird bereits seit Jahren sowohl in der anwendungsorientierten Forschung als auch in der Grundlagenforschung an adsorptions-minimierenden Oberflächen, bzw. an den molekularen Grundlagen der Biomoleküladsorption geforscht. Hierbei muss man, um die Mechanismen vollständig zu verstehen, bis auf die molekulare Ebene (nm-Bereich) gehen.

Neben der ungewollten Proteinadsorption, gibt es weiterhin auch Anwendungen (Bioprozesstechnik und Biomedizin oder auch „Drug Targeting“ zum zielgenauen Einsatz von Medikamenten im menschlichen Körper) bei denen die Anbindung von Proteinen gezielt gesteuert werden soll. Hierbei werden die Moleküle meistens über einen chemischen Linker an die Oberflächen angebracht, wobei es möglichst, im Vergleich zu ungebundenen Proteinen, zu keinem Verlust der Funktionen (z.B. proteolytische Funktionen) kommen soll.

Im Rahmen dieser Arbeit wurde die Adsorption von Modellproteinen und -peptiden auf anorganischen Oberflächen (SiO_2 und Al_2O_3) mit Hilfe von Matrix-Assisted Laser Desorption / Ionization Time-of-Flight Mass Spectrometry (MALDI ToF-MS), Atomic Force Microscopy (AFM), Quartz Crystal Microbalance (QCM), Reverse Phase High Performance Liquid Chromatography (RP-HPLC), Protein Assays (BCA Assay) und fluoreszenz-gelabelten Proteinen (FITC-BSA) untersucht.

Es war möglich mit Hilfe einer neuen MALDI ToF-MS gestützten „Ablagerungs“-Methode stark und schwach bindende Peptide aus einem komplexen Gemisch heraus zu identifizieren und deren Sequenzen über einen Datenbankabgleich zu erhalten. Diese Peptide wurden auf ihre Adsorptionskräfte hin mit Hilfe von AFM-Kraft-Abstandskurven analysiert. Weiterhin konnten erste Untersuchungen von Adsorptionscharakteristika (Konturlängen, Peakmuster) von Chymotrypsin und Lysozym mit Hilfe des AFM durchgeführt werden. Sie gaben Aufschluss darüber, wie

Einzel-Molekül-Kraftkurven aussehen. Das Auftreten von Peaks in diesen Kraftkurven könnte vermutlich das Brechen von Disulfidbrücken verursacht worden sein. Es ist allerdings auch nicht auszuschließen, dass mehrere gleichzeitig gebundene Proteine für die Erzeugung von Peaks in den Kraftkurven verantwortlich sind. Hier sind weitere Untersuchungen notwendig, um eindeutige Aussagen machen zu können.

Weiterhin wurde die Immobilisierung von Proteasen (Chymotrypsin) an kolloidalen Partikeln durchgeführt und es konnte gezeigt werden, dass die enzymatische Aktivität erhalten bleibt. Weiterhin wurden die Einflüsse der Immobilisierung auf die Verdau-Kinetik analysiert. Abschließende Äquivalenz-Experimente zeigten bei einem Vergleich von *in-solution-digests* mit immobilisierten Proben, dass etwa 1-10% der ursprünglich eingesetzten Proteinmenge für die Immobilisierung benötigt wird, um dieselben Peptidpeaks wie in den *in-solution-digests* zu erzeugen.

Der adsorptionsminimierende Effekt von Plasmabehandlungen (PICVD) von Borosilikatglas bezogen auf die adsorbierte Menge von Proteinen konnte eindeutig mit MALDI ToF-MS nachgewiesen werden. Die abschließende Analyse von Adsorptionskinetiken des Proteins Lysozym zeigte einen bereits in der Literatur beschriebenen „Overshooting“-Effekt, der erstmals mit MALDI ToF-MS nachgewiesen und auch mit QCM validiert werden konnte.

1 Introduction

1.1 Adsorption at a glance

General. The phenomenon of the adsorption of biomolecules onto inorganic surfaces can be found in various areas ranging from daily life problems up to intrinsic scientific questions. Beside many other sections, the adsorption can occur at technical interfaces such as solar panels or at medical surfaces e.g. at contact lenses, drug storage devices or medical surfaces that are in contact to human body fluids or cells. Researchers try to investigate the interactions between DNA, peptides and proteins and inorganic surfaces at the single molecule level or even atomic resolution. The results of these experimental as well as theoretical investigations can help to understand molecular mechanisms of adsorption and desorption processes. The main goal is to control these processes by choosing an appropriate (coated) surface or counteract adsorption through specific molecular mechanisms. Beside the unspecific physisorption of molecules to surfaces, another aim is to find covalent binding protocols for targeted immobilization of biofunctional molecules. Control of molecular adsorption to nanoparticles or colloidal particles can be used for protein drug transport in human bodies whereas immobilized enzymes or antibiotics can be used in medical flat surfaces. Nevertheless there are still a lot of challenges in this field of research. Which are the driving forces of biomolecular adsorption and how can we control adhesion – or adhesion-prevention? Which peptides tend to adhere to which surface and how can we identify these peptides in a fast and certain way?

Physisoption. Physisorption describes the adsorption of molecules, especially proteins or peptides, to interfaces through non-specific physical interactions [1-3]. These interactions can be described by H-bonds, electrostatic and Van-der-Waals forces induced by fluctuating dipole-dipole interplays. In contrast to chemisorption the physisorption-driven adsorption is weak. Many studies have been executed about the physisorption of proteins using different techniques [4], for example QCM for the on-time-view of kinetics, AFM for visual and nano-mechanical analysis [5,6] or spectroscopic techniques (CD- or fluorescence-spectroscopy, IR-spectroscopy) for

quantitation of adsorbed molecules. The latter can also reveal structural information about molecules in adsorbed state.

It was reported that after exposition of molecules to a surface and a succeeded adsorption, conformational changes can occur [7-9]. These rearrangements can cause desorption or, in contrast, strengthen the adsorbed state. Also the number, magnitude, location and distribution of charges at the protein and substrate surface can influence the adsorption. For example, it was found that β-Lactoglobulin and fibronectin perform a re-orientation on the surface followed by a decreased binding energy that is causing an increased desorption rate [1]. This re-orientation is induced by protein surface charges (see Figure 1-1).

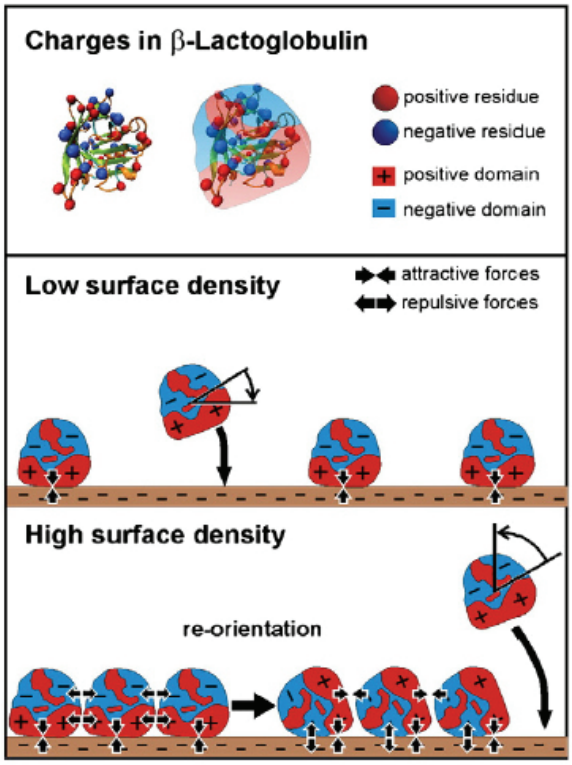

Figure 1-1. Top: β-Lactoglobulin exhibiting charges and surface charge distributions. Middle: If no steric inhibitions occur, protein-surface interactions are mainly forcing the adsorption state. Bottom: At a high protein concentration on surfaces, re-orientation can occur due to protein-protein interactions. (Adopted from Seeger et al., 2011, [1])

After adsorption has taken place, molecules can also be displaced by others that feature a higher affinity to the substrate. This effect was described originally by Vroman in 1962 [10] and was the basis for further experimental investigations confirming the initial results [11]. The analysis of interactions between molecules and nanoparticles or colloidal particles was also extended during the last years. To understand these interactions, well-known model proteins like Bovine Serum Albumin (BSA) or Lysozyme were chosen to achieve information of model-particle interactions [12-15].

Peptides. Many analytical techniques and theoretical analysis demand the down-scaling of systems to be investigated because of technical or computational limitations. Therefore many experiments are performed using peptides as an easy-to-handle model [16-22]. The identification of peptides that bind either strongly or weakly to inorganic substrates has become a wide field of research [23-25]. Most techniques, e.g. the phage display, are based on random chosen peptide sequences presented on phage-surfaces. After binding studies to specific surfaces, promising candidates are chosen, analyzed and amplified for a new adhesion test-cycle. This random-based technique is widely used but needs a highly technical, financial and temporal effort. Figure 1-2 shows a comprehensive overview of the pathway for the identification of binding peptides, beginning with the analysis up to the design of new biotechnological relevant peptides [26].

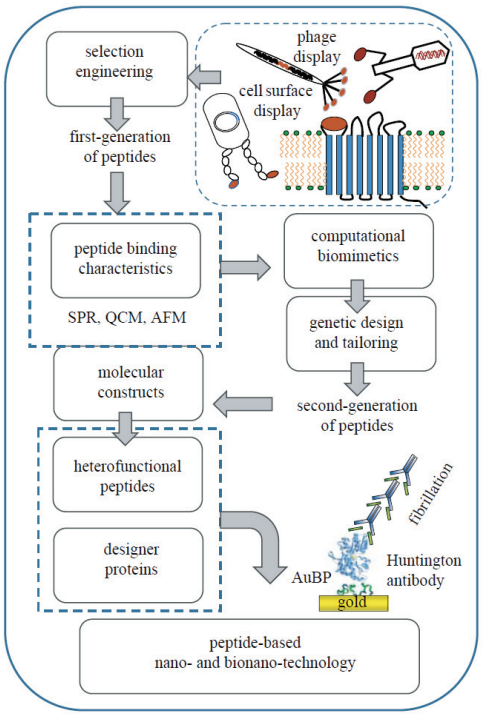

Figure 1-2. Overview of identification, analytical characterization and design of inorganic material binding peptides. (Adopted from Tamerler & Sarikaya, 2009, [26])

Kinetics. One of the main fields in molecular adsorption research is the analysis and modeling of adsorption kinetics. Within the last years many theoretical models have been developed to describe the adsorption on surfaces and interfaces. The basic model was introduced from Langmuir, describing the adsorption from a bulk solution towards a surface (Equation 1-1).

$$\frac{d\theta}{dt} = k^{on} \cdot c_s \cdot (1 - \frac{\theta}{\theta_{\max}}) - k^{off} \cdot \theta \qquad (1\text{-}1)$$

In this basic model θ describes the protein surface coverage and k^{on} and k^{off} are the on- and off-rate constants, respectively. θ_{max} is the maximum coverage at which no more binding sites are available. Although this model comprises binding sites that can be occupied or freely available, the complexity of natural binding kinetics demands for more detailed parameters [27]. These can be the Vroman effect, the consideration of electrochemical or steric interactions with neighboring molecules or the states of adsorbed molecules (e.g. distorted or extended, end-on or side-on adhesion). The latter can be accompanied by confomational changes in tertiary structure leading to a possible decrease of protein functionalities. A comprehensive overview of recent adsorption kinetics is given in [1].

Control of molecule adsorption. The targeted control of molecular adhesion has come an extensive field of research. On the one hand the immobilization of proteins is widely used and on the other hand many investigations were done to find strategies to prevent adhesion of proteins [28-30] or cells [31]. The latter is an important field for biomedical research: The production of implants or medical surfaces that are resistant to adhesion can avoid inflammations or allergic reactions in patients. An intended immobilization of proteins can be used for drug delivery or biotechnological applications e.g. were a fast and easy removal of enzymes from reaction batches is demanded.

The prevention of molecule adhesion was experimentally analyzed by using self-assembled monolayers (SAMs) [32-34], consisting of polymers with varying end-groups. A survey of SAM-modified surfaces and their adhesion behavior can be found in [28].

Polyethylene glycol (PEG) as a classical SAM [35-37], but also proteins were used to analyse the effect of adhesion minimization [38]. In this context the RGD-peptide was investigated in depth, e.g. to prevent osteoblast adhesion [39]. Proteins of the cell surface represent the first contact point in the adhesion process and therefore play a crucial role in this context (see Fig. 1-3).

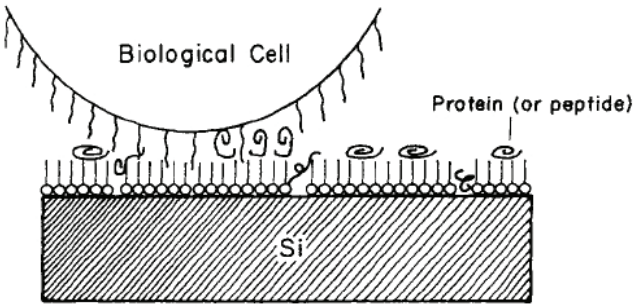

Figure 1-3. Schematic of cell adhesion driven by protein-protein interactions forces. Cells exhibit proteins on their membrane surface for interactions with foreign (cell-) surfaces. (Adopted from Sogah et al., 1993, [32])

1.2 Biomolecules

Biomolecules is the superior term for any kind of molecule in living organisms. They are responsible for the structure of cells, the interaction of cells among each other, the reproduction of organisms, including the storage of genetic information, cell metabolism and much other functionality [40]. The main focus in this work was on the adsorption of proteins and peptides, therefore these will be explained in more detail in the following.

1.2.1 Proteins and Peptides

Proteins are polymers built of amino acids acting as monomers. There are twenty two proteinogenic amino acids; they build the basis for all proteins that are synthesized in the human body. Amino acids have generally the same composition of a center-located alpha-carbon atom and a NH_2- and COOH- terminus. These termini can, as a function of solvent pH value, be protonated or deprotonated. Amino acids can therefore feature a total positive, negative or neutral charge, respectively. Polymerization occurs via the terminal groups through binding of one amine group with the neighboring carboxyl group under elimination of H_2O. Beside a single hydrogen atom, a fourth chemical group, R, is attached to the alpha-carbon as it can be seen in figure 1-4.

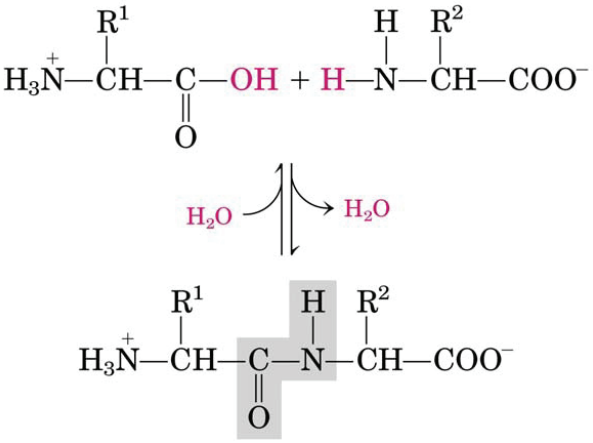

Figure 1-4. Two amino acids with side chains R^1 and R^2 are linked under elimination of H_2O and build a di-peptide. This reaction can be repeated several times to form a polypeptide chain (protein). Reverse reaction is possible including the uptake of H_2O (hydrolysis). Adopted from Lehninger, 2001 [40].

This side chain R is mainly responsible for the chemical and physical properties of the amino acids and, later on, of the proteins. The side chains can either be charged (positively and negatively) or have polar / non-polar and hydrophobic / hydrophilic characteristics, respectively. The primary structure (sequential arrangement of amino acids) takes place inside the cell body. Two ribosomal subunits assemble around the freshly transcribed mRNA and translate the information from a three letter code of nucleotide pairs (Adenine, Thymine, Guanine, Cytosine) into amino acids that are provided by tRNA. The amino acid side chain properties and their positioning play also a crucial role in the folding of proteins. Due to the forming of hydrogen bonds among single atoms of side chains or the development of disulfide bonds especially between cysteine residues, the secondary structure of proteins is predetermined. Beside the linear arrangement of amino acids (random coil), β-sheets and α-alpha helices are characteristic structures of secondary ordered amino acid chains. The rearrangement of these structures to large amino acid complexes builds the tertiary structure. As a last step several (tertiary-) protein subunits can aggregate to each other and form a quaternary structured protein (see Figure 1-5).

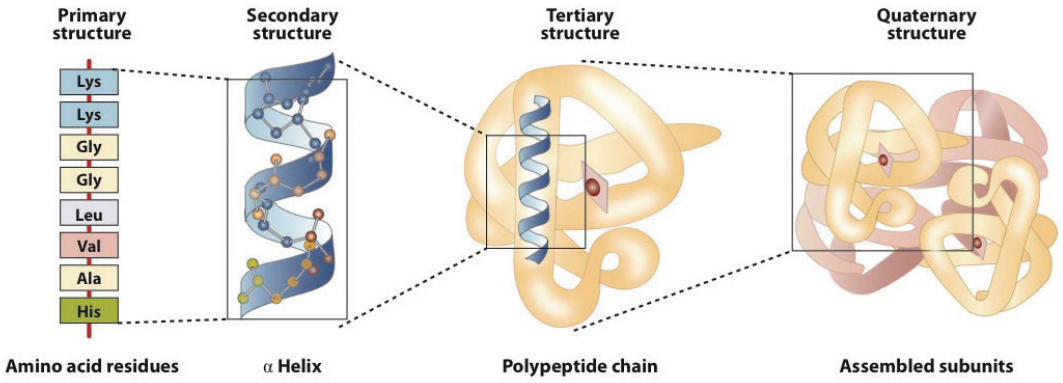

Figure 1-5. Protein structure levels. Starting from a chain with single amino acid residues (primary structure) α-helices and β-sheets (not depicted) can be assembled as secondary structures. These chains can build a tertiary and a quaternary structure (by assembled tertiary structure subunits). Adopted and changed from Lehninger, 2001 [40].

Proteins can hold a number of functions within cellular functions. Enzymes are involved in many biochemical reaction cascades and metabolism pathways e.g. in citric acid cycle that provides intermediates products for biosynthesis and is responsible for the production of energy. They are also introduced into transcription as well as DNA repair. Enzymes enable many chemical reactions that are energetically non-favorable by

opening up reaction paths that usually are hindered. Thus, reaction rates are immensely increased so that reaction products are formed faster than in non-catalyzed reactions. Structural proteins are responsible for the stability of cells (cytoskeleton) and muscles or biological matter like hair or nails and often exhibit a fibrous shape. Typical structural proteins are collagen, elastin, keratin or actin. Proteins can be furthermore involved in cell-cell- or cell-material-interactions. (Trans-) Membrane proteins that are incorporated into cell membranes display an important role regarding cell-cell-interactions as well as cell-material- interactions. They can be responsible for the first contact to inorganic materials and play a crucial role in scientific adsorption studies.

1.3 Surfaces

Concerning the adhesion of proteins and peptides onto inorganic surfaces, the focus in this work was set to silica and alumina surfaces. They are physically well characterized and can therefore be also used for e.g. computational simulations. Due to these facts, these materials will be briefly introduced below.

1.3.1 SiO_2

SiO_2 is commonly used in process technology and semiconductor technology as well as in paints or adhesives (as particles). One of the main fields of application for SiO_2 is glass, which is used for optical solutions or in laboratory equipment.

Structure. Silica is built from silicon connected to four oxygen atoms, forming a SiO_4 tetrahedron. In SiO_2 these tetrahedron molecules are linked by sharing oxygen atoms. Each silicon atom is linked to four bridging oxygen atoms while each oxygen atom is connected to two silicon atoms. This 4:1 stoichiometry is solved in SiO_2 structures where Si-O-Si bonds link SiO_4 tetrahedra (Figure 1-6 C). These bonds can vary in angle and length which is the reason for the appearance of crystalline polymorphs. A schematic of an α-quartz can be found in figure 1-6 A, beside a model for an amorphous SiO_2 network (Figure 1-6 B) [41].

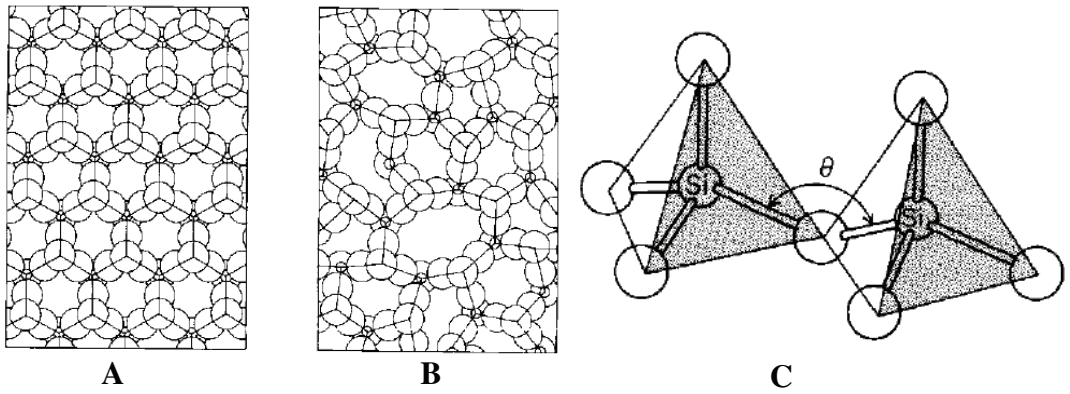

Figure 1-6. Schematic images of (A) α-quartz and (B) amorphous SiO_2. The bond between two silicon atoms via a oxygen atom can vary in length and angle θ (C). Adopted from [41].

1.3.2 Al_2O_3

Due to its mechanical, physical and chemical properties, alumina is used in a wide range of applications. Beside the usage as an insulator in technical applications like televisions or satellites, its mechanical properties make it very appropriate for the production of light weight constructions (cars, airplanes). Due to its inertness it is also widely used in biomedical applications. Many body implants (e.g. joint replacements) or dental solutions are made of aluminum oxide [42].

Fabrication. Al_2O_3 is produced by the Bayer process. Within this process, *bauxite* (natural form of alumina including contaminants) is crushed into pieces and then washed with a liquor obtained from downstream processes. After addition of NaOH and CaO the mixture is digested using high pressure and heat. Alumina is then dissolved and reacts with NaOH to AlO_2Na. This product is precipitated from liquor as $Al_2O_3*3H_2O$. The last step involves calcination of this trihydrate using high temperatures again. The so calcinated α-alumina particles have a typical size of 0.5 to 10 µm [42].

Properties. The most stable version of alumina is α-Al_2O_3 which occurs in the corundum crystal structure. It is composed of a hexagonal close-packed structure with lattice parameters of 4.8 Å (a) and 13.0 Å (c) at 20°C. Some selected material properties are given in table 1-1, derived from [43].

Table 1-1. Selected properties of α-Al_2O_3. Adopted and changed from [43].

Property (Unit)	**Value at 20°C**
Density (g/cm^3)	3.984
Elastic modulus (GPa)	416
Hardness, Vickers (GPa)	15
Specific heat ($J*kg^{-1}*K^{-1}$)	755
Tensile strength (MPa)	267
Thermal conductivity ($W*m^{-1}*K^{-1}$)	33
Thermal diffusivity (cm^2/s)	0.111

1.4 Aims of this work

Regarding the previously introduced fields of research, the aim of this work is to investigate protein adsorption phenomena using various analytical techniques. The here presented results from physisorption experiments as well as findings from immobilization experiments attempt to deepen the understanding of molecule-surface-interactions.

1.5 Structure of this work

Chapter two addresses the analytical techniques which were used for this work. Each technique will be explained separately. Chapter three will discuss results of a new depletion technique used for identification of putative strong and weak binding peptides on inorganic surfaces using matrix assisted laser desorption ionization mass spectrometry (MALDI ToF-MS). The investigation of some of these identified peptides using single molecule force spectroscopy (SMFS) measurements is shown in chapter four. Additionally, in this part further preliminary SMFS results from non-digested proteins will be discussed. To cover the area of research considering targeted immobilization of biomolecules, chapter five will show the results of activity measurements of enzyme immobilization onto silica and alumina colloidal particles. Chapter six deals with general adsorption experiments and will illustrate if chemical surface treatment is able to influence the adsorption of proteins. Chapter seven will show results from protein adsorption experiments investigating the kinetics, especially from lysozyme, followed by the last chapter that will briefly conclude this work.

1.6 References

[1] M. Rabe, D. Verdes, S. Seeger. Understanding protein adsorption phenomena at solid surfaces. Adv. Colloid Interfac., 162:87-106, 2011

[2] K. Nakanishi, T. Sakiyama, K. Imamura. On the adsorption of proteins on solid surfaces, a common but very complicated problem. J. Biosci. Bioeng., 91: 233-244, 2001

[3] S. J. Marshall, S. C. Bayne, R. Baier, A. P. Tomsia, G. W. Marshall. A review of adhesion science. Dent. Mater., 26: 11-16, 2010

[4] V. Hlady, J. Buijs, H. P. Jennissen. Methods for studying protein adsorption. Methods Enzymol. 309: 402-429, 1999

[5] A. P. Serro, K. Degiampietro, R. Colaco, B. Saramago. Adsorption of albumin and sodium hyaluronate on UHMWPE: A QCM-D and AFM study. Colloid. Surface B, 78:1-7, 2010

[6] M. P. Gispert, A. P. Serro, R. Colaco, B. Saramago. Bovine serum albumin adsorption onto 316L stainless stell and alumina: a comparative study using depletion, protein radiolabeling, quartz crystal microbalance and atomic force microscopy. Surf. Interface Anal. 40: 1529-1537, 2008

[7] P. Roach, D. Farrar, C. C. Perry. Interpretation of protein adsorption: Surface-induced conformational changes. J. Am. Chem. Soc. 127: 8168-8173, 2005

[8] M. van der Veen, M. C. Stuart, W. Norde. Spreading of proteins and ist effect on adsorption and desorption kinetics. Colloid. Surface B 54: 136-142, 2007

[9] T. Ballet, L. Boulange, Y. Brechet, F. Bruckert, M. Weidenhaupt. Protein conformational changes induced by adsorption onto material surfaces: an important issue for biomedical applicationsof material science. B. Pol. Acad. Sci.-Tech. 58: 303-315, 2010

[10] L. Vroman. Effect of adsorbed proteins on the wettability of hydrophilic and hydrophobic solids. Science 196: 476-477, 1962

[11] S.-Y. Jung, S.-M. Lim, F. Albertino, G. Kim, M. C. Gurau, R. D. Yang, M. A. Holden, P. S. Cremer. The Vroman effect: A molecular description of fibrinogen displacement. J. Am. Chem. Soc. 125: 12782-12786, 2003

[12] K. Rezwan, L. P. Meier, M. Rezwan, J. Vörös, M. Textor, L. J. Gauckler. Bovine serum albumin adsorption onto colloidal Al_2O_3 particles: A new model based on zeta potential and UV-Vis measurements. Langmuir 20:10055-10061, 2004

[13] S. H. Brewer, w. R. Glomm, M. C. Johnson, M. K. Knag, S. Franzen. Probing BSA binding to citrate-coated gold nanoparticles and surfaces. Langmuir 21: 9303-9307, 2005

[14] N. Basar, L. Uzun, A. Güner, A. Denizli. Spectral characterization of lysozyme adsorptionon dye-affinity beads. J. Appl. Polym. Sci. 108: 3454-3461, 2008

[15] K. Rezwan, L. P. Meier, L. J. Gauckler. Lysozyme and bovine serum albumin adsorption on uncoated silica and AlOOH-coated silica particles: the influence of positively and negatively charged oxide surface coatings. Biomaterials 26: 4351-4357, 2005

[16] K. Imamura, Y. Kawasaki, T. Nagayasu, T. Sakiyama, K. Nakanishi. Adsorption characteristics of oligopeptides composed of acidic and basic amino acids on titanium surface. J. Biosci. Bioeng. 103: 7-12, 2007

[17] T. Hayashi, K.-I. Sano, K. Shiba, K. Iwahori, I. Yamashita, M. Hara. Critical amino acid residues for the specific binding of the Ti-recognizing recombinant ferritin with oxide surfaces of titanium and silicon. Langmuir 25: 10901-10906, 2009

[18] T. Pirzer, T. Hugel. Adsorption mechanism of polypeptides and their location at hydrophobic interfaces. Chem. Phys. Chem. 10: 2795-2799, 2009

[19] C. Tamerler, E. E. Oren, M. Duman, E. Venkatasubramanian, M. Sarikaya. Adsorption kinetics of an engineered gold binding peptide by surface plasmon resonance spectroscopy and a quartz crytsal microbalance. Langmuir 22: 7712-7718, 2006

[20] C. Whitehouse, J. Fang, A. Aggeli, M. Bell, R. Brydson, C. W. G. Fishwick, J. R. Henderson, C. M. Knobler, R. W. Owens, N. H. Thomson, D. A. Smith, N. Boden. Adsorption and self-assembly of peptides on mica substrates. Angew. Chem. Int. Ed. 44: 2-5, 2005

[21]D. Horinek, A. Serr, M. Geisler, T. Pirzer, U. Slotta, S. Q. Lud, J. A. Garrido, T. Scheibel, T. Hugel, R. R. Netz. Peptide adsorption on a hydrophobic surface results from an interplay of salvation, surface, and intrapeptide forces. PNAS 105: 2842-2847, 2008

[22] M. Goebel-Stengel, A. Stengel, Y. Tache, J. R. Reeve jr. The importance of using the optimal plasticware and glassware in studies involving peptides. Anal. Biochem. 414: 38-46, 2011

[23] J. S. Evans, R. Samudrala, T. R. Walsh, E. E. Oren, C. Tamerler. Molecular design of inorganic-binding peptides. MRS Bull. 33: 514-518, 2008

[24] K. Shiba. Exploitation of peptide motif sequences and their use in nanobiotechnology. Curr. Opin. Biotech. 21: 412-425, 2010

[25] O. Mermut, R. L. York, D. C. Phillips, K. R. McCrea, R. S. Ward, G. A. Somorjai. Directions in peptide interfacial science. Biointerphases 1, 2006

[26] C. Tamerler, M. Sarikaya. Molecular biomimetics: nanotechnology and bionanotechnolgy using genetically engineered peptides. Phil. Trans. R. Soc. A 367: 1705-1726, 2009

[27] A. J. Clark, A. Kotlicki, C. A. Haynes, L. A. Whitehead. A new model of protein adsorption kinetics derived from simultaneous measurement of mass loading and changes in surface energy. Langmuir 23: 5591-5600, 2007

[28] E. Ostuni, R. G. Chapman, R. E. HolmLin, S. Takayama, G. M. Whitesides. A survey of structure-property relationships of surfaces that resist the adsorption of protein. Langmuir 17: 5605-5620, 2001

[29] Z. Ademovic, D. Klee, P. Kingshott, R. Kaufmann, H. Höcker. Minimization of protein adsorption on poly(vinylidene fluoride). Biomol. Eng. 19: 177-182, 2002

[30] J. Li, D. Tan, X. Zhang, H. Tan, M. Ding, C. Wan, Q. Fu. Preparation and characterization of nonfouling polymer brushes on poly(ethylene terephtalate) film surfaces. Colloid. Surface B 78: 343-350, 2010

[31] E. Ostuni, R. G. Chapman, M. N. Liang, G. Melulini, G. Pier, D. E. Ingber, G. M. Whitesides. Self-assembled monolayers that resist the adsorption of proteins and the adhesion of bacterial and mammalian cells. Langmuir 17: 6336-6343, 2001

[32] S. Margel, E. A. Vogler, L. Firment, T. Watt, S. Haynie, D. Y. Sogah. Peptide, protein, and cellular interactions with self-assembled monolayer model surfaces. J. Biomed. Mater. Res. A 27:1463-1476, 1993

[33] L. Li, S. Chen, S. Jiang. Protein adsorption an alkanethiolate self-assembled monolayers: Nanoscal surface structural and chemical effects. Langmuir 19: 2974-2982, 2003

[34] E. Ostuni, B. A. Grzybowski, M. Mrksich, C. S. Roberts, G. M. Whitesides. Adsorption of proteins to hydrophobic sites on mixed self-assembled monolayers. Langmuir 19: 1861-1872, 2003

[35] X. Khoo, P. Hamilton, G. A. O´Toole, B. D. Snyder, D. J. Kenan, M. W. Grinstaff. Directed assembly of PEGylated-peptide coatings for infection-resistant titanium metal. J. Am. Chem. Soc. 131: 10992-10997, 2009

[36] N. Xia, Y. Hu, D. W. Grainger, D. G. Castner. Functionalized poly(ethylene glycol)-garfted polysiloxane monolayers for control of protein binding. Langmuir 18: 3255-3262, 2002

[37] S. Bozzini, P. Petrini, M. C. Tanzi, S. Zürcher, S. Tosatti. Poly(ethylene glycol) and hydroxy functionalized alkane phosphate mixed self-assembly monolayers to control nonspecific adsorption of proteins on titanium oxide surfaces. Langmuir 26: 6529-6534, 2010

[38] S. Pillai, A. Arpanaei, R. L. Meyer, V. Birkedal, L. Gram, F. Besenbacher, P. Kingshott. Preventing protein adsorption from a range of surfaces using an aqueous fish portein extract. Biomacromolecules 10: 2759-2766, 2009

[39] J. Michael, L. Schönzart, I. Israel, R. Beutner, D. Scharnweber, H. Worch, U. Hempel,B. Schwenzer. Oligonucleotide-RGD peptide conjugates for surface modification of titanium implants and improvement of osteoblast adhesion. Bioconjugate Chem. 20: 710-718, 2009

[40] David Nelson, Michael Cox. Lehniger Biochemie, Springer Verlag, 3. Auflage, 2001

[41] F. J. Grunthaner, P. J. Grunthaner. Chemical and electronic structure of the SiO_2 / Si interface. Materials Science Reports 1: 65-160, 1986

[42] K. Davis. Material Review: Alumina (Al_2O_3). School of Doctoral Studies (European Union) Journal, 2010

[43] R. G. Munro. Evaluated Material Properties for a sintered α-Alumina. J. Am. Ceram. Soc. 80: 1919-1928, 1997

2 Methodology

This chapter is focused on an overview of the basic principles of the methods that were used in this work. While this chapter gives a general introduction to the methodology, the detailed experimental parameters can be found in the following chapters in which these techniques were used.

2.1 Matrix-Assisted Laser Desorption / Ionization Time of Flight Mass Spectrometry (MALDI ToF-MS)

MALDI ToF mass spectrometry can reveal information about the exact masses of organic and inorganic molecules in a range of few hundred Dalton (e.g. amino acids and peptides) up to several thousands of Dalton (proteins). MALDI ToF-mass spectrometers can be divided mainly into three compartments: The ion source chamber where the molecules are desorped and ionized (1), followed by (2) the flight tube and finally (3) the detector section. A schematic overview of a typical MALDI ToF-mass spectrometer is shown in figure 2-1.

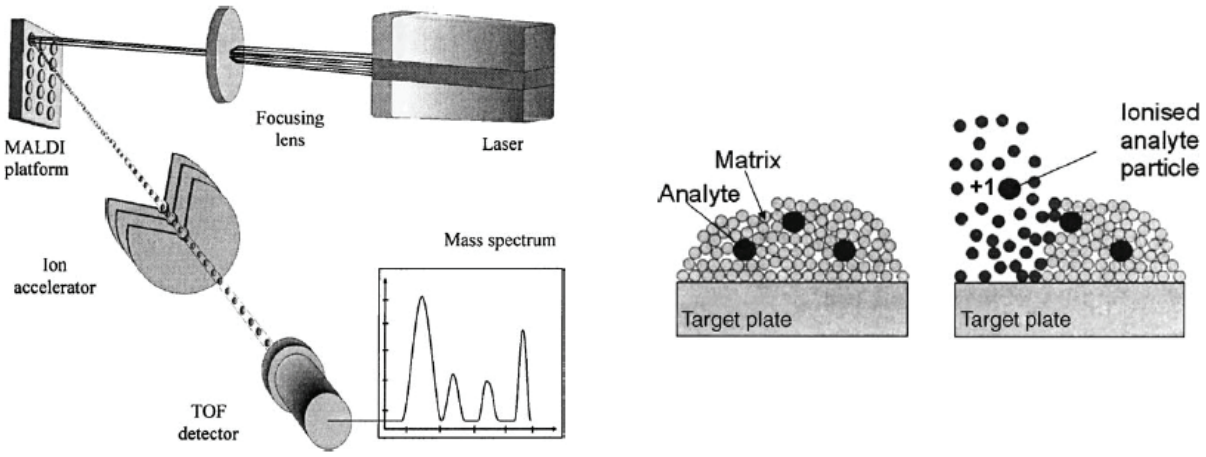

Figure 2-1. Left. Scheme of MALDI ToF-MS principle. Different from text, this scheme shows no ion mirror. Right: Target plate with matrix with embedded analyte molecues. After laser shot analytes are ionized by H^+ transfer. Adopted and changed from Silberring et al. 2004 [1].

Molecules are prepared onto targets made of either polymers or polished steel and then mixed with an appropriate matrix substance which separates the molecules from each

other, adsorbs the energy from ionization induced by laser light and transfers ions (in the case of MALDI ToF-MS mainly H^+) to the molecules. The preparation of MALDI samples can influence spectral results and should therefore be adjusted to the specific experimental situations [2]. Inside the ion source chamber sample molecules are ionized by shots of a laser beam (inducing a micro-explosion cloud, the so called MALDI plume) followed by the application of an acceleration voltage. Samples are then accelerated, pass the flight tube and hit the detector after being reflected by an ion mirror. This mirror adapts time-of-flight discrepancies caused by an inaccurate distribution of molecules inside the MALDI plume and therefore increases the peak resolution. The detection is often realized by multichannel plates, detecting the collision of sample molecules with the inner walls of microchannels. This causes an electron-cascade which amplifies the detection signal. By measuring the exact time which molecules need to pass the flight tube (Time-of-Flight) statements can be made about the mass of the molecules. Equation (2-1) shows the connection between the experimental mass of molecules and the flight-time.

$$\frac{1}{2}mv^2 = zeU \rightarrow v^2 = \frac{s^2}{t^2} \rightarrow \frac{m}{z} = \frac{2eU}{s^2}t^2 \rightarrow m = Kt^2 \quad (2\text{-}1)$$

The kinetic energy of accelerated molecules can be written as $\frac{1}{2}mv^2$ where m is the mass and v the velocity of the sample molecule. This is equal to the charge state z, electron charge e and the acceleration voltage U. Substitution of v^2 with $\frac{s^2}{t^2}$ gives $\frac{m}{z} = \frac{2eU}{s^2}t^2$ and, finally, the connection of mass m with flight-time t^2 while all other constant values are summarized in constant K (see equation (2-1)).

This equation assumes that only one H^+-ion is transferred to the molecule (z=1). It should be taken into account that other ionization techniques (e.g. electrospray ionization, ESI) can reveal several charge states for one molecule. The calibration of MALDI ToF mass spectrometers using molecules with well known masses can reveal information about masses of so far unknown molecular parameters.

MALDI ToF-MS peak areas were also used before for quantitation of unknown molecule concentrations using standard dilution series [3] or internal standards [4]. MALDI ToF-MS can reveal information about molecule amounts and protein films on surfaces [5-7].

Beside the exact determination of ion masses, this technique can be used to reveal more intrinsic information about proteins. The digestion of a protein using an appropriate enzyme will lead to peptides that can be detected with MALDI ToF-MS. If the used protease is known, a list of peptide peaks (masses) can then be used to be compared with data base entrances. Considering technical and experimental tolerances it is possible to identify the sample protein, as long as it is already registered in the data base. This method is called protein mass fingerprint (PMF). Further, it is even possible to scan enzymatically treated biological tissue with MALDI ToF-MS and reveal information about protein distributions within a sample area. Statistical methods like principal component analysis are used to analyse the information. “Protein-maps” or, in general, images can be generated (MALDI Imaging) [8-13]. In addition, MALDI ToF-MS can be also used for biochemical questions concerning e.g. viral proteins or antigens, as described previously [14,15].

2.2 Atomic Force Microscopy (AFM)

Atomic force microscopy was introduced by Binnig, Quate and Gerber in 1986 for the first time. Beside many other experimental possibilities which arised due to the technical development of this instrument within the last years, it was mainly used in this work for the three basic kinds of measurements. First, it can give insight into intramolecular nanomechanics of unfolding events of proteins. Secondly it can measure the interaction forces of molecules towards surfaces or, finally, image biomolecules under native circumstances (concerning measurements in liquids with controlled pH, temperature, ionic strength).

An atomic force microscope consists of a flexible flat spring, the cantilever, with a small and sharp tip at the end. A laser beam is aligned onto the backside of this cantilever and reflected into a photo diode. Any event causing a deflection of the cantilever results in a change of the position of the reflected laser spot on the photo diode. This change can be recalculated into a height at which the cantilever was deflected (Figure 2-2, left). Taking into account the spring constant k of the cantilever,

the deflected height z is equivalent to a force F acting on the cantilever. This relationship can be described by the simple equation (2-2).

$$F = k * z \qquad (2\text{-}2)$$

Samples to be investigated are moved relative to the cantilever in x,y and z- direction by piezo crystals. A feedback loop (PI controller) regulates the piezo movement considering user-set parameters. Integral and proportional gains can be used to control piezo elements to react with experimental conditions. It is possible to vary the force which the cantilever carries out on the surface and change the reaction velocity and strength at emerging barriers such as proteins, molecules or uneven substrates. With regard to AFM for imaging, two distinct modes can be used for measurements. Contact mode describes the scanning of surfaces with the tip including piezo movements upon barriers like proteins (controlled by integral and proportional gain). A further development is the tapping mode in which the cantilever oscillates at a constant frequency to reduce surface contact. This mode can be used to image soft matter like cells or protein films. In several experiments AFM imaging has been used to reveal information about adsorbed proteins or protein layers [16-18]. The basic principle of the measured force-distance curves is shown in figure 2-2.

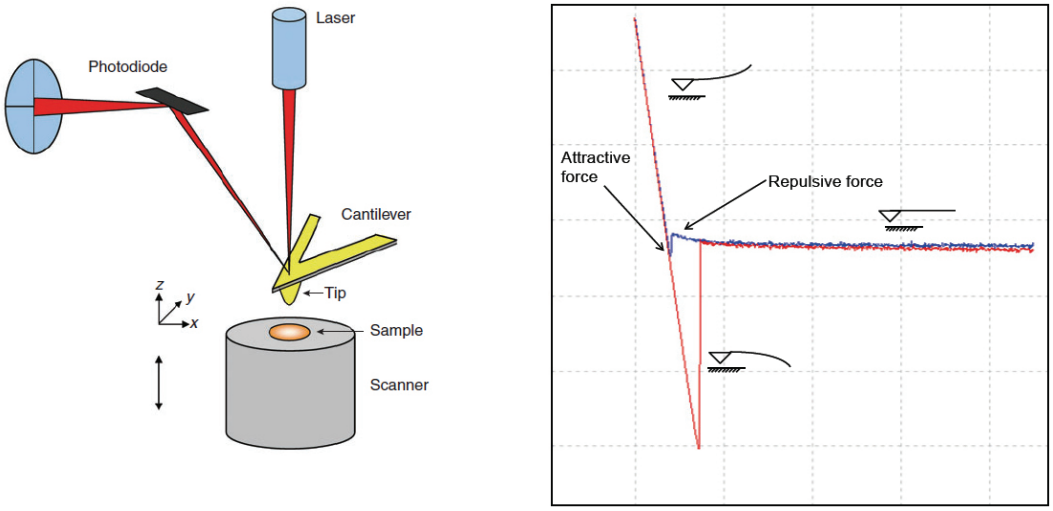

Figure 2-2. Left: Scheme of an Atomic Force Microscope. A laser beam is reflected on the backside of a cantilever into a photodiode. Any events between tip and surface that cause a deflection of the cantilever will be detected and displayed as images or force curves, respectively. Adopted from Hinterdorfer & Dufrene, 2006 [19]. Right: Exemplary force-distance curve from AFM experiment. The blue line indicates approach towards the surface and red indicates the retract curve including possible adhesion peaks. A weak repulsive force followed by an attractive "snap-on" peak can be observed due to electrostatic interactions.

Apart from imaging, force curves as indicated in figure 2-2 (right) can be collected. The approaching line (blue) proceeds linear until first non-specific interactions between tip and surface cause a “snap-on” event. Afterwards the curve increases due to pressing the tip onto the surface until a specific setpoint is reached. Retraction from the surface (red) decreases the force to the surface until the tip-surface contact gets lost. Any interactions between tip and the surface will be indicated by one or more force peaks. The peak can be analysed regarding the size or shape and reveal information about adhesion forces or mechanical surface properties [20]. Furthermore, molecules can be chemically linked to the tip [21] and used for Single Molecule Force Spectroscopy (SMFS). Subsequent, SMFS measurements can be conducted to identify interactions between molecules and inorganic substrates [22-27], molecules and molecules (linked to the substrate) [28-31] or to obtain detailed information about intramolecular unfolding events [32].

2.3 Quartz Crystal Microbalance with Dissipation (QCM-D)

Quartz crystal microbalances are able to measure smallest amounts of adsorbed molecules on flat surfaces [33]. A quartz crystal (which can be also covered with gold or other materials) is set to vibrate at a constant frequency. The deposition of molecules onto the crystal induces a shift in frequency that can be measured and plotted over time leading to a kinetic. Beside measurements in gases, a flow of solvent containing an analyte is widely used. The solvent is allowed to contact the crystal at a specific flow rate. If any molecules (e.g. proteins) adhere to the crystal surface a frequency shift is observable. An increasing negative shift is related to an increasing mass of adsorbed molecules. In 1959 Sauerbrey proposed a theory to describe the relationship between frequency shift and adsorbed mass regarding hard layers, e.g. in gas adsorption [34]. Hence, the frequency shift can be recalculated into adsorbed mass (see Equation (2-3)).

$$\Delta F = -\frac{2f_0^2}{A\sqrt{\rho\mu}}\Delta m \qquad (2\text{-}3)$$

F is the measured frequency shift, f_0^2 is the resonance frequency, A is the active crystal area, ρ is the density of the quartz, μ is the shear modulus of the quartz and Δm depicts the change in adsorbed mass.

For experiments considering the adsorption of soft matter like protein films, cells or viruses, the dissipation signal is important (QCM with dissipation: QCM-D). Dissipation quantifies the damping of the sensor frequency due to viscoelastic properties of adsorbed matter. Beside the basic resonance frequency (n=1) nowadays overtones (n=5 to =13) are measured to increase signal clarity. In this context, QCM-D was used for several investigations on proteins or protein films [35-37] and peptides [38,39]. It was further used for specific analysis like phage adhesion [40], protein binding to nano particles [41] or even protein digestion kinetics [42].

2.4 Reverse Phase High Performance Liquid Chromatography (RP-HPLC)

Liquid chromatography is widely used to separate analyte molecules from each other starting with a high complex sample mixture. Beside many modifications that are available nowadays, in this work Reverse Phase High Performance Liquid Chromatography (RP-HPLC) was used for analytical experiments. RP-HPLC systems consist of three compartments, namely (1) the pump / injection unit, (2) the separation unit (usually a column packed with separating material) and finally a detection compartment (Figure 2-3).

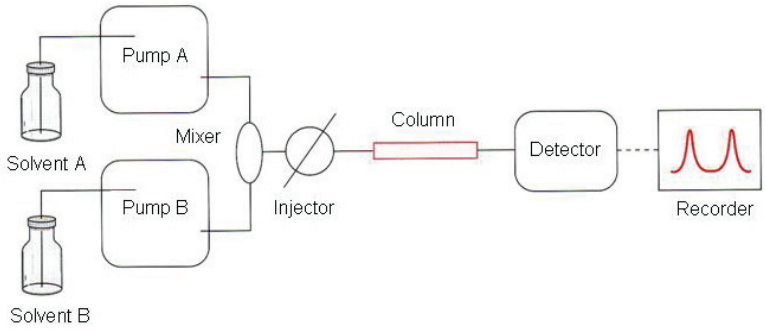

Figure 2-3. Principle of RP-HPLC systems. Solvent reservoirs, pumps and injector represent the first compartment of HPLC systems, followed by the separation achieved by a column and the detector [43].

In the case of RP-HPLC, sample solutions are injected to the system either by hand (via syringes) or with a pump. The analyte solution is then pumped into the column that can differ in size and package material, called stationary phase. A widely used stationary phase for e.g. protein separation is C18 chains connected to silica beads. Proteins interact with the C18 chains due to hydrophobic / hydrophilic interactions and tend to

stay inside the column. In a next step the proteins are removed by washing the column material with a solvent (mobile phase) comprising an increasing percental concentration of polar solvents. The control of elution-solvent gradient over time, the system pressure and the packing of column material can be used to increase the analyte separation. Especially the influence of the package of stationary phase inside the column can be a critical factor due to analyte diffusion effects during separation [44]. The re-elution of samples into the mobile phase is controlled by the strength of interactions with the stationary phase and mobile phase, respectively. The time (retention time) at which proteins are re-eluted can be simply measured by UV detector signals. The mixture components can then be collected and used for further experiments. By using standard curves it is even possible to conduct an exact quantification of the amount of analytes inside a complex mixture [45].

2.5 Bicinchoninic Acid Assay (BCA-Assay)

The BCA assay is a colorimetric assay that can be used to quantify the amount of proteins in solutions. It is a two-step assay. The first step contains the reduction of Cu^{2+} (from copper sulfate) to Cu^{+} ions caused by the presence of proteins. This reaction is equivalent to the amount of proteins in solution. In the second step the reduced Cu^{+} ions can build a chelate complex with two Bicinchoninic Acid molecules. This chelate complex has a purple color and adsorbs light at the specific wavelength of 562 nm which can be easily measured by a photometer (see for example [46]). The darker the color, the more protein is contained in the solution which makes it even possible to make relative and rough statements about protein concentrations without any technical equipment. By using a standard curve with known protein concentrations it is possible to make predictions about the protein amount of unknown samples. This method is widely used because of its robustness against detergents and the high sensitivity.

2.6 Fluorescence Measurements (FITC)

Fluorescein isothiocyanat (FITC) is a label molecule that can be simply used to link to proteins and peptides. The molecule is functionalized with an isothiocyanate (-N=C=S) group that can react with primary amines of proteins and peptides (see Figure 2-4) [47].

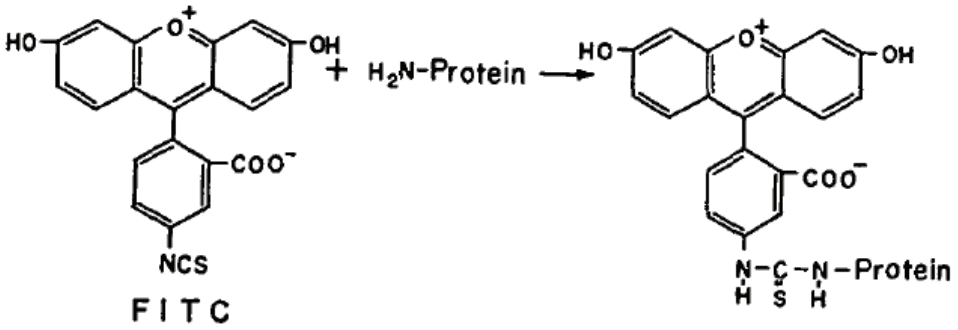

Figure 2-4. Fluorescein isothiocyanate (FITC) reacts with primary amine groups of proteins. The so labelled proteins and peptides can then be detected at a wavelength of 518 nm. Adapted from Tomita et al. 1973 [47].

These labeled proteins can then easily be detected by excitation the label molecule with energy (light) at a wavelength of 494 nm. The emission of light is measured at a wavelength of 518 nm and can either be analysed statistically or visually. In protein research FITC is widely used and fluorescein isothiocyanate labelled bovine serum albumin (BSA-FITC) was e.g. suggested as a model protein drug [48].

2.7 References

[1] A. Gorecka-Drzazga, S. Bargiel, R. Walczak, J. A. Dziuban, A. Kraj, T. Dylag, J. Silberring. Desorption/ionization mass spectrometry on porous silicon dioxide. Sens. Actuat. B-Chem. 103: 206-212, 2004

[2] C. Chen, A. K. Walker, Y. Wu, R. B. Timmons, G. R. Kinsel. Influence of sample preparation methology on the reduction of peptide matrix-assisted laser desorption/ionization ion signals by surface-peptide binding. J. Mass Spectrom. 34: 1205-1207, 1999

[3] A. K. Walker, C. M. Land, G. R. Kinsel, K. D. Nelson. Quantitative determination oft he peptide retention of polymeric substrates using matirx-assisted laser desorption/ionization mass spectrometry. J. Am. Soc. Mass Spectrom. 11: 62-68, 2000

[4] E. Szajili, T. Feher, K. F. Medzihradszky. Investigating the quantitative nature of MALDI-TOF MS. Mol. Cell. Proteomics 7.12: 2410-2418, 2008

[5] P. Kingshott, H. A. W. St. John, H. J. Griesser. Dircet detection of proteins adsorbed on synthetic materials by Martix-Assisted Laser Desorption Ionization-Mass Specrtometry. Anal. Biochem 273: 156-162, 1999

[6] P. Kingshott, H. A. W. St. John, R. C. Chatelier, H. J. Griesser. Matrix-assisted laser desorption ionization mass spectrometry detection of proteins adsorbed *in vivo* onto contat lenses. J. Biomed. Mater. Res. 49:36-42, 2000

[7] N. Xia, C. J. May, S. L. McArthur, D. G. Castner. Time-of-flight ion mass spectrometry analysis of conformational changes in adsorbed protein films. Langmuis 18: 4090-4097, 2002

[8] . Stoeckli, P. Chaurand, D. E. Hallahan, R. M. Caprioli. Imaging mass spectrometry: A new technology for the analysis of protein expression in mammalian tissues. Nat. Med. 7: 493-496, 2001

[9] R. L. Caldwell, R. M. Caprioli. Tissue profiling by mass spectrometry. Mol. Cell. Proteomics 4.4: 394-401, 2005

[10] E. H. Seeley, R. M. Caprioli. Molecular imaging of proteins in tissues by mass spectrometry. PNAS 105: 18126-18131, 2008

[11] A. Walch, S. Rauser, S.-O. Deininger, H. Höfler. MALDI imaging mass spectrometry for direct tissue analysis: a new frontier for molecular histology. Histochem. Cell Biol.130: 421-434, 2008

[12] S.-O. Deininger, M. P. Ebert, A. Fütterer, M Gerhard, C. Röcken. MALDI imaging combined with hierarchical clustering as a new tool fort he interpretation of complex human cnacers. J. Proteome Res. 7: 5230-5236, 2008

[13] . L. Norris, D. S. Cornett, J. A. Mobley, M. Andersson, E. H. Seeley, P. Chaurand, R. P. Caprioli. Processing MALDI mass spectra to improve mass spectral direct tissue analysis. Int. J. Mass. Spectrom. 260: 212-221, 2007

[14] Y. J. Kim, A. Freas, C. Fenselau. Analysis of viral glycoproteins by MALDI-TOF Mass Spectrometry. Anal. Chem. 73: 1544-1548, 2001

[15] D. Suckau, J. Köhl, G. Karwath, K. Schneider, M. Casaretto, D. Bitter-Suermann, M. Przybylski. Molecular epitope identification by limited prteolysis of an immobilized antigen-antibody complex and mass spectrometric peptide mapping. PNAS 87: 9848-9852, 1990

[16] D. T. Kim, H. W. Blanch, C. J. Radke. Direct imaging of lysozyme adsorption onto mica by atomic force microscopy. Langmuir 18: 5841-5850, 2002

[17] H. X. You, C. R. Lowe. AFM studies of protein adsorption. J. Colloid Interf. Sci. 182: 586-601, 1996

[18] C.A. Johnson, Y. Yuan, A. M. Lenhoff. Adsorbed layers of ferritin at solid and fluid interfaces studies by atomic force micrsocopy. J. Colloid Interf. Sci. 223:261-272, 2000

[19] P. Hinterdorfer, Y. F. Dufrene. Detection and localization of single molecular recognition events using atomic force microscopy. Nat. Methods 3: 347-355, 2006

[20] A. L. Weisnenhorn, M. Khorsandi, S. Kasas, V. Gotzos, H.-J. Butt. Deformation and height anomaly of soft surfaces with an AFM. Nanotechnology 4: 106-113, 1993

[21] R. Barattin, N. Voyer. Chemical modifications of AFM tips for the study of molecular recognition events. Chem. Comm. 13: 1513-1532, 2008

[22] J. Landoulsi, V. Dupres. Probing peptide-inorganic surface interaction at the single molecule level using force spectroscopy. Chem.Phys.Chem. 12: 1310-1316, 2011

[23] S. Manohar, A. R. Mantz, K. E. Bancroft, C.-Y. Hui, A. Jagota, D. V. Vezenov. Peeling single-stranded DANN from graphite surface to determine oligonucleotide binding energy by force specrtoscopy. Nano Lett. 8: 4365-4372, 2008

[24] M. Geisler, D. Horinek, T. Hugel. Single molecule adhesion mechanics on rough surfaces. Macromolecules 42: 9338-9343, 2009

[25] C. Friedsam, H. E. Gaub, R. R. Netz. Probing surfaces with single-polymer atomic force microscope experiments. Biointerphases 1: 1-21, 2006

[26] A. Serr, R. R. Netz. Pulling adsorbed polymers from surfaces with the AFM: stick *vs.* slip, peeling *vs.* gliding. Europhys. Lett. 73: 292-298, 2006

[27] K. E. Bremmell, P. Kingshott, Z. Ademovic, B. Winther-Jensen, H. J. Griesser. Colloid probe AFM investigations of interactions between fibrinogen an dPEG-likeplasma polymer surfaces. Langmuir 22: 313-318, 2006

[28] A. Yersin, H. Hirling, P. Steiner, S. Magnin, R. Regazzi, B. Hüni, P. Huguenot, P. De Los Rios, G. Dietler, S. Catsicas, S. Kasas. Interactions between synaptic vesicle fusion proteins explored by atomic force microscopy. PNAS 100: 8736-8741, 2003

[29] M. E. Drew, A. Chworos, E. Oroudjev, H. Hansma, Y. Yamakoshi. A tripod tip for single molecule ligand-receptor force spectrosocopy by AFM. Langmuir 26: 7117-7125, 2010

[30] B.-H. Kim, N. Y. Palermo, S. Lovas, T. Zaikova, J. F. W. Keana, Y. L. Lyubchenko. Single-molecule atomic force micsocopy force spectroscopy study of Aβ-40 interactions. Biochemistry 50: 5154-5162, 2011

[31] D. Pastre, L. Hamon, I. Sorel, E. Le Cam, P. A. Curmi, O. Pietrement. Specific DNA-protein interactions on mica investigated by atomic force microscopy. Langmuir 26: 2618-2623, 2010

[32] Q. Peng, H. Li. Atomic force microscopy reveals parallel mechanical unfolding pathways of T4 lysozyme: Evidence for a kinetic partitioning mechanism. PNAS 105: 1885-1890, 2008

[33] M. A. Tenan, D. M. Soares. The quartz crystal microbalance: A toll for probing viscous/viscoelastic properties of thin films. Braz. J. Phys. 28: 405-412, 1998

[34] G. Sauerbrey. Verwendung von Schwingungen ur Wägung dünner Schichten und zur Mikrowägung. Zeitschrift für Physik 155: 206-222, 1959

[35] D. Shen, M. Huang, L.-M. Chow, M. Yang. Kinetic profile of the adsorption and conformational change of lysozyme on self-assembled monolayers as revealed by quartz crystal resonator. Sensor Actuat. B-Chem. 77: 664-670, 2001

[36] A. P. Sierro, K. Degiampietro, R. Colaco, B. Saramago. Adsorption of albumin and sodium hyaluronate on UHMWPE: A QCM-D and AFM study. Colloid. Surface B 78: 1-7, 2010

[37] M. P. Gisbert, A. P. Serro, R. Colaco, B. Saramago. Bovine serum albumin adsorption onto 316L stainless steel and alumina: a comparative study using depletion, protein radiolabeling, quartz crystal microbalance and atomic force microscopy. Surf. Interface Anal. 40: 1529-1537, 2008

[38] C. Tamerler, E. E. Oren, M. Duman, E. Venkatasubramanian, M. Sarikaya. Adsorption kinetics of an engineered gold binding peptide by surface plasmon resonance spectroscocopy and a quartz crystal microbalance. Langmuir 22: 7712-7718, 2006

[39] O. Mermut, R. L. York, D. C. Phillips, K. R. McCrea, R. S. Ward, G. A. Somorjai. Directions in peptide interfacial science. Biointerphases 1: 5-11, 2006

[40] H. Chen, X. Su, K.-G. Neoh, W.-S. Choe. QCM-D analysis of binding mechanism of phage particles displaysing a constrained heptapeptide with specific affinity to SiO_2 and TiO_2. Anal. Chem. 78: 4872-4879, 2006

[41] S. H. Brewer, W. R. Glomm, M. C. Johnson, M. K. Knag, S. Franzen. Probing BSA binding to citrate-coated gold nanoparticles and surfaces. Langmuir 21: 9303-9307, 2005

[42] A. Huenerbein, C. E. H. Schmelzer, R. H. H. Neubert. Real-time monitoring of peptic and tryptic digestions of bovine β-casein using quartz crystal microbalance. Anal. Chim. Acta 584: 72-77, 2007

[43] F. Lottspeich, J. W. Engels. Bioanalytik. Spektrum Akademischer Verlag, 2. Auflage, 2006

[44] J. J. Van Deemter, F. J. Zuiderweg, A. Klinkenberg. Longitudinal diffusion and resistance to mass transfer as causes of nonideality in chromatography. Chem. Engng. Sci. 5: 271-289, 1956

[45] E. O. Keith, M. Boltz, R. Gadh, R. Ghorsriz, D. Mangatt. L. E. Janoff. Adhesion of tear proteins to contact lenses and vials. Biotechnol. Appl. Biochem. 34: 5-12, 2001

[46] P. E. tyllianakis, S. E. Kakabakos, G. P. Evangelatos, D. S. Ithakissios. Direct colorimetric determination of solid-supported functional groups and ligands using bicinchoninic acid. Anal. Biochem. 219: 335-340, 1994

[47] M. Hiramatsu, N. Okabe, K.-I. Tomita. Preparation and properties of lysozyme modified by fluorescein-isothiocyanate. J. Biochem. 73: 971-978, 1973

[48] C.Wischke, H.-H. Borchert. Fluorescein isothiocyanate labelled bovine serum albumin (FITC-BSA) as a model protein drug: opportunities and drawbacks. Pharmazie 61: 770-774, 2006

3 Identification of materials binding peptide sequences

Parts of this chapter where supported by the work of Dr. Julian Schneider (Molecular Dynamics simulations), Linda Gätjen (QCM-D measurements) and Klaus Rischka (Peptide synthesis) in cooperation with the Fraunhofer IFAM Bremen. All other results were obtained by Sascha Steckbeck. This chapter is published in *Analytical Methods* (DOI 10.1039/c3ay42042f, 2014)

3.1 Introduction

Protein adsorption is an ubiquitous phenomenon that takes place both in daily-life situations, for instance on the surface of contact lenses [1], and in very specific cases, for example when protein-based drugs adhere on the walls of glass storage packages [2]. In the body, the adsorption of proteins on biomedical implants is the first step of a reaction cascade, which results in the adhesion of cells and thus regulates the host response upon implantation [3]. Also the development of bacterial biofilms on materials' surfaces, which can influence the chemical, physical, mechanical or hygienic properties of materials, is initiated by the adsorption of a protein conditioning layer [4].

In the 1990s, seminal works by Stanley Brown revealed that oligopeptides can selectively bind to inorganic mineral surfaces in a process reminiscent of biomolecular recognition [5]. Several groups have recently contributed to the selection of a variety of sequences that "recognise" certain materials' classes, inorganic compounds or even crystallographic facets of the same material. In the last decade up to the present day the field has been expanding with impressive speed, due to the highly promising applications that selective peptide-materials binding opens up in bionanotechnology [6-12].

To date, the search for peptides that bind selectively to a certain inorganic phase is mainly confined to random selection using biotechnological methods, e.g. from phage-display libraries [7]. It is therefore an open challenge to develop new techniques both to identify specific materials binding motifs and to make conclusions about the underlying adhesion mechanisms [13]. In this work, we present a novel and rapid technique based on matrix assisted laser desorption ionization time-of-flight mass spectrometry (briefly MALDI-MS) that can be used as an initial guess to guide the discrimination between strong and weak materials-binding peptides. MALDI-MS is commonly used to assess

the purity of protein solutions and has also been applied to investigate the adhesion between molecules and inorganic substrates [1, 14-19, 20]. Differently from these previous works, the basic idea of our method relies upon time-resolved, sensitive measurements of the MALDI-MS peak signals acquired from a solution containing several peptides placed in contact with an inorganic surface, in our case amorphous SiO_2.

Specifically, we show that samples taken at various incubation times present different time evolutions of the peaks assigned to different peptides, as a result of their different binding affinities. Supported by additional experiments using bicinchoninic acid assay (BCA), high-performance liquid chromatography (HPLC), atomic force microscopy (AFM) and quartz crystal microbalance (QCM-D), we demonstrate the advantages and limitations of the method to discriminate strong from weak binding sequences from a mixture solution. Additional molecular dynamics (MD) simulations suggest a possible hydrophobic driving force for the affinity of tryptophan-containing sequences for the silicon oxide surface.

3.2 Experimental

Materials. SiO_2 nanoparticles were purchased from FiberOpticCenter Inc. (New Bedford, USA), with a diameter of 150 nm and a BET specific surface area of 30 m^2/g. Glass vessels were provided by Schott AG (Mainz, Germany). These included both standard borosilicate glass vials and so-called Type I Plus glass vials, whose inner walls were coated with pure amorphous SiO_2 by plasma impulse chemical vapor deposition (PICVD) in order to prevent unspecific protein adhesion. Both types of vials had the same height and diameter dimensions of 40 mm of 22 mm (wall thickness: 1 mm). The Si wafers for the AFM investigations were purchased from silchem Handelsgesellschaft GmbH (Freiberg, Germany)

Lysozyme digestion. The digestion of lysozyme (Sigma-Aldrich, Steinheim, Germany, Cat. No. L4919-5G) was performed following the protocol in [21] through incubation with Trypsin (Sigma-Aldrich, T6567-5X20UG, Proteomics Grade) over night at 37°C in 400 mM NH_4HCO_3 buffer, at a trypsin/lysozyme (wt/wt) ratio of 1/50. Before the digestion, lysozyme was reduced with DTT (Dithiotreitol, 45 mM) at 50°C for 15 min and then alkylated with 100 mM Iodacetamid (IAA) at room temperature for 15 min to

achieve better cleavage results. The digestion was stopped by freezing the solution in liquid N_2. Afterwards, the peptides were diluted to the concentration needed for the MALDI-MS experiments and used immediately. Digested peptides were identified using MASCOT Peptide Mass Fingerprint software from Matrix Science. Peptides were searched against SwissProt data base with a tolerance of 0.5 Da and Carbamidomethylation as fixed modification.

MALDI ToF-MS measurements. MALDI ToF-MS measurements were performed on a Voyager-DE^{TM} PRO Biospectrometry Workstation from Applied Biosciences controlled by the Voyager Control Panel Software (Foster City, CA, USA). The analysis was performed with the Data Explorer 4.0 software from Applied Biosystems. All measurements were carried out on polished steel targets coated with a CHCA (α-Cyano-4-hydroxycinnamic acid, Sigma, Germany, C-2020-10G) thin-film matrix. The latter was freshly prepared with a saturated CHCA solution in 100% Acetone, which was allowed to dry immediately before starting the MALDI–MS experiments. The matrix / sample ratio for spot preparation was 1:1 using 0.5 µL of matrix and sample. Tests of other different preparation parameters have been performed as described in figure 3-1.

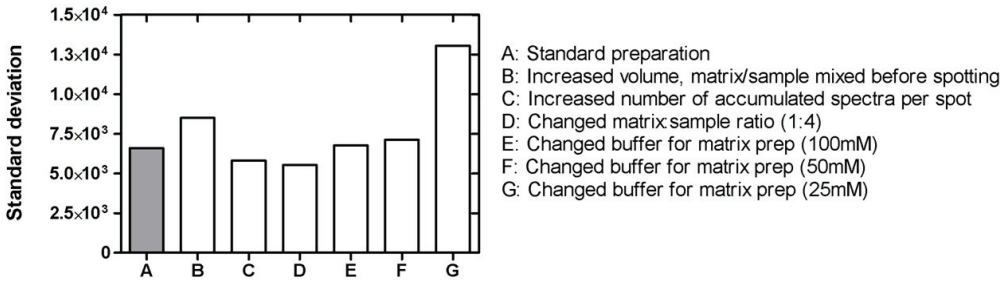

Figure 3-1. Influence of different preparation methods for MALDI ToF-MS on the standard deviations associated with the peak area value of a solution of the SBP peptide (1,467 Da) in series of nine measurements for each preparation method. Our standard procedure (grey bar) leads to a standard deviation comparable or even smaller than other preparation methods. Variations from standard protocol (A) are as follows: B: matrix and sample were mixed before spotting using an increased volume to minimize pipette errors (50 µl of sample and matrix, respectively). C: Increased amount of accumulated spectra (10 instead of 5). D: Matrix/Sample ratio was adjusted to 1:4 (before: 1:1). E-G: Molarity of buffer (NH_4HCO_3) that was used for sample dissolving was decreased to 100, 50 and 25 mM instead of 400 mM.

Lysozyme adsorption. The lysozyme adhesion experiments were performed in the same buffer as used for the digestion protocol (400 mM NH_4HCO_3). Four mL of protein solution at a concentration of 0.5 mg/mL were filled into borosilicate glass vials and 0.5µL solution samples were collected at 0, 2, 4, 20, 22, 24, 26, 28, 44, 46 and 48 hours. During this time the solution was shaken at 100 RPM on an orbital shaker (IKA KS 260 basic, Staufen, Germany). On the one hand, each sample for the MALDI-MS measurement was pipetted directly on the target coated with the CHCA matrix and allowed to dry at RT for MALDI-MS analysis. In order to obtain statistically relevant measurements, at each time step we collected 5 spectra with 200 laser shots from 10 separate samples (spots). The acceleration voltage was adjusted to 25,000 V and the delay time to 750 nsec. The observed mass range was 5 to 20 kDa in reflector mode. On the other hand, comparative BCA assays of supernatants were performed following the instructions from the supplier (Pierce™ BCA Protein Assay Kit no. 23227, Thermo Fisher Scientific Inc., Rockford, IL USA). The protein detection was carried out at a wavelength of 560 nm in a multimode microplate reader (Mithras LB 940, Berthold Technologies GmbH, Bad Wildbad, Germany).

Peptide adsorption. Evaluation of the adsorption of digested peptides as well as synthetic peptides were performed in protein LoBind tubes (Eppendorf, Hamburg, Germany) containing 2 mg SiO_2 nanoparticles in 400 mM NH_4HCO_3 buffer. The concentration of the synthetic peptides amounts to $7*10^{-9}$ mol, which corresponds to the theoretical digest peptide concentration, assuming a complete and perfect digest (e.g., without any mis-cleavages). We note, however, that the activity of trypsin is pH-dependent and may be lower than expected at pH 8.4. This may lead to an actual concentration of cleaved peptides slightly different (smaller) than the theoretical one. During incubation, the samples were shaken at 20°C and 1,400 RPM in a thermomixer to avoid sedimentation of the nanoparticles and to assure an adequate mixing of particles and peptides. After 1, 120, 360 and 1,440 minutes (24 hours) of incubation, samples of the supernatant were collected after 5 minutes of centrifugation at 21,000 x *g*. Samples (0.5 µL) were then subsequently spotted on MALDI-MS steel targets where CHCA has been applied before (0.5 µL). For calibration of the MALDI-MS a peptide standard kit (P2-3143-00, AB SCIEX, Framingham, MA, USA) was used.

For the MALDI-MS analysis, the acceleration voltage was adjusted to 20,000 V and the delay time was 120 nsec. Five spots were measured for each incubation time and

peptide, recording spectra in the range of 0.4 to 2.6 kDa with 100 laser shots per spectrum (other preparation parameters were tested and the corresponding results regarding the variability of the MALDI-MS peak areas are presented in Figure 3-1).

Synthesis of peptides. Solid-phase-peptide-synthesis (SPPS) was performed adopting the Fmoc-strategy, using an automated ABI 433A Peptide Synthesizer (Foster City, CA, USA) applying the FastMoc protocol [22]. Amino acids and preloaded Tritylchloride polystyrene (TCP) resins were purchased from IRIS Biotech GmbH (Marktredwitz, Germany) and PepChem (Reutlingen, Germany), respectively. The activation of the carboxyl groups was performed by a mixture of HBTU (2-H(1-*H*-Benzotriazole-1-yl)-1,1,3,3-tetramethyluronium hexafluorophosphate) and HOBt (1-Hydroxybenzotriazole) at 0.5 M in DMF (N,N- Dimethylformamide). After synthesis, the peptides were cleaved from the resin by adding 3.6 mL trifluroacetic acid (TFA), 0.2 mL Triisopropylsilane (TIPS) (Roth, Karlsruhe, Germany) and 0.2 mL H_2O. The obtained solution was shaken briefly and left at RT for 2 hours. The peptides were purified by solution filtering and direct precipitation in ice-cold *tert*-Butylmethylether (Cat. No. T175.1, Sigma-Aldrich, Steinheim, Germany). After centrifugation at 3,500 rpm for 10 minutes the supernatant was removed, the pellet was frozen with liquid N_2 and freeze-dried in 15 mL centrifuge tubes (VWR, Darmstadt, Germany). In analogy with the peptides obtained via lysozyme digestion, all cysteine residues of the synthetic peptides were alkylated with 100 mM IAA at room temperature for 15 min. All synthesised peptides were then tested by means of MALDI ToF-MS for the correct masses. A list of the six peptides employed in this work is presented in Table 3-1.

Table 3-1. Peptides used in this study.

Name	Sequence	Mass	Origin	Note
P1	TPGSR	517 Da	This work	Strong SiO_2 binder
P2	NTDGSTDYGILQINSR	1754 Da	This work	Weak SiO_2 binder
P3	GCRL	447 Da	This work	Unclear SiO_2 affinity
P4	WWCNDGR	936 Da	This work	Unclear SiO_2 affinity
WBP	CINQEGAGSKDK	1249 Da	Oren et al., 2007	Weak binder to quartz
SBP	PPPWLPYMPPWS	1467 Da	Oren et al., 2007	Strong binder to quartz

HPLC experiments. The HPLC (BioCat 700E system from Applied Biosystems, CA, USA) comparison with the MALDI-MS data was performed preparing the samples as for the peptide adsorption experiments. After the centrifugation step, two 100 µL supernatant samples were injected into the HPLC C18-column (Polaris 5µ, 250 x 4.6 mm, Agilent, Boblingen, Germany) after 1 and 1,440 minutes (24 hours), during which time the solution was shaken at 1,400 rpm (thermomixer). The gradient for the HPLC separation was from 0 to 7 min equilibration time with 100% solvent B (v/v). Afterwards (7 to 27 min) the peptides were eluted from the column by increasing the amount of solvent A to 70% (v/v). This was followed by 5 minutes (27 to 32 min) holding that gradient. The last step (32 to 39 min) involved the decrease of solvent A to 0% (v/v) and increase of B to 100% (v/v). Solvent A consisted of 100% (v/v) acetonitrile (HPLC grade, Roth, Karlsruhe, Germany) with 0.1% (v/v) trifluoroacetic acid (TFA, Roth, Karlsruhe, Germany). Solvent B was 90% (v/v) H_2O (HPLC grade, Roth, Karlsruhe, Germany) and 10% (v/v) acetonitrile with 0.1% (v/v) TFA. The flow rate was adjusted to 1 mL / min and peptides were detected using an UV detector at a wavelength of 215 nm.

QCM-D experiments. QCM measurements were performed using a Q-Sense E4 System from Biolin Scientific (Stockholm, Sweden). All tested peptides were prepared in the same concentration of 0.1 mg/mL in 400 mM NH_4HCO_3 buffer. The quartz crystal (Q-Sense, QSX 303, SiO_2) was first allowed to equilibrate in air for 30 min and then in buffer for at least another 30 min. The flow rate was adjusted to 80 µL/min. The recorded frequency shifts and dissipation were analysed by the PRISM software (v. 5.01, GraphPad Software Inc., San Diego, CA, USA). The temperature was controlled permanently to 25 °C.

AFM Imaging. A JPK Nanowizard III AFM (JPK Instruments AG, Berlin, Germany) was used to record surface images in liquid (AC mode) with silicon nitride probes (DNP-S10, Bruker, Germany) with a nominal spring constant of 0.35 N/m and a tip radius of 10 nm. The visual analysis was performed with JPK Data Processing software (v. spm-4.2.16). AFM Imaging on oxidised Si was carried out after cutting a Si wafer into pieces of appropriate size. Each piece was cleaned in isopropanol in an ultrasonic bath and then thoroughly rinsed with doubly distilled water (ddH_2O). Drop of peptide solutions (1 mg/mL in NH_4HCO_3 buffer) were incubated on each wafer surface for 120 minutes followed by rinsing with ddH_2O. The samples were then transferred directly to

an AFM liquid cell. Images (1x1 µm) were collected at a scan rate of 1 Hz (512 x 512 lines) at RT in NH_4HCO_3 buffer.

Molecular Dynamics Simulation. The classical equilibrium Molecular Dynamics (MD) simulations were performed using the AMBER force field [23] and the TIP3P water model in combination with an own force field for the interactions between oxidised Si surfaces and protein containing water solutions [24,25]. The surface was modelled with a realistic structure of the natively oxidized (100) Si surface obtained and employed in previous works [26, 24-28]. This surface features both neutral silanol groups as well as negatively charged deprotonated silanol terminations (surface charge density of -0.136 C/m^2). The surface model covers an area of 43.49 x 43.49 $Å^2$. Na^+ counterions were included to ensure charge neutrality of the system. The simulations were performed using the LAMMPS [29] code. The time step was set to 1 fs, the non-bonded interactions were cut off at a distance of 12.0 Å, and the electrostatic interactions were described by the particle-particle particle-mesh (ppm) method as implemented in the code. The structure of the peptide was equilibrated in solution for 6 ns at 450 and 300 K, before it was placed in close contact with the substrate, where it was once more equilibrated at 450 K for 1 ns and at 300 K for 10 ns. This protocol was repeated several times in order to explore different possible adsorbed peptide conformations.

3.3 Results and Discussion

When a protein solution comes in contact with a solid material surface, adhesion at the solid/liquid interface may occur, accompanied by a decrease of the protein concentration in solution. In fact, quantitative estimates of the amount of adsorbed proteins are often obtained by analysing the concentration decrease in the liquid phase with various spectroscopic or colorimetric techniques. Here we have performed MALDI ToF-MS measurements on samples of a protein solution placed in contact with SiO_2 surfaces over a specific time range, assuming that protein adsorption should be accompanied by a decrease of the protein peak areas.

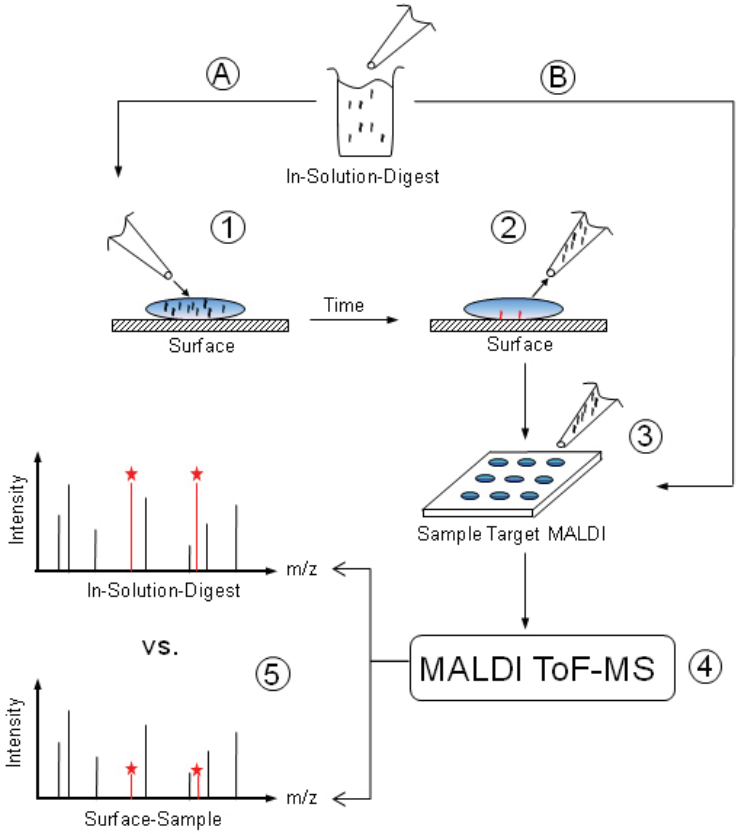

Figure 3-2. Scheme of the MALDI ToF-MS depletion technique used for the identification of material-binding peptide sequences. An in-solution-digest of a protein is split into two sample ways (A and B). Sample B is transferred immediately to the MALDI target for comparison with sample A and protein mass fingerprint. Sample A is applied to the surface to be tested (1). After specific time steps samples are taken from solution (2). Samples are prepared on MALDI targets, co-crystallizing with HCCA matrices (3). MALDI ToF-MS measurements reveal changes in peaks areas due to peptide adsorption (4 and 5). After a data base search, noticeable peaks can be assigned to specific peptide sequences.

After validating this concept with whole lysozyme proteins and mixtures of standard MALDI-MS calibration peptides, we apply the method to digested lysozyme fragments, whose sequences can be assigned to specific mass/charge ratios (i.e. to specific MALDI-MS peaks) by means of a database search. This permits an analysis of the adhesion behaviour of many single peptides with defined sequences at the same time. A schematic overview of the method is presented in Figure 3-2.

Adsorption of whole lysozyme. We stored a solution of whole lysozyme for two days in uncoated borosilicate glass vials typically used as packages for pharmaceutical solutions, in particular protein-based drugs. The MALDI-MS protein peak area as well as the protein amount (BCA absorbance) measured for samples in solution taken at increasing time intervals clearly decreased within the first 5 hours, indicating a loss of free proteins in solution and thus lysozyme adhesion on the vial's walls (Fig. 3-3, top). On the basis of calibration curves relative to BCA and MALDI-MS (Fig. 3-3, bottom), the fraction of adhered proteins within these first 5 hours can be estimated as 20% or 40% of the total protein amount, respectively. An exact quantification, however, is prevented by the large uncertainties of the time-resolved data acquired in both assays.

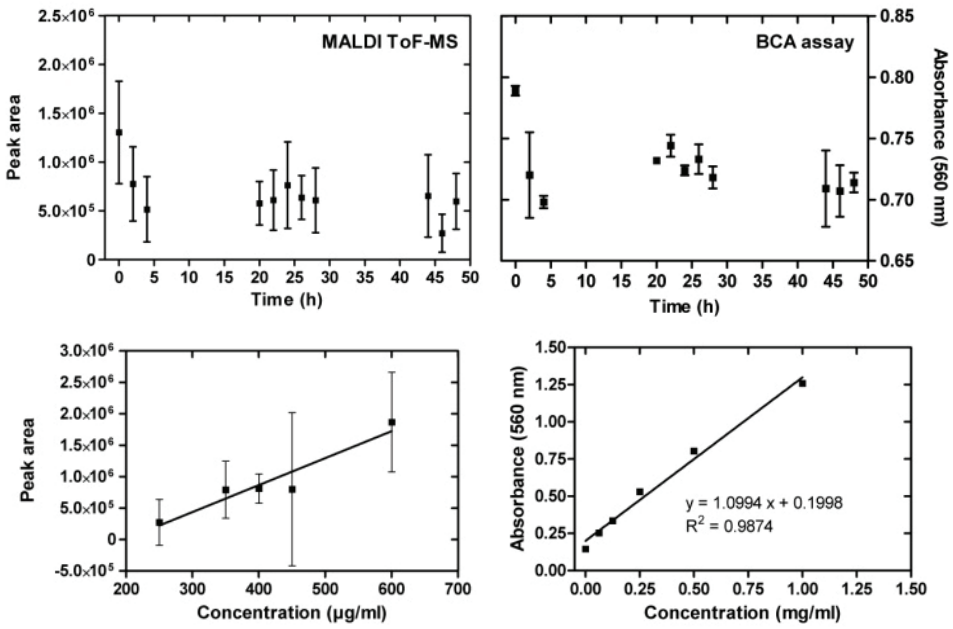

Figure 3-3. Top: Adsorption of non-digested lysozyme on the wall of a borosilicate glass vial, as obtained from MALDI ToF-MS depletion (left) and BCA assay measurements (right). The squares are the experimental values. Bottom: Standard curve of correlation between lysozyme concentration and MALDI peak area (left) and measured BCA absorbance in context to lysozyme concentration (right).

Validation with mixtures of standard calibration peptides. In order to assess whether different concentration ratios of peptide mixtures can be estimated by means of MALDI-MS measurements, we performed a set of validation experiments using mixtures of three standard calibration peptides (PC1: Sequence NTDGSTDYGILQINSR, PC2: Sequence CINQEGAGSKDK, PC3: Sequence: PPPWLPYMPPWS). We prepared three solutions at different concentration ratios (see Figure 3-4). Namely: the concentration of PC3 remains the same in the solutions A, B, C; the concentration of PC2 decreased by 1/4 and 1/10 in solutions B and C with respect to solution A, respectively; the concentration of PC1 decreased by 1/10 in solution B and increased again to 1/4 in solution C. The three mixtures are analysed by means of MALDI-MS and the peak areas of all three peptides are reported in Figure 3-4.

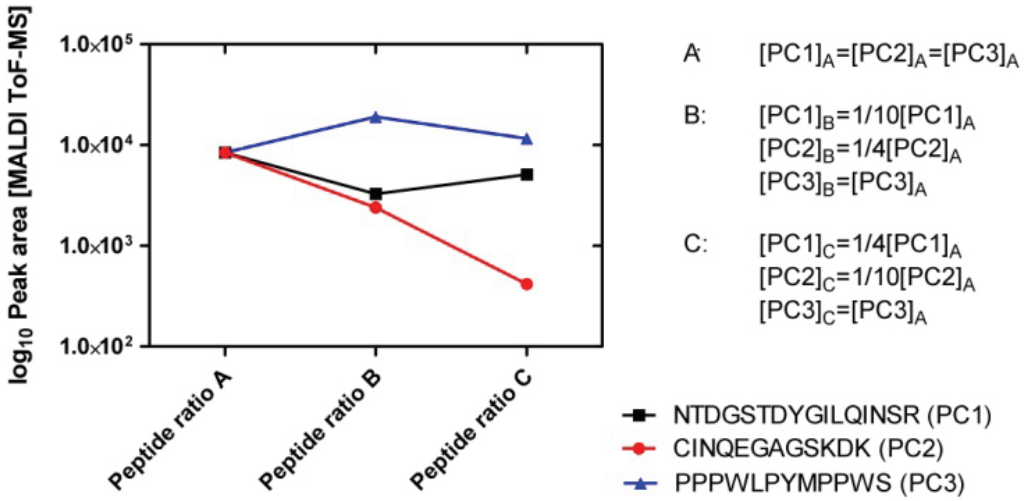

Figure 3-4. Variation of the MALDI peak areas of three different calibration peptides mixed in different concentration ratios in three solutions A, B, C (total concentration: 100 µg/mL) .The concentrations in each solution are reported next to the graph. Note the logarithmic scale of the y axis and the normalization of the MALDI data to match the intensity values of the three peptides when their concentrations are equal (case A).

It can be seen peak areas of peptide PC3 (constant concentrations) changed only weakly in the three measurements. The peak areas of peptide PC2 decreased in the expected way, and the peak areas of PC1 also followed the same trend as the concentrations. Note, from the variations of the peak areas it is not possible to gain quantitative knowledge about the original concentration ratios. This may due either to the intrinsic large variation of the MALDI-MS measurements (see Figure 3-1) or to ionisation

suppression effects due to the presence of several peptides in the MALDI-MS samples. In any case, it is important that the measured peak areas qualitatively follow the same trend of the concentration ratios in the three solutions. Therefore, we conclude from this experiment MALDI-MS measurements can be applied to peptide mixture monitoring qualitatively the change of their concentrations in adsorption experiments. Furthermore, it is possible to obtain information about their different binding affinity to the same material surface.

Adsorption of peptide mixtures from digested lysozyme. A mixture of several different peptides was obtained after digestion of lysozyme as described in the experimental section. Using the MASCOT database search algorithm [30] we were able to assign a sequence to each mass/charge peak with total sequence coverage of 78%. The peptide mixture was placed in contact with both borosilicate glass and the SiO_2-coated glass surfaces of pharmaceutical vials. The SiO_2 coating was produced by plasma treatment using plasma-induced chemical vapour deposition (PICVD) to prevent protein adhesion [31]. The evolution of the peaks with time demonstrated a drastic reduction of the amount of peptides in solution upon contact with borosilicate glass, irrespective of their sequences. In contrast, no or only a slight decrease of the peptide concentration in solution is observed on the SiO_2-coated surface (Figure 3-5), confirming the expected effect of adhesion minimization after plasma treatment.

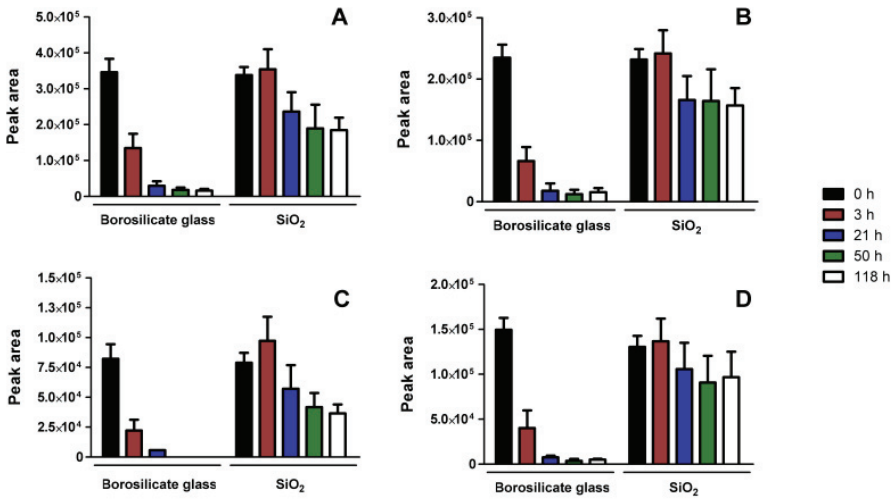

Figure 3-5. Four representative peptide adsorption plots from lysozyme digest on uncoated and SiO_2-coated borosilicate glass surfaces. The change of peak areas quantifying the amount of peptides remaining in solution is reported as a function of time, over a long incubation period. The peptide sequences are as follows: A: NRCK (518 Da), B: HGLDNYR (875 Da), C: FESNFNTQATNR (1429 Da) and D: GTDVQAWIR (1046 Da).

We note that, as a result of the small surface area displayed by the vials, we are not able to draw any conclusion about the specific adsorption behaviour of different peptide sequences on the SiO_2-coated glass. For this reason, we performed a further MALDI-MS depletion assay placing the digested lysozyme solution in contact with SiO_2 nanoparticles and collecting solution samples over a time frame of 24 hours. In this experiment we can distinguish between peptide sequences that display a more or less marked reduction of MALDI-MS peak areas, and thus a higher or weaker affinity for the SiO_2 nanoparticle surface (Figure 3-6).

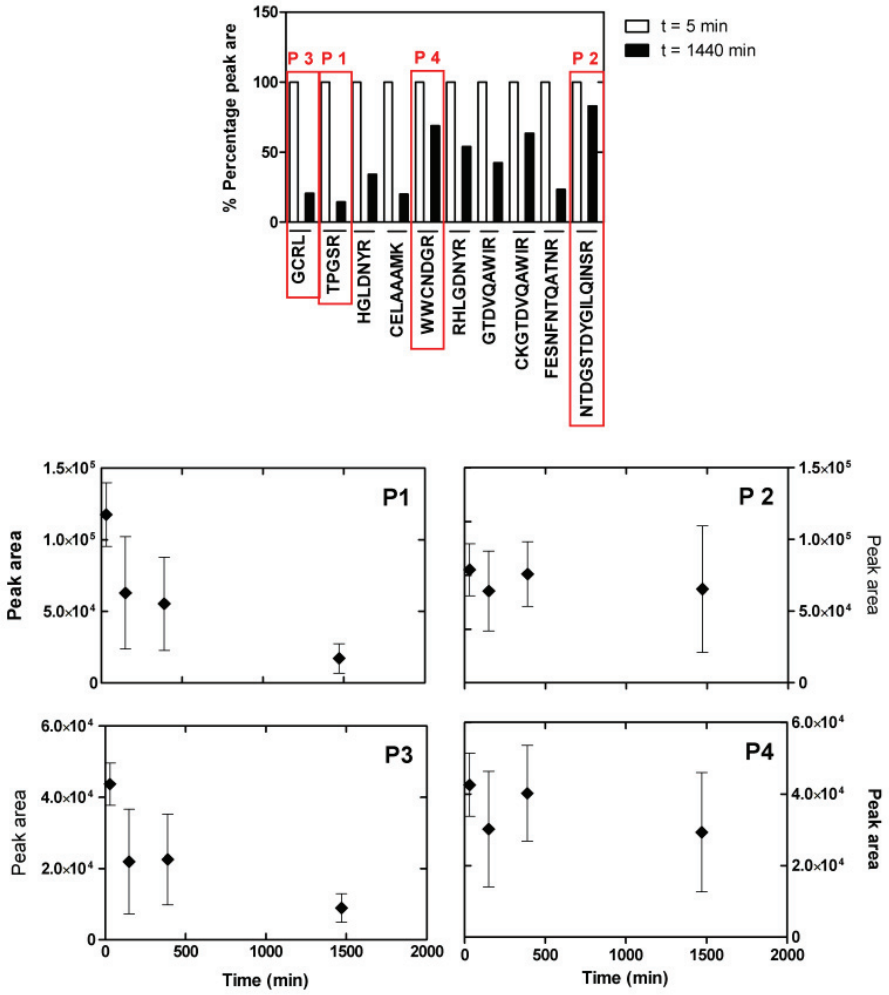

Figure 3-6. Comparison of the adhesion behaviour of peptides from a lysozyme digest mixture on amorphous SiO_2 nanoparticles measured with the MALDI ToF-MS depletion technique. The diagram (upper figure part) shows the differences of peptide amounts in solution between the start of experiment (t = 5 min) and after 24 hours (t = 1,440 min) of incubation with the nanoparticles. Two peptides are selected as putative strong binders (P1: TPGSR and P3: GCRL) and two as putative weak binders (P2: NTDGSTDYGILQINSR and P4: WWCNDGR). A more detailed plot with time evolution of data points for these four peptides is shown in the lower figure part.

We realised in these experiments the possible adsorption of the peptides to the vial's walls influence the results only to a negligible extent due to the much larger surface area of the nanoparticles. Control experiments addressing this issue are shown in figure 3-7.

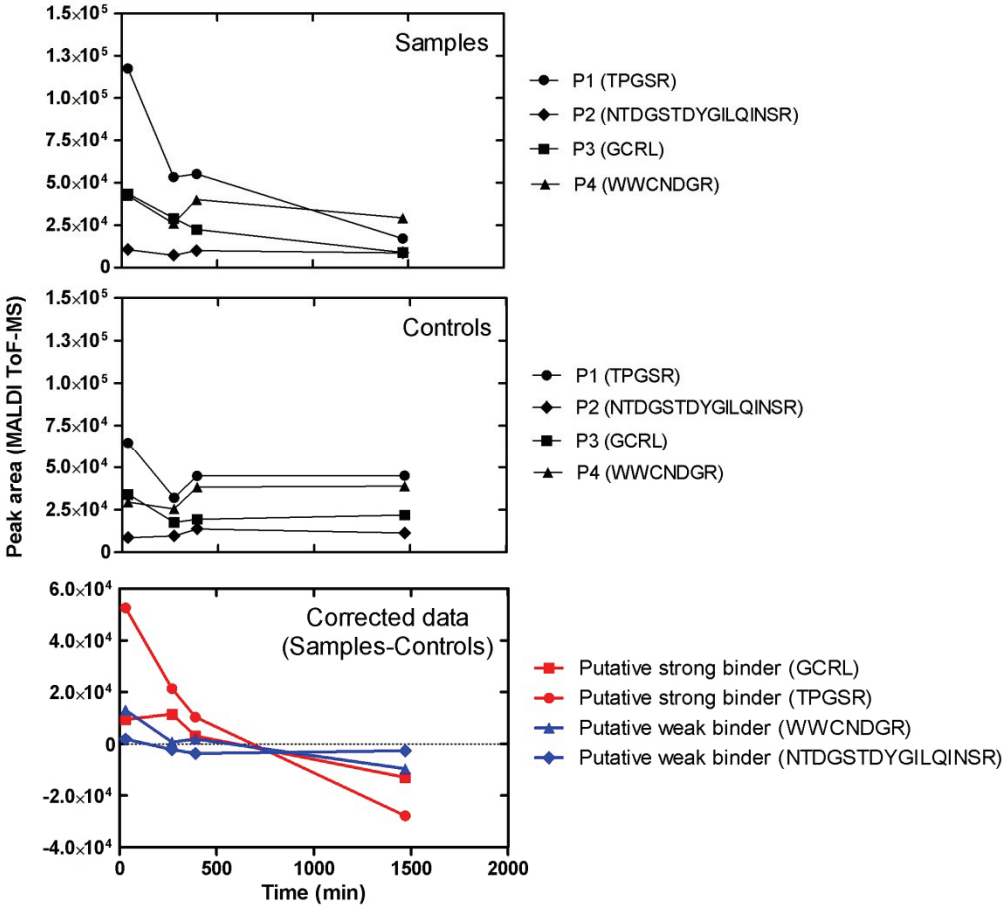

Figure 3-7. Time evolution of peptide adsorption as measured with MALDI-ToF MS depletion technique. Sample (upper image) describes the adsorption of peptides on SiO_2 nano particles in Eppendorf tubes. Controls (middle) shows peptide adsorption plots on Eppendorf tubes without nano particles. The corrected data (lower image) was calculated by subtraction of controls from sample values. Although for P1 and P3 a weak adsorption onto tubes (controls) can be assumed within first 120 minutes, signals remain stable or increase slightly until 1,440 minutes.

It should be noted that different peptides possess different ionization potentials and thus accelerate differently in MALDI-ToF MS experiments, leading to different absolute values of the peak areas. Moreover, each individual experiment is subjected to relatively large error bars concerning the peak area quantifications. Therefore, this technique can only be used as a rough and qualitative mean of estimating the surface-binding affinity of different peptides, when focusing on relative changes of the same peak during the course of one and the same experiment.

Despite these limitations, we were able to classify, for instance, the sequences TPGSR (named henceforth P1, 517 Da) and GCRL (henceforth P3, 447 Da) as strong binding peptides and the sequences NTDGSTDYGILQINSR (henceforth P2, 1754 Da) and WWCNDGR (henceforth P4, 936 Da) as weak binding peptides. In particular, the peptides P1 and P3 showed a decrease of peak area starting within the first minutes after placing the solution in contact with SiO_2 nanoparticles and continuously decreasing until about 1,440 minutes (see Figure 3-6). This behaviour was not observable for peptides P2 and P4.

It is worth noting that the identification has been performed starting from a complex mixture of peptides, with the strong advantage of rapid detection over other techniques based on biotechnological assays. A disadvantage is represented by the large error fluctuations intrinsic in the MALDI-MS depletion measurements (see Figure 3-1). Moreover, at this point nothing can be said about the influence of clustering, weakening or amplifying phenomena caused by the existence of other peptides in solution on the binding affinity of a specific sequence. In fact, the existence of more than one kind of biomolecule in a solution inevitably leads to a competition for binding sites on surfaces [36], as a generalisation of the well-known Vroman effect. For these reasons, in the next section we present complementary investigations of the binding affinity of pure oligopeptides synthesised with solid phase peptide synthesis (SPPS). MALDI-ToF MS spectra in Figure 3-8 illustrate the level of purity of our synthetic peptides.

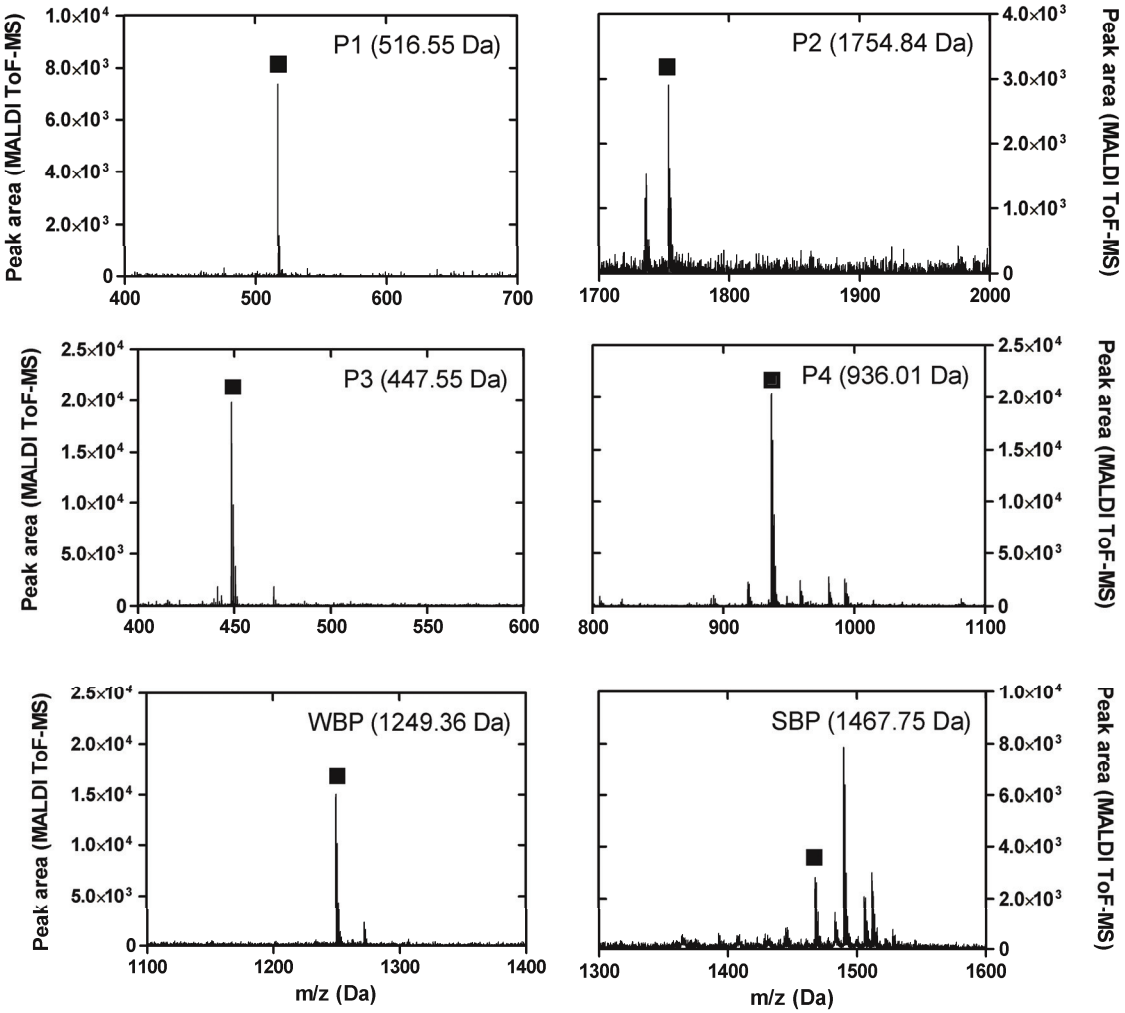

Figure 3-8. MALDI ToF-MS of the solution of synthetic peptides P1, P2, P3, P4, WBP, SBP used in our study, as a mean of assessing the purity of the peptides after SPP synthesis. Black squares indicate the specific peptide peaks. MALDI ToF-MS is a common technique to identify peptide purity after synthesis procedure and was therefore used in this context. Given peptide masses are without modifications (e.g. alkylation). As it can be seen, peaks of interest can be separated easily from potential foreign peaks (if existing).

Adsorption of single synthetic peptides. In order to verify the adsorption behaviour of the pure peptides, for instance to avoid competition effects in the peptide mixture, we synthesised all four peptides P1 to P4 by means of SPPS. The results are compared in particular with two other synthetic peptides which have been identified as a strong binder to quartz (sequence PPPWLPY-MPPWS, henceforth strong binding peptide, SBP) and a weak-binder to quartz (sequence CINQEGAGSKDK, henceforth weak-binding peptide, WBP) in previous works [32, 33].

All six peptides were investigated individually with our MALDI ToF-MS depletion technique. The results are presented in Figure 3-9. As a mean of comparison, the concentration depletion in the pure peptide solutions was also measured independently by RP-HPLC immediately and 1,440 minutes after incubation with the nanoparticles. To highlight the differences in binding affinity among the different peptides, we scaled their MALDI-MS peak areas so that they all present the same values a t = 1 min (this reflects the usage of equal initial concentrations in all cases). We arbitrarily take the value of peptide P1 as the reference to obtain the scaling factors for all other peptides at all times. The initial peak area value is highlighted with black dotted lines in all panels of Figure 3-9.

The obtained MALDI-MS peak areas evolutions confirm the strong binding character of peptides P1, P3 and SBP and the weak binding character of P2 and WBP. The HPLC results are in fairly good agreement with the MALDI-MS measurements, although a slight increase of the HPLC area is visible for the P3 peptide.

Interestingly, a clear decrease of the MALDI-MS peak area of P4 visible in Figure 3-9 (synthetic peptides) was not observed using the peptide digestion mixture (Figure 3-6). This may be because of interactions with other peptides which result in a depletion prevention of the P4 peak in the former case. Alternatively, the oxidation of tryptophane residues could result in a spurious decrease of the MALDI-MS peak due to the mass change associated with oxidation.

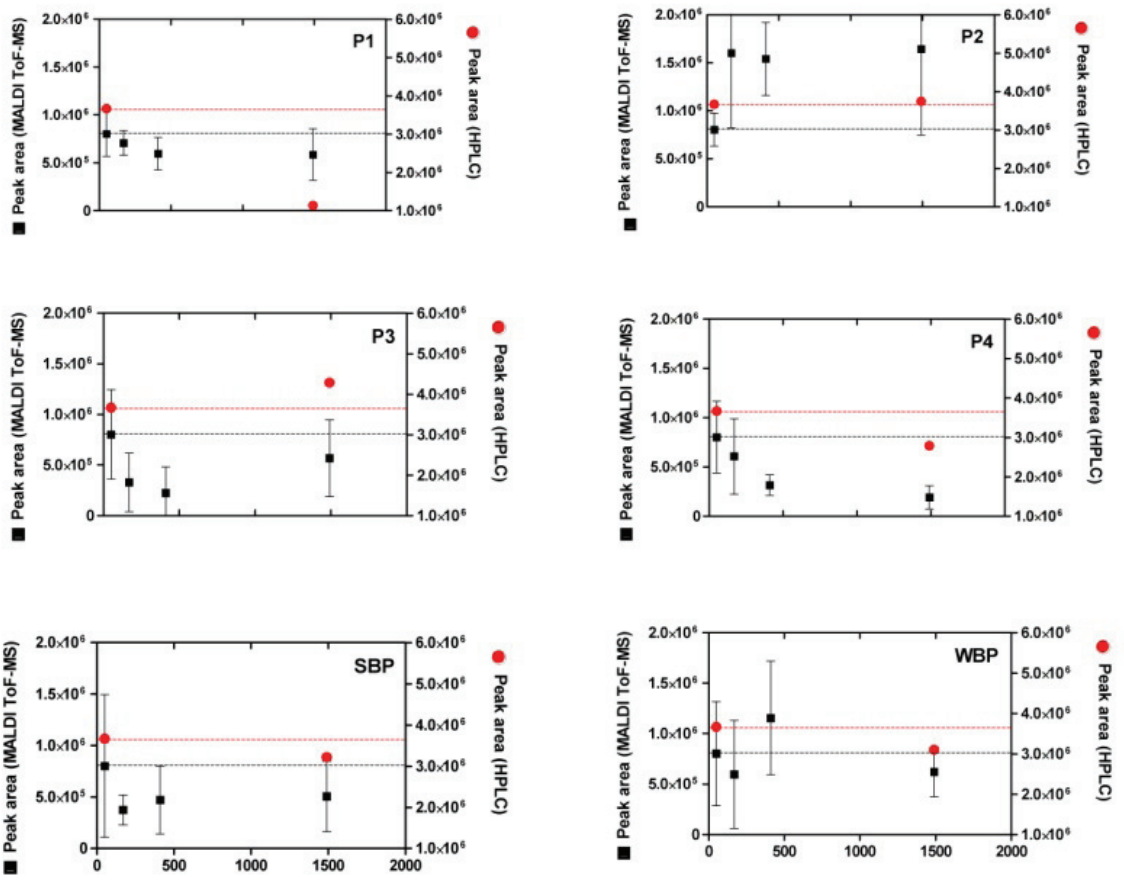

Figure 3-9. Time evolution of the MALDI-MS peak areas (black squares) of four isolated peptides (P1 to P4) identified from Figure 3-6 and two previously identified peptides [32] (SBP: strong binding peptide, WBP: weak binding peptide) in contact with SiO_2 nanoparticles. As a comparison, the results of HPLC depletion assays are reported as red circles. All peptides were synthesized by SPPS and cysteine residues were alkylated to permit comparisons to peptides from lysozyme digest. The MALDI-MS data were normalized as described in the text.

However, additional tests showed only a negligible amount of Trp oxidation during the course of the experiments thus seem to exclude this hypothesis (Figure 3-10).

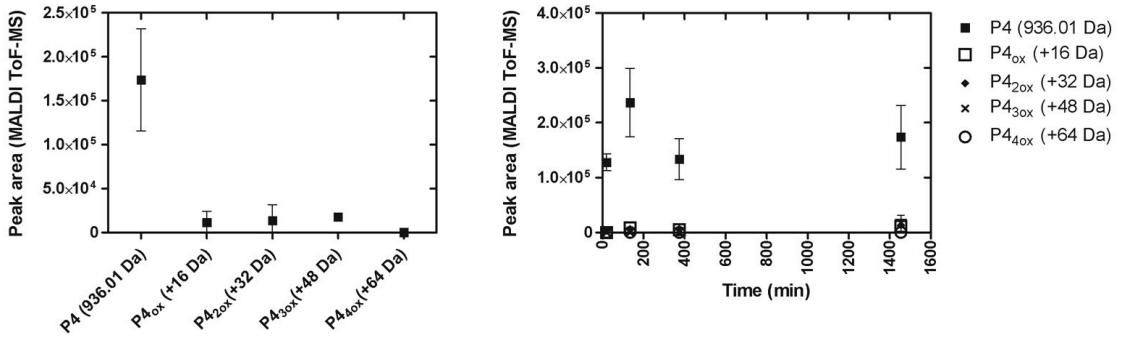

Figure 3-10. MALDI peak areas associated with the non-oxidized or with oxidized states of tryptophan in peptide P4 (WWCNDGR). The occurrence of peaks corresponding to oxidized states after 24 hours incubation is negligible (left). The abundance of oxidation peaks did not change significantly with time during incubation of the peptide with SiO_2 nanoparticles (right).

Other spurious effects as a result of the synthesis process, e.g. remaining impurities (Figure 3-8) [34] or ionization suppression effects cannot be excluded. We also note that the high sensitivity of the MALDI-MS technique to small changes of peptide concentration, while being an advantage in detecting the adhesion of peptides for small surface areas (Figure 3-5), is also a source of error, for instance due to inhomogeneities of the solution arising from incomplete mixing.

The slow evolution and decomposition of peptide coronas around the used SiO_2 nanoparticles can be a further source of uncertainty [35]. This may explain unexpected increases of the MALDI-MS and HPLC peak areas during the adsorption experiments (visible especially in Figure 3-9 for P2 and WBP). However, the observed clear decrease of the peak areas for strong binding peptides is most probably a signature of strong surface affinity.

QCM-D and AFM investigations. In order to further confirm the strong or weak binding character of the peptides for silicon oxide surfaces, we performed complementary AFM imaging on an oxidised Si wafer and QCM-D analysis using a sensor coated with SiO_2. The QCM-D results (Figure 3-11) showed weak but clear

attenuations of the oscillation frequencies (and corresponding slight increases of the dissipation signals) within the first 1,500 seconds after surface contact, as expected for surface adsorption [38]. In particular, the very small frequency changes (less than 1 Hz) indicated that only few peptides interact with the surface, in agreement with the results obtained for SiO_2-coated glass vials (see Figure 3-5).

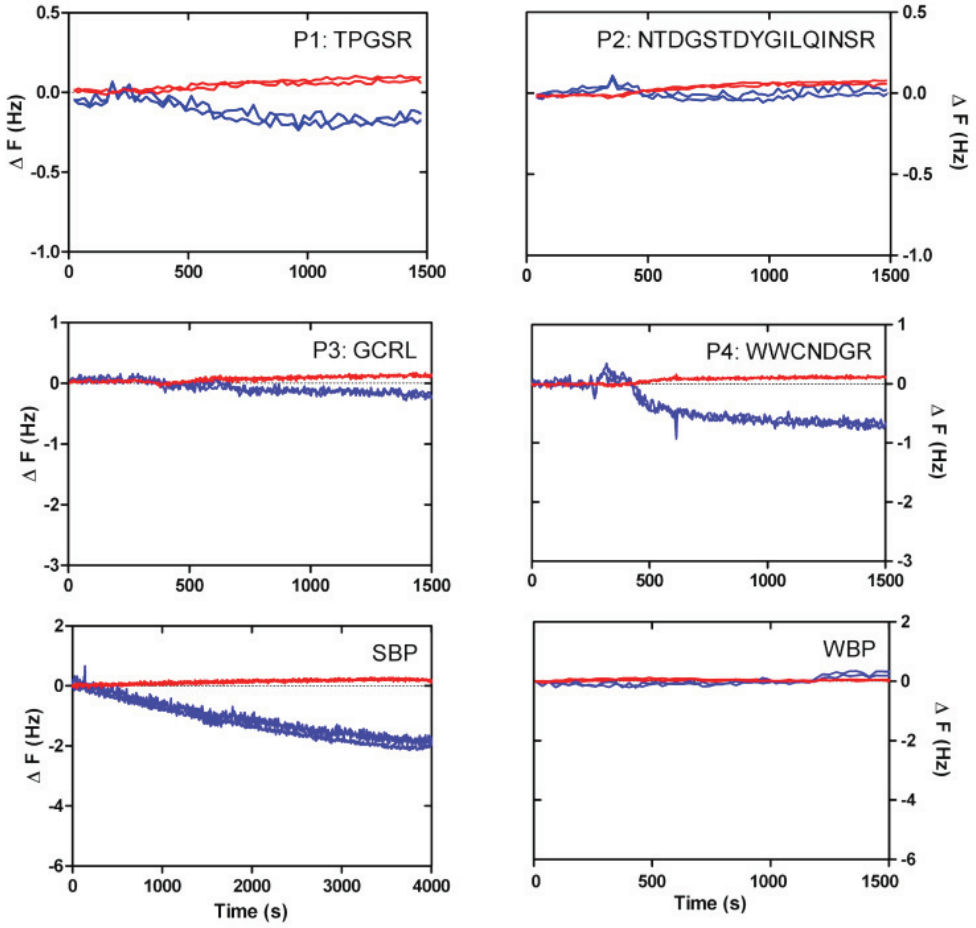

Figure 3-11. Changes of frequency (blue lines) and dissipation (red lines) obtained in QCM-D experiments (7th and 11th overtone frequencies) after placing solutions of the individual peptides P1, P2, P3, P4, SBP and WBP on SiO_2-coated sensor surfaces.

In particular, the reference peptide SBP produced the largest QCM-D frequency shift over a long measurement time, while no frequency shift at all is obtained for the WBP peptide, as expected [32]. Similar trends are obtained for the newly identified SiO_2-binder P1 with respect to the weak-binder P2. Notably, also the AFM images and in

particular the different roughness of typical line sections (Figure 3-12) suggest that a higher adsorbed amount of P1 with respect to P2, despite the larger size of the latter peptide. For peptides P3 and P4 the situation remains less clear. Peptide P3 leads to a very small (albeit detectable) QCM-D frequency shift. This may indicate some binding affinity of the peptide for SiO_2 surfaces, in agreement with the MALDI-MS results obtained for peptide mixtures (Figure 3-6) and the isolated peptide (Figure 3-9). The AFM imaging also indicated a slight amount of adsorption, since the obtained roughness is larger than for the clean Si wafer, although below 0.5 nm, also due to the very small peptide size. As for P4, both the QCM-D analysis and the AFM imaging suggest binding of the peptide to the surface, which we could detect by means of MALDI-MS using synthetic peptides (Fig. 3-9) but not for peptides in digest solution (Fig. 3-6). Discrepancies may arise from the different nature of the surfaces investigated (amorphous SiO_2 nanoparticles in the MALDI-MS experiments, SiO_2-coated QCM-D sensors and oxidised Si wafer for the AFM).

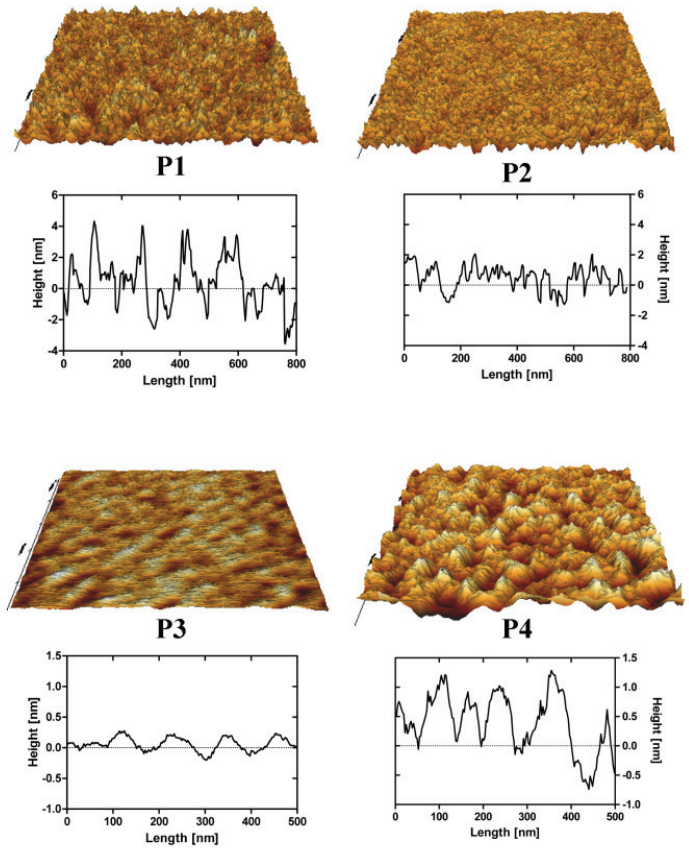

Figure 3-12. AFM 3D-rendered images and representative line sections of the peptides P1, P2, P3 and P4 adsorbed on an oxidised Si wafer (image areas 1x1µm). The overall appearances and the height profiles of the peptide-adsorbed surfaces are comparable with previous AFM studies performed by other groups [29].

Molecular Dynamics Simulations. In order to investigate a possible driving force for the adsorption of the P4 peptide, we performed all-atom Molecular Dynamics simulations using a realistic model of the natively oxidised Si surface and a carefully tuned force field for the SiOx/water/peptide interface [25]. After placing the equilibrated peptide in proximity of the surface and starting constant-temperature simulations in explicit water solvent, it spontaneously adsorbed on the surface. Two principal adsorption sites are identified in several independent simulations carried out in order to explore different possible adsorbed peptide conformations (Figure 3-13). Namely, (1) the negatively charged surface terminations attract polar residues, particularly the positively charged R residue as well as the N-terminal ammonium group. These groups reside in regions of increased water density at the surface, where they form hydrogen bonds with surface groups and physisorbed water molecules, similar to our previous findings of the interaction between RGD and RKLPDA peptides on oxidised Ti surfaces [26, 39]. Furthermore, (2) in almost all adsorbed conformations obtained in our simulations, P4 additionally binds to the surface via its two aromatic tryptophan residues, which lie above hydrophobic surface regions with decreased water density. In detail, the aromatic rings are able to form a stable anchor between the surface and patches of high water density, as displayed in Figure 3-13. We could speculate that this "hydrophobic" adsorption mode may be prevented for the case of highly hydrophilic SiO_2 nanoparticles, but not for flat oxidised Si wafer or QCM-D sensor surfaces.

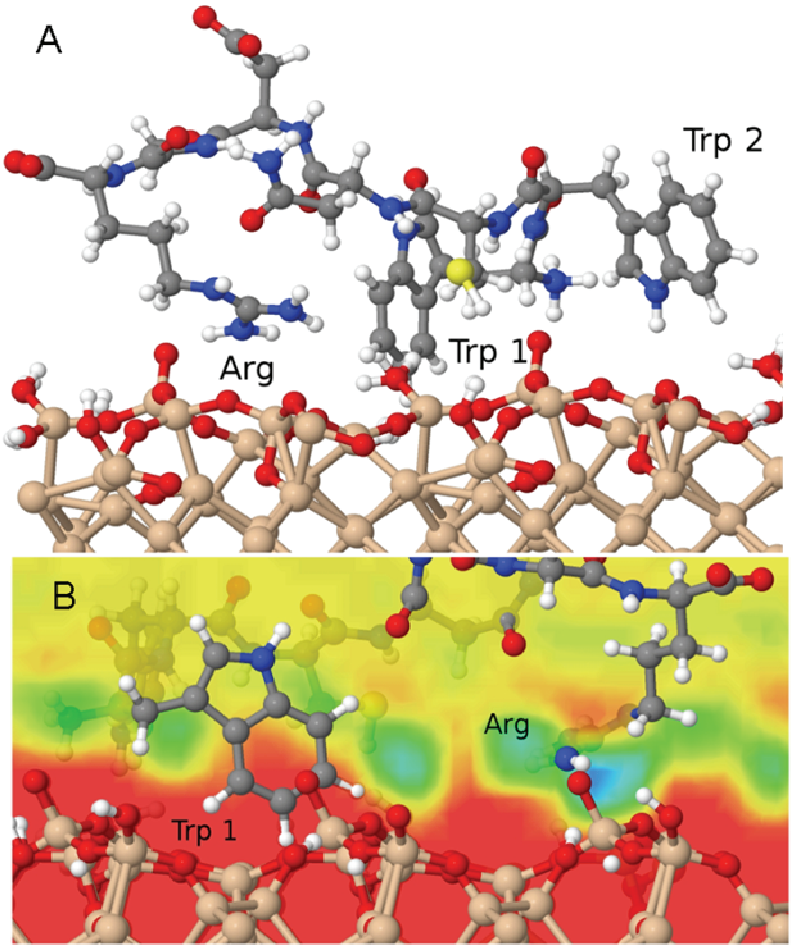

Figure 3-13. (A) Snapshot of a typical adsorbed configuration of the P4 (WWCNDGR) peptide on an oxidized Si surface model obtained in molecular dynamics simulations. (B) The interplay of the hydrophobic W (Trp) and hydrophilic R (Arg) residues with the local variations of the water density above the surface is displayed. The water density in the absence of peptides is shown as a colour map (red corresponds to zero, blue corresponds to high density) within a vertical plane that includes the Trp ring as well as the Arg side chains.

3.4 Conclusions

MALDI-ToF mass spectrometry has been used in the past to detect the presence of proteins on materials surfaces [1, 14, 16-19]. We have shown here that it can be also exploited for qualitative investigations of the affinity and kinetics of adsorption of proteins and peptides on materials surfaces. In particular, in our study we have used it to show that a plasma-SiO_2 coating of borosilicate glass surfaces reduces the adsorption of peptides drastically with respect to uncoated surfaces (see Figure 3-5). More importantly, it can enable an unbiased initial discrimination between strong and weak materials-binding peptide sequences, starting from complex peptide mixtures (see Figures 3-2 and 3-6). However, due to the large error bars intrinsic in the MALDI-MS

spectral analysis and to the numerous sources of uncertainty regarding specific surface affinity when working with peptide mixtures, its combination with more established and sensitive methods such as QCM-D remains unavoidable. Only via a combination of various methods we could clearly identify the sequence TPGSR as a novel strong SiO_2-binding motif. In the case of other peptide sequences the MALDI-MS prediction were not unequivocally confirmed by further analysis.

In particular, the sequence WWCNDGR seems to be affine to certain type of silicon oxide (e.g. the native oxide layer of Si wafer or the SiO_2 coating of QCM sensor surfaces). Molecular Dynamics simulations suggest that such affinity is most probably due to the peculiar properties of the oxidised Si surface to bind both hydrophilic (Arg) and hydrophobic (Trp) residues (see Figure 3-13), as a consequence of the recognition capability of amino acids sequences for local variations of the water density at the solid/liquid interface [26].

In summary, we conclude that the technique introduced in this work can provide an initial guess to guide the identification of strong vs. weak materials binding peptides. It may be considered as a viable alternative to commonly used methods, such as phage display library screening, probably at the expenses of quantitative selectivity, but gaining in rapidity and simplicity. This may be important in industrial applications when a quick assessment of the adsorption affinity of proteins or protein segments is required, such as during the development of anti-adherent coatings of pharmaceutical glass packaging for protein-based drugs [2].

Moreover, the developed depletion assay can be used to estimate which regions (peptide sequences) of a larger protein can be expected to strongly bind to a certain material, thus giving an indication on the binding orientation over the surface [37]. Finally, especially when used in combination with atomistic modelling, it can help rationalise fundamental mechanisms of materials/peptide interaction and thus support a rational design and synthesis of novel hybrid biomaterials based on the biomolecular recognition of inorganic surfaces.

3.5 References

[1] Kingshott P, St.John HAW, Chatelier RC, Griesser HJ (2000) *J. Biomed. Mater. Res.* 49: 36-42

[2] Kraut A, Marcellin M, Adrait A, Kuhn L, Louwagie M, Kieffer-Jaquinod S, Lebert D, Masselon CD, Dupuis A, Bruley C, Jaquinod M, Garin J, Gallagher-Gambarelli M (2009) *J. Proteome Res.* 8: 3778-3785

[3] Puckett SD, Taylor E, Raimondo T, Webster TJ (2010) *Biomaterials* 31: 706-713

[4] Hayashi T, Sano K-I, Shiba K, Kumashiro Y, Iwahori K, Yamashita I, Hara M (2006) *Nano Lett.* 6: 515-519

[5] Brown S (1997) *Nat. Biotechnol*. 15: 269-272

[6] Whaley SR, English DS, Hu EL, Barbara PF, Belcher AM (2000) *Nature* 405: 665-668

[7] Shiba K (2010) *Curr. Opin. Biotech*. 21: 412-425

[8] Sarikaya M, Tamerler C, Jen AK-Y, Schulten K, Baneyx F (2003) *Nat. Mater*. 2: 577-585

[9] Nam K T, Kim D-W, Yoo PJ, Chiang C-Y, Meethong N, Hammond PT , Chiang Y-M, Belcher AM (2006) *Science* 312: 885-888

[10] Demir HV, Seker UOS, Zengin G, Mutlugun E, Sari E, Tamerler C, Sarikaya M (2011) *ACS Nano* 5: 2735-2741

[11} Kuang Z, Kim SN, Crookes-Goodson WJ, Farmer BL, Naik RR (2010) *ACS Nano* 4: 452-458

[12] Khatayevich D, Gungormus M, Yazici H, So C, Cetinel S, Ma H, Jen A, Tamerler C, Sarikaya M (2010) *Acta Biomater.* 6: 4634-4641

[13] Peelle BR, Krauland EM, Wittrup KD, Belcher AM (2005) *Langmuir* 21: 6929-6933

[14] Doucette A, Craft D, Li L (2000) *Anal. Chem.* 72: 3355-3362

[15] Agrawal K, Wu H-F (2008) *Rapid Commun. Mass Spectrom.* 22: 283-290

[16] Griesser HJ, Kingshott P, McArthur SL, McLean KM, Kinsel GR, Timmons RB (2004) *Biomaterials* 25: 4861-4875

[17] McLean KM, McArthur SL, Chatelier RC, Kingshott P, Griesser HJ (2000) *Colloids Surfaces B: Biointerfaces* 17: 23-35

[18] Kingshott P, St John, HAW, Griesser HJ (1999) *Anal Biochem* 273: 156-162

[19] Leize E M, Leize EJ, Leize C, Voegel J-C, Dorsselaer AV (1999) *Anal Biochem* 272: 19-25

[20] McArthur SL, McLean K M, St John HAW, Griesser HJ (2001) *Biomaterials* 22: 3295-3304

[21] The protein protocols handbook, edited by J.M. Walker, second edition, Humana Press, 2002

[22] *Applied Biosystems, **09/2002***: User Bulletin No 33: FastMocTM Chemistry: HBTU Activation in Peptide Synthesis on the Model 4331A

[23] Cornell, W. D., Cieplak, P., Bayly C. I., Gould I. R., Merz Jr. K. M., Ferguson D. M., Spellmeyer D.C. Fox T., Caldwell J. W., Kollman P. A. *J. Am. Chem. Soc.*, **1995**, 117, 5179-5197

[24] Cole D. J., Csányi G., Payne M.C., Spearing S. M., Colombi Ciacchi L. *J. Chem. Phys.,* **2007**, 127, 204704-204715

[25] Butenuth A., Moras G., Schneider J., Koleini M., Köppen S., Meissner R., Wright L. B., Walsh T. R., Colombi Ciacchi L. P*hys. Status Solidi B*, **2012**, 249, 292-305

[26] Schneider J., Colombi Ciacchi L. *J. Am. Chem. Soc.*, **2012**, 134, 2407-2413

[27] Colombi Ciacchi L., Payne M. C. *Phys. Rev. Lett*., **2005**, 96, 196101-196104

[28] Colombi Ciacchi L., Cole D. J., Payne M. C., Gumbsch P. *J. Phys. Chem. C* **2008**, 112, 12077-12080

[29] Plimpton S. J. *J. Comp. Phys.,* **1995**, 117, 1-19

[30] Perkins D N, Pappin D J C, Creasy D M, Cottrell J S (1999) *Electrophoresis* 20: 3551-3567

[31] Walther M, Heming M, Spallek M (1996) *Surf CoatTechnol* 80: 200-202

[32) Oren EE, Tamerler C, Sahin D, Hnilova M, Seker UOS, Sarikaya M Samudrala R (2007) *Bioinformatics* 23: 2816-2822

[33] Oren E E, Notman R, Kim IW, Evans JS, Walsh TR, Samudrala R, Tamerler C, Sarikaya M (2010) *Langmuir* 26: 11003-11009

[34] Richter K, Diaconu G, Rischka K, Amkreuz M, Müller FA, Hartwig A (2012) *Bioinspired, Biomimetic and Nanomaterials* 2: 45-53

[35] Cedervall T, Lynch I, Lindman S, Berggard T, Thulin E, Nilsson H, Dawson K A, Linse S (2007) PNAS 104: 2050-2055

[36] Jung S-Y, Lim S-M, Albertorio F, Kim G, Gurau MC, Yang RD, Holden MA, Cremer PS (2003) *J Am Chem Soc* 125: 12782-12786

[37] Lundqvist M, Andresen C, Christensson S, Johansson S, Karlsson M, Broo K, Jonsson B-H (2005) *Langmuir* 21: 11903-11906

[38] Mermut, O, Phillips D C (2006) *J Am Chem Soc* 128: 3598-3607

[39] Schneider, J, Colombi Ciacchi, L (2011) *J Chem Theor Comput* 7: 473-484

4 Single molecule force spectroscopy (SMFS)

4.1 Introduction

The adsorption of proteins and peptides was experimentally investigated by AFM in many preceding studies. Due to the great variety of possible applications of the atomic force microscope it became an important technique in surface adsorption experiments [1-3]. Starting with imaging in non-contact mode it is possible to display surfaces while they are exposed to protein solutions. The amount, conformation or reactions of adsorbed molecules is then visually observable [4-9]. The technical improvement of atomic force microscopes leads to high resolution pictures which make it possible to view the morphology of single molecules such as proteins, DNA or even the chemical structure of surfaces in atomic resolution. [10].

On the other hand many analyses were done considering desorption forces and interacting forces between surfaces and molecules to make statements about the strength and energy of surface binding [11-21]. Beside the force needed to detach molecules from surfaces, protein unfolding events were also widely investigated. By analyzing force-distance curves from proteins that are stretched nanomechanically by AFM, conclusions about structural sub-domains or intramolecular structures (formed by hydrogen bonds or disulfide bonds) can be made [22-24]. Even the interaction between two molecules, one attached to the surface and the other at the AFM tip, were investigated. This makes it possible to investigate protein-protein or protein-DNA interactions at a molecular scale [25-31].

This chapter describes single molecule force spectroscopy (SMFS) measurements of peptides or proteins covalently attached to the AFM cantilever tip. After some peptides were identified by MALDI depletion technique (see chapter 3), within this chapter these peptides were tested for their interaction forces with silica surfaces. Considering putative weak or strong interactions of the peptides, SMFS experiments should help to make predictions about these assumptions. Furthermore, exemplary force distance curves from proteins will be shown and analyzed for preliminary results.

4.2 Experimental

Origin of proteins and peptides. Peptides WWCNDGR and GCRL were identified by MALDI depletion experiments as previously described in chapter 3. By analyzing the peptide peak areas, these peptides were chosen for further analysis considering SMFS measurements. It was possible to identify these peptides via data base search and therefore locate the position inside the originary protein (lysozyme) as depicted in figure 4-1.

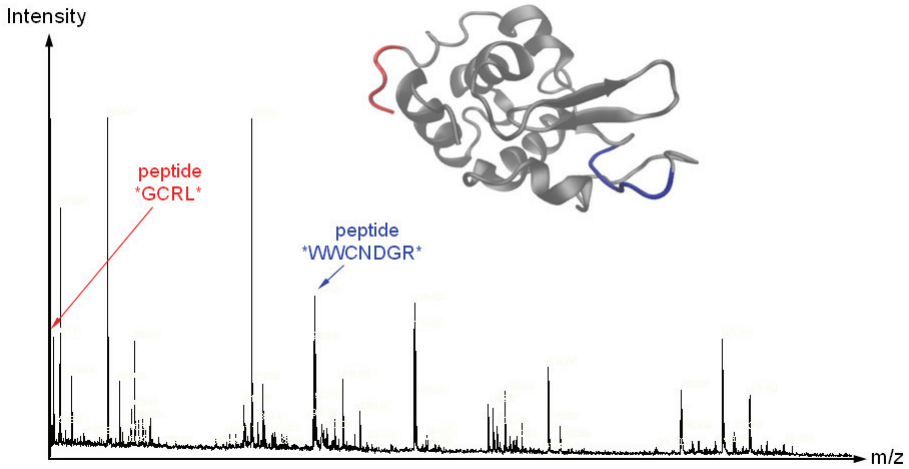

Figure 4-1. Typical spectrum of LSZ digest using trypsin as protease. Due to data base search single peptide peaks can be assigned to peptide sequences and then located in LSZ 3D view.

Peptides CINQEGAGSKDK and PPPWLPYMPPWS were described before as putative weak and strong binder respectively by Oren et al. 2007 [32]. They were chosen for analogous experiments to verify the results from SMFS experiments from peptides WWCNDGR and GCRL. All four peptides were synthesized by SPPS. Furthermore, proteins lysozyme and chymotrypsin were purchased from Sigma Aldrich.

SPPS. Peptides used for this study were synthesized using solid phase peptide synthesis (SPPS) as described before in chapter 3. Briefly, the SPPS peptide synthesis was performed adopting the Fmoc-strategy, using an automated ABI 433A Peptide Synthesizer (Foster City, CA, USA) applying the FastMoc protocol. Amino acids and preloaded Tritylchloride polystyrene (TCP) resins were purchased from IRIS Biotech GmbH (Germany) and PepChem (Reutlingen, Germany), respectively. After synthesis, the peptides were cleaved from the resin by adding 3.6 mL Triflouroacidic acid (TFA),

0.2 mL Triisopropylsilane (TIPS) (Roth, Germany) and 0.2 mL H_2O. The peptides were purified by solution filtering and direct precipitation in ice-cold *tert*-Butylmethylether (Cat. No. T175.1, Sigma, Germany). Supernatant was removed, the pellet was frozen with liquid N_2 and freeze-dried in 15 mL centrifuge tubes (VWR, Germany). All synthesised peptides were then tested by means of MALDI ToF-MS for the correct masses.

AFM linker chemistry. For the chemical linkage of proteins and peptides to AFM tips the tips were first cleaned with piranha solution (Sulfuric acid (conc.): Hydrogenperoxide (30%); 7:3) and rinsed thoroughly with H_2O. Afterwards they were silanized using a 1%-solution of (3-Aminopropyl)triethoxysilane (APTES, purchased from Sigma Aldrich) in toluol. Tips were then incubated in this solution for 5 minutes, rinsed again and directly carried to a polyethylene glycol N-hydroxysuccinimide (PEG-NHS, from Sigma Aldrich) solution (2.5% in H2O) for 60 minutes. As last step AFM tips were incubated in peptide or protein solution, respectively. For all force measurements equal molarities of peptides were used. Modified tips were directly transferred to AFM and used for force curve experiments. A scheme of linked peptides is shown in figure 4-2.

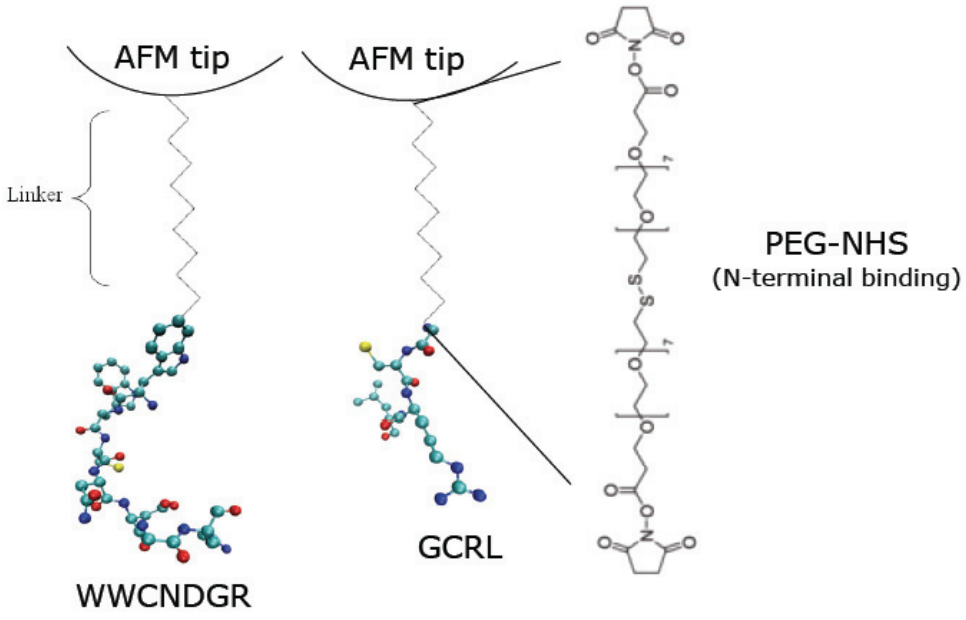

Figure 4-2. Schematic plot of chemistry for linking peptides and proteins onto AFM tips for SMFS experiments. All tip modifications were done by silanization of surfaces using APTES followed by chemical linker PEG-NHS. Peptides and proteins are able to attach to this linker and can then be used for measurements.

AFM measurements. A JPK Nanowizard III AFM was used to record force curves of proteins and peptides in liquid (contact mode) with silicon nitride probes (DNP-S10, Bruker) with a nominal spring constant of 0.33 N/m and a tip radius of 10 nm. Tip speed ranged from 0.4 to 1 µm/s. Peptides and proteins were chemically linked to AFM tips by using PEG-NHS as described above. The visual analysis was performed with JPK Data Processing software (v. spm-4.2.16). AFM curves on oxidised Si were carried out after cutting a Si wafer into pieces of appropriate size. Each piece was cleaned in isopropanol and acetone in an ultrasonic bath and then thoroughly rinsed with doubly distilled water (ddH_2O).

Peak picking. To detect peaks within force distance curves from SMFS measurements of proteins a simple and quick peak picking algorithm was used. This algorithm compares each x,y-data point of a SMFS curve to the subsequent one. As long as this next data point has a smaller y-value it will be quoted as new minimum value. This procedure is repeated until the next data point has a higher value leading to the assumption that the preliminary value is the minimum of a force peak; following values should then increase again. This point-to-point analysis is repeated until a new point of inflexion is reached and values starting to decrease again (a maximum was reached). Each identified maximum and minimum value (x, y-coordinates) is noticed separately in a maximum and minimum list, respectively. In this study only minimum values depicting force peaks were considered. The maximum list, including all maxima, was not further used for analysis. To prevent the detection of very small peaks, a tolerance parameter ("delta-value") was implemented. For each two-data-point-comparison the delta-value was considered. Only if the subsequent point is located outside the actual value minus / plus the delta-value, it is accepted as true subsequent data-point for further analysis. Due to the usage of this parameter it is possible to minimize false detection of diminutive peaks, e.g. within noisy SMFS curves.

4.3 Results and Discussion

4.3.1 SMFS of peptides

Figure 4-3 shows a typical AFM force distance curve of a single peptide. To test some of the peptides that were identified in chapter 3 several force curves as depicted in this figure were collected and statistically analyzed. For the analysis of the curves two parameters were chosen to prove if the measurement was successful. In literature, it can be found that forces between peptides and inorganic surfaces cover a force range of 50 - 500 pN, dependent on the size and amino acid composition of the peptides and the surface properties, respectively [13]. Therefore only curves showing values in this magnitude were provided for further analysis.

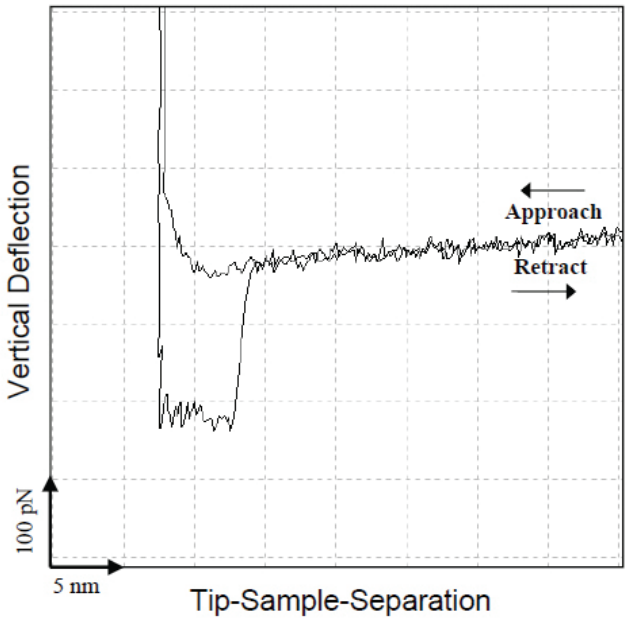

Figure 4-3. Exemplary force-distance curve of a peptide (sequence: WWCNDGR).

Secondly, the tip-sample-distance between last surface contact of the tip and the final desorption force peak was measured (tip-sample-separation). The used PEG-NHS linker has a nominal length of 7.8 nm and the length of the peptides was calculated by 0.36 nm per amino acid. Therefore it was possible to make a prediction of the maximum stretching length of molecule and linker (length linker + length peptide). All SMFS curves that fulfill these criteria were used for analysis. A dot plot of the tip-sample-separation over desorption forces for two peptides (GCRL and WWNCDGR) is shown

in figure 4-4. It can be found that these two peptides reveal forces distributed very close to each other, which is also observable in figure 4-5.

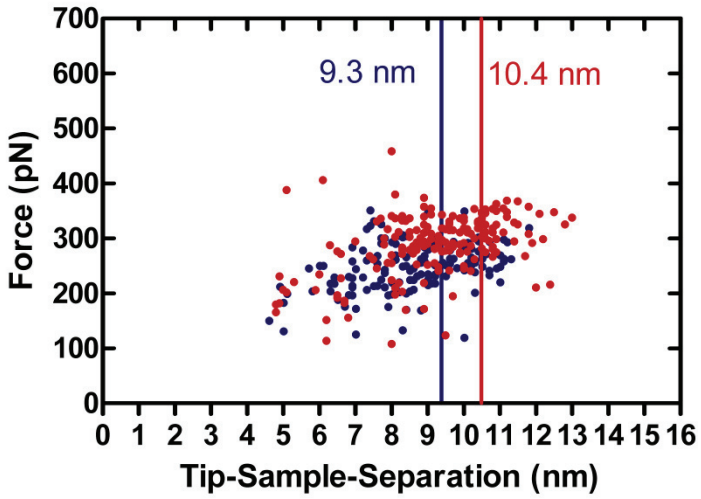

Figure 4-4. Dot plot of tip-sample-separation in context of measured desorption forces. Values of peptide WWCNDGR are depicted in red, GCRL is shown as blue dots. The nominal length of WWCNDGR is 10.4 nm (peptide+linker = 2.6+7.8) and for GCRL 9.3 nm (peptide+linker=1.5+7.8). Only slight differences in tip-sample-separations and forces can be observed, respectively.

To check the influence of the chemical linker several blank curves without biomolecules were tested on the same surface. The results show that attractive forces between linker and surface are much higher and can be clearly separated and therefore do not influence the peptide measurements. Additionally, it can be found that WWCNDGR (309 pN) reveals slightly higher average desorption forces than GCRL (249 pN) peptide. In addition two more peptides that were identified by Oren et al. in 2007 as strong (Strong binding Peptide, SBP) and weak (weak binding peptide, WBP) quartz binding peptide were investigated using SMFS measurements. The results of this analysis are shown in figure 4-6. It can be found that the average desorption forces are 131 and 271 pN, respectively.

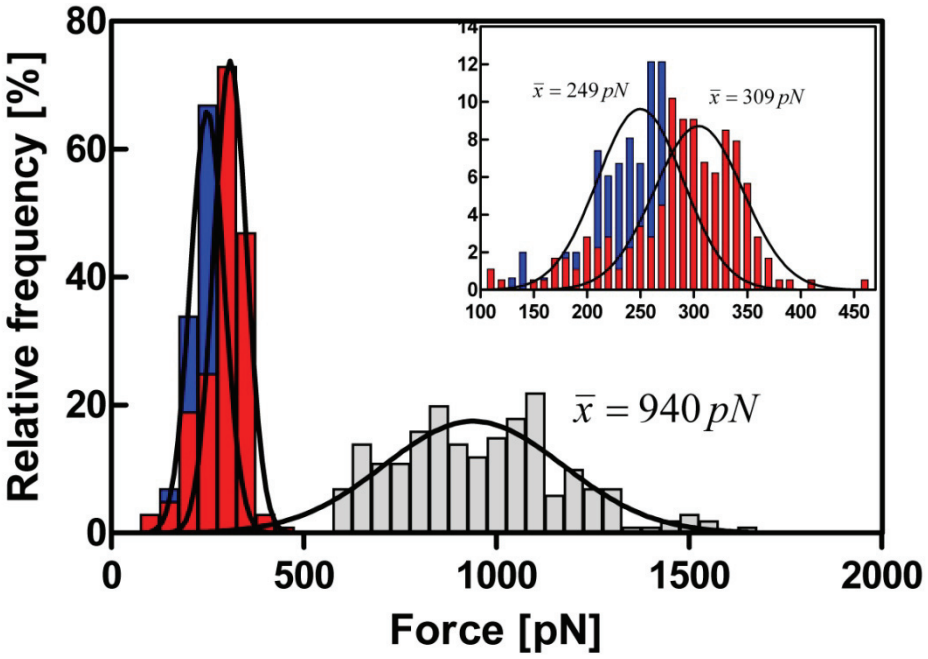

Figure 4-5. Frequency distribution (relative) of desorption forces of peptides WWCNDGR (red) and GCRL (blue). The used linker were APTES and PEG-NHS. Blank AFM measurements (only linker) are depicted in grey. All samples were measured on SiO_2 wafer. Peptide WWCDNGR: Number of samples was n=768 and number of analyzed samples was n=176 (22.9%). Peptide GCRL: Number of samples was n=512 and number of analyzed samples was n=148 (28.9%). Number of samples for blank curves was n=200.

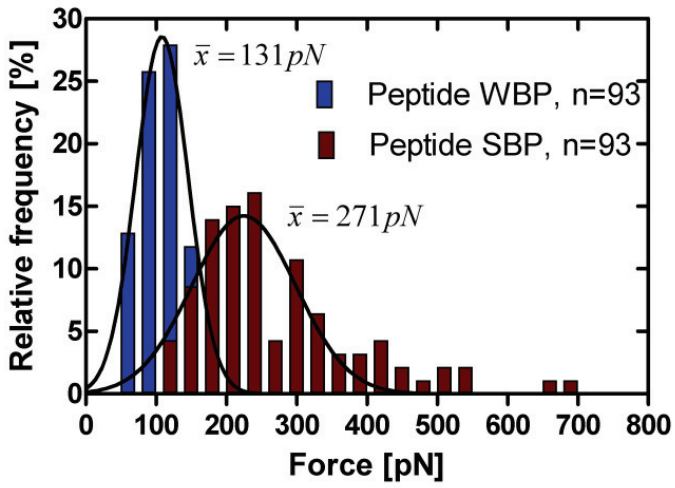

Figure 4-6. Frequency distribution of desorption forces of peptides SBP and WBP (identified by Oren et al. 2007, [32]) from SMFS measurements. Samples were measured on a clean SiO_2 wafer surface. The used linker were APTES and PEG-NHS.

WBP and SBP as previously well defined and analyzed peptides from literature were chosen to verify the measurements of unknown peptides WWCNDGR and GRCL. In particular, it can be concluded that the amino acid composition of WWCNDGR and GCRL can be consulted to explain the higher desorption forces of WWCNDGR. These higher unbinding forces can be predicted due to aromatic and hydrophobic tryptophan (W) residues in WWCNDGR. From computational and experimental view it was found that this amino acid tends to interact with hydrophobic surfaces by removal of water structure on the surface [32]. In this manner, a correlation between model peptides and surfaces with increasing hydrophobicity was measured before by SPR experiments. Here it was obvious that increasing hydrophobicity properties of surface increase the desorption force of peptides [13]. Theoretical studies about the adsorption of model peptides using computer simulation methods revealed also that the arginine (R) residue plays an important role in anchoring the peptide to silica surfaces [33]. In conclusion, the here presented results concerning desorption forces are in agreement with preceding studies (chapter 3) and show the high impact of hydrophobic / hydrophilic properties of single amino acids in the context of adsorption modes.

4.3.2 SMFS of proteins

Two exemplary protein force displacement curves of lysozyme (LSZ) and chymotrypsin (CHT) are shown in figure 4-7. In contrast to single peptide force curves, a complex peak pattern is observable.

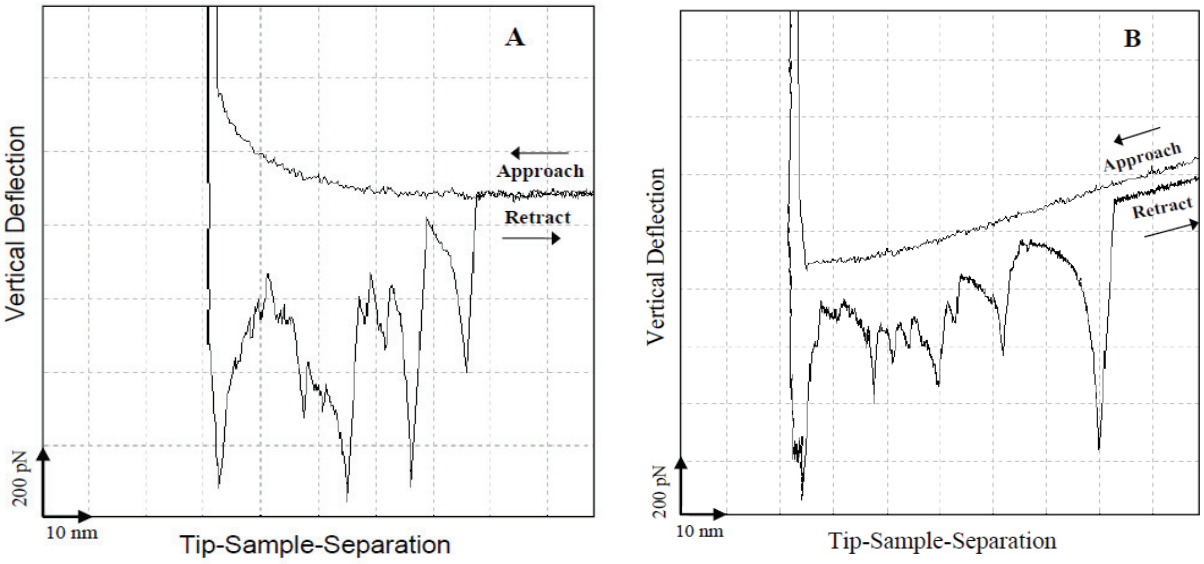

Figure 4-7. Exemplary SMFS curves of LSZ (A) and CHT (B) linked to AFM tips via PEG-NHS and measured on clean SiO_2 wafer.

As a first preliminary analysis, the tip-sample-distance between the last surface contact of the tip and the last desorption force peak from chymotrypsin were measured from several experiments for statistical analysis. This tip-sample distance leads to the maximum stretching of protein before desorption from surface occurs. The result is depicted in figure 4-8 and reveals a distribution of maximum tip-sample-distribution of 20 - 70 nm. As it can be seen in a theoretical map (figure 4-9) chymotrypsin consists of three chains connected via disulfide bonds. The PEG-NHS linker that was used for binding the protein to an AFM tip, binds to NH_2 groups of amino acids and the N-terminus of all three amino acid chains of chymotrypsin. Considering that PEG-NHS binds ideally to only one N-terminus of one chain, a statistical prediction about the maximum stretching length can be made. In this consideration all pathways from each N terminus along the chains were analysed for the number of amino acids. The number of these amino acids was multiplied by 0.36 nm to get a rough estimation of nano

mechanical stretching of chymotrypsin. The average value of all stretching pathways is 35 nm (see figure 4-8), agreeing well with the experimentally measured distribution. This theoretical assumption was done considering the fact that all three N-termini are located on or very close to the chymotrypsin isosurface and are therefore achievable for chemical linkage.

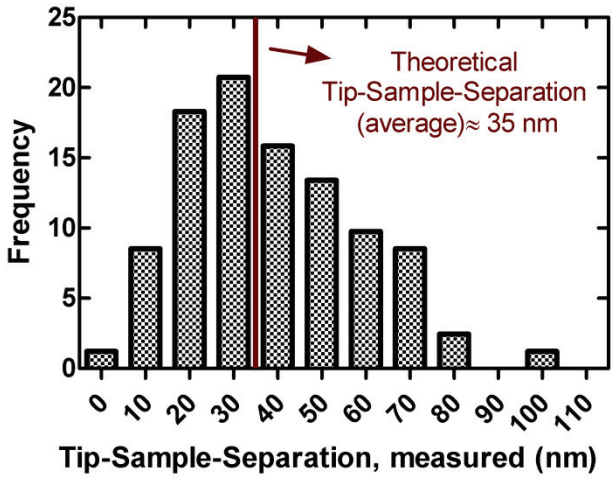

Figure 4-8. Distribution of tip-sample-separation of final force peaks before protein desoprtion. CHT was linked to AFM tips and measured on SiO_2 surface.

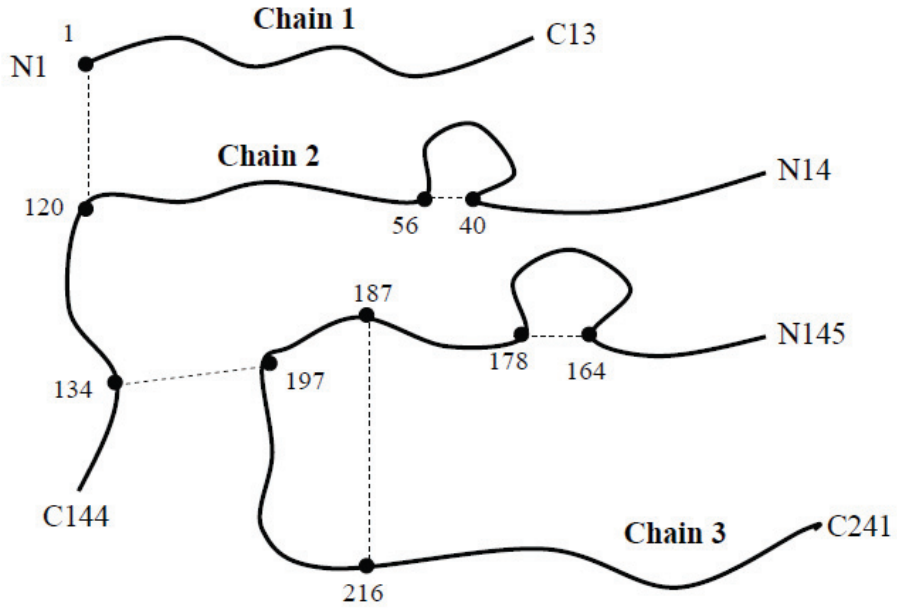

Figure 4-9. Schematic map of CHT built by three peptide chains (chain 1-3) that are connected via two disulfide bonds (dotted lines). This map can be used for analysis of tip-sample-separation distribution plots (see figure 4-8) of SMFS curves. (Adapted from S: Köppen, 2012)

The second protein to be analysed by AFM was lysozyme, consisting of 129 amino acids and four intramolecular disulfide bonds (see figure 4-10).

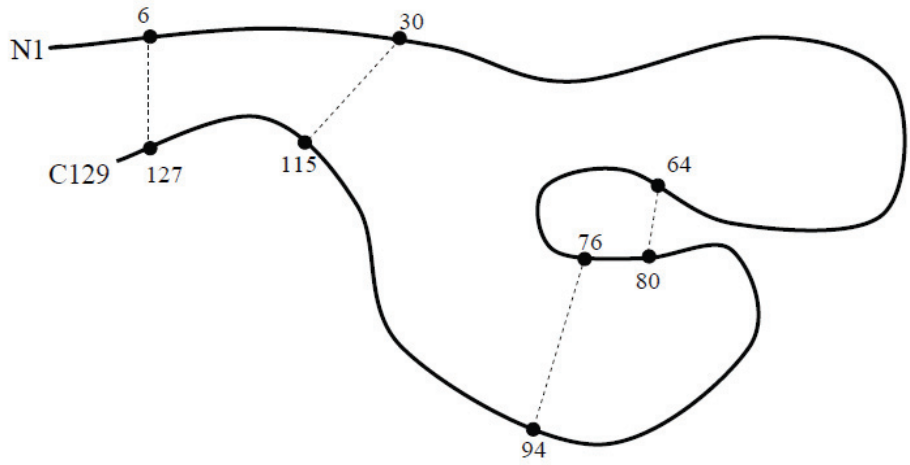

Figure 4-10. Schematic map of LSZ built by one peptide chain exhibiting four intramolecular disulfide bonds. This map can be used for analysis of peak distances in Figure 4-11.

By applying a peak picking algorithm it was possible to identify the distances between peaks within each force distance curve from nanomechanical stretching of lysozyme (figure 4-11 B, red dots). The experimental distribution of peak distances from 40 curves (figure 4-11 A) reveals values mainly distributed around 5 – 40 nm.

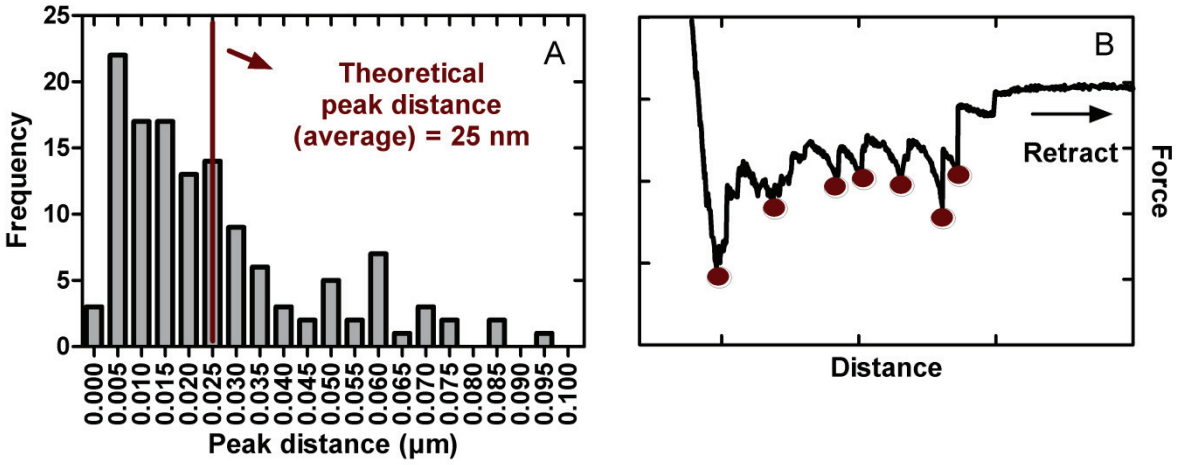

Figure 4-11. Analysis of lysozyme force distance curves with n = 40. Distribution of experimentally determined peak distances is shown in A. The theoretical distance between peaks formed by disulfide bonds is 25 nm as depicted in A. B shows on e exemplary retraction curve from force measurements after applying the peak picking algorithm.

Assuming that each clear detectable peak is induced by breaking a disulfide bond, a statement about the stretching mechanisms of lysozyme can be made. If the PEG-NHS linker binds, as theoretical expected, to the N-terminus and the chain is maximal elongated, a theoretical average peak distance value can be calculated. This value was determined with 25 nm, as it can be seen in figure 4-11 A.

Figure 4-11 A shows also that the experimental peak distance distribution is skewed to smaller values. This could be explained by the fact that mostly disulfide bonds close to the tip and surface contact points are disrupted. An extended elongation of lysozyme including the rupture of disulfide bonds far away from tip and surface contact is less abundant. Hence, the experimental distribution of peak distances and the theoretical average value for breaking all protein disulfide bonds are agreeing well. It should be noticed that this result is strongly influenced by the chosen “delta-value” parameter used for peak detection within the force curves. If the parameter is too strictly selected, the number of putative peaks is high and peak distances will decrease. On the other hand a slack parameterization will end in few detected peaks and increase the peak distances extraordinary. However, it should be noted that, beside the rupture of disulfide bonds, other artefacts could explain the abundance of peaks within force-distant curves. Multiple protein-binding to one tip would also lead to force peaks by detaching these proteins from the surface. Beside this, uncertainties about free linkers and their surface interactions or impurities on the surface must be taken into account. Therefore these results are preliminary and have to be investigated in more detail.

4.4 References

[1] A. Janshoff, M. Neitzert, Y. Oberdörfer, H. Fuchs. Kraftspektroskopie an molekularen Systemen - Einzelmolekülspektroskopie an Polymeren und Biomolekülen. Angew. Chem., 112: 3346-3374, 2000

[2] A. R. Bizzarri, S. Cannistraro. Atomic Force Spectroscopy in Biological Complex Formation: Strategies and Perspectives. J. Phys. Chem. B, 113(52): 16449-16464, 2009

[3] R. Barattin, N. Voyer. Chemical modifications of AFM tips for the study of molecular recognition events. Chem. Comm., 1513-1532, 2008

[4] D. T. Kim, H. W. Blanch, C. J. Radke. Direct Imaging of Lysozyme Adsorption onto Mica by Atomic Force Microscopy. Langmuir 18: 5841-5850, 2002

[5] H. X. You, C. R. Lowe. AFM Studies of Protein Adsorption. 2. Characterization of Immunoglobulin G Adsorption by Detergent Washing. J. Colloid Interface Sci. 182: 586-601, 1996

[6] C. A. Johnson, Y. Yuan, A. M. Lenhoff. Adsorbed Layers of Ferritin at Solid and Fluid Interfaces Studied by Atomic Force Specrtoscopy. J. Colloid Interface Sci. 223: 261-272, 2000

[7] A. P. Serro, K. Degiampietro, R. Colaco, B. Saramago. Adsorption of albumin and sodium hyaluronate on UHMWPE: A QCM-D and AFM study. Colloids Surfaces B: Bionterfaces, 78: 1-7, 2010

[8] M. Jastrzebska, I. Mroz, B. Barwinski, R. Wrzalik, S. Boryczka. AFM investigations of self-assembled DOPA-melanin nano-aggregates. J. Mater. Sci., 45(19): 5302-5308, 2010

[9] D. Pastre, L. Hamon, I. Sorel, E. Le Cam, P. A. Curmi, O. Pietrement. Specific DNA-Protein Interactions on Mica Investigated by Atomic Force Microscopy. Langmuir, 26(4): 2618-2623, 2010

[10] K. Voitchovsky, J. J. Kuna, S. A. Contera, E. Tosatti, F. Stellacci. Direct mapping of the solid-liquid adhesion energy with subnanometre resolution. Nat. Nanotechnol., 5: 1-5, 2010

[11] J. Landoulsi, V. Dupres. Probing Peptide-Inorganic Surface Interaction at the Single Molecule Level Using Force Spectroscopy. ChemPhysChem., 12:1310-1316, 2011

[12] M. Rief, H. Clausen-Schaumann, H. E. Gaub. Sequence-dependent mechanics of single DNA molecules. Nat. Struct. Biol., 6(4): 346-349, 1999

[13] Y. Wei, R. A. Latour. Correlation between Desorption Force Measured by Atomic Force Microscopy and Adsorption Free Energy Measured by Surface Plasmon Resonance Spectroscopy for Peptide-Surface Interactions, Langmuir 26(24): 18852-18861, 2010

[14] S. Manohar, A. R. Mantz, K. E. Bancroft, C.-Y. Hui, A. Jagota, D. V. Vezenov. Peeling Single-Stranded DANN from Graphite Surface to determine Oligonucleotide Binding Energy by Force Spectroscopy. Nano Lett.8(12): 4365-4372, 2008

[15] M. Geisler, T. Pirzer, C. Ackerschott, S. Lud, J. Garrido, T. Scheibel, T. Hugel. Hydrophobic and Hofmeister effects on the Adhesion of Spider Silk Proteins onto Solid Substrates: An AFM-Based Single-Molecule Study. Langmuir, 24: 1350-1355, 2008

[16] M. Geisler, D. Horinek, T. Hugel. Single Molecule Adhesion Mechanics on Rough Surfaces. Macromolecules. 42: 9338-9343, 2009

[17] F. Sbrana, M. Lorusso, C. Canale, B. Bochicchio, M. Vassalli. Effect of chemical cross-linking on the mechanical properties of elastomeric peptides studied by single molecule force spectroscopy. J. Biomech., 44:2118-2122, 2011

[18] P. Hinterdorfer, Y. F. Dufrene. Detection and localization of single molecular recognition events using atomic force microscopy. Nat. Methods., 3(5): 347-355, 2006

[19] C. Friedsam, H. E. Gaub, R. R. Netz, Probing surfaces with single-polymer atomic force microscope experiments. Biointerphases, 1(1): 1-21, 2006

[20] A. Serr, R. R. Netz, Pulling adsorbed polymers from surfaces with the AFM: stick vs. slip, peeling vs. gliding, Europhys. Lett., 73(2): 292-298, 2006

[21] K. E. Bremmell, P. Kingshott, Z. Ademovic, B. Winther-Jensen, H. J. Griesser. Colloid Probe AFM Investigation of Interactions between Fibrinogen and PEG-Like Plasma Polymer Surfaces, Langmuir, 22: 313-318, 2006

[22] Q. Peng, H. Li, Atomic force microscopy reveals parallel mechanical unfolding pathways of T4 lysozyme: Evidence for a kinetic partitioning mechanism. PNAS, 105(6): 1885-1890, 2008

[23] H. J. Kreuzer, S. H. Payne, Stretching a macromolecule in an atomic force microscope: Statistical mechanical analysis. Phys. Rev. E, 63: 021906-1-021906-4, 2001

[24] A. Marsico, D. Labudde, T. Sapra, D. J. Muller, M. Schroeder. A novel pattern recognition algorithm to classifiy membrane protein unfolding pathways with high-throughput single-molecule force spectroscopy. Bioinformatics, 23: 231-236, 2006

[25] A. Yersin, H. Hirling, P. Steiner, S. Magnin, R. Regazzi, B. Hüni, P. Huguenot, P. de los Rios, G. Dietler, S. Catsicas, S. Kasas. Interactions between synaptic vesicle fusion proteins explored by atomic force microscopy. PNAS, 100(15): 8736-8741, 2003

[26] M. E. Drew, A. Chworos, E. Oroudjev, H. Hansma, Y. Yamakoshi. A Tripod Tip for Single Molecule Ligand-Receptor Force Spectroscopy by AFM, Langmuir, 26(10): 7117-7125, 2010

[27] C. Verbelen, J. Antikainen, T. K. korhonen, Y. F. Dufrene. Exploring the molecular forces within and between CbsA S-layer proteins using single molecule force spectroscopy, Ultramicoscopy, 107: 1004-1011, 2007

[28] B.-H. Kim, N. Y. Palermo, S. Lovas, T. zaikova, J. F. W. Keana, Y. L. Lyubchenko, Single-Molecule Atomic Force Microscopy Force Spectroscopy Study of Aβ-40 Interactions, Biochemistry, 50:5154-5162, 2011

[29] T. Okada, M. Sano, Y. Yamamoto, H. Muramatsu, Evaluation of Interaction Forces between Profilin and designed Peptide Probes by Atomic Force Microscopy, Langmuir, 24: 4050-4055, 2008

[30] C. Verbelen, . J. Gruber, Y. F. Dufrene. The NTA-His_6 bond is strong enough for AFM single-molecule recognition studies. J. Mol. Recognit., 20:490-494, 2007

[31] F. Kühner, L. T. Costa, P. M. Bisch, S. Thalhammer, W. M. Heckl, H. E. Gaub. LexA-DNA Bond Strength by Single Molecule Force Spectroscopy, Biophys. J., 87(4): 2683-2690, 2004

[32] E. E. Oren, C. Tamerler, D. Sahin, M. Hnilova, U. O. S. Seker, M. Sarikaya, R. Samudrala. A novel knowleedge-based approach to design inorganic-binding peptides. Bioinformatics, 23(21): 2816-2822, 2007

[33] J. Schneider, L. C. Ciacchi. Specific Material Recognition by Small Peptides Mediated by the Interfacial Solvent Sructure. J. Am. Chem. Soc. 134: 2407-2413, 2012

5 Immobilization of proteins onto surfaces

The experiments and results within this chapter were obtained in cooperation with Bioceramics Group, University of Bremen. The immobilization of chymotrypsin onto colloidal particle samples was done by Ludmilla Derr. The experimental results regarding MALDI ToF-MS measurements including the data analysis were done by Sascha Steckbeck.

5.1 Introduction

Due to their catalysing properties and high selectivity, enzymes have been used since many years in numerous biotechnological applications and for a variety of chemical reactions e.g. requiring mild processing conditions [1-4]. As the employment of free enzymes is often hampered by several factors e.g. difficult recovery, lack of long-term stability and cyclic re-usability, enzyme immobilisation onto solid supports is considered a promising strategy to overcome these main drawbacks. Immobilisation of the enzyme onto inorganic supports, e.g. polymers, magnetic nanoparticles or metal oxides [5] enables a more convenient handling of the enzyme, facile product separation, prevention from autolysis or auto-digestion and may be beneficial to maintain or increase enzyme stability under both operation and storage conditions [6]. All these aspects have made enzyme immobilisation particularly attractive for e.g. down streaming processes or for proteolysis in proteomic analysis [7-8]. Several studies on enzyme immobilisation have been carried out and three main factors influencing the performance of immobilised enzyme have been identified: 1) the properties of the enzyme, 2) immobilisation method employed and 3) properties of the support material.

For example, phosphorylated pepsin immobilised on alumina nanoparticles showed higher thermal stability and retained much higher enzymatic activity due to the lack of diffusion limitations of the substrate. Diffusional limitations were observed for pepsin immobilised inside the pores of microsized porous alumina, causing decreased accessibility for the substrate hemoglobin [9]. In addition, multipoint covalent attachment of chymotrypsin (CT) by linking its amino groups to agarose-aldehyde gels caused a 60,000-fold increase in enzyme availability, associated with a loss in enzymatic activity of only 35% [10]. Moreover, a strong reduction of the autolytic

cleavage of CT has been recently observed when the enzyme was immobilised onto magnetic bead cellulose [11].

Despite the significant attention paid to the development of enzyme immobilisation strategies on various supports, a still major challenge in this field is the scarce availability of reliable methods enabling a direct characterisation of enzyme activity and overall enzymatic performance at different operation and storage conditions [12-14].

In this study we investigated at a semi-quantitative level the enzymatic catalytic activity of CT covalently immobilised on alumina and silica colloidal particles. Apart from being affordable and highly available, they feature high chemical, thermal stability and are of particular relevance for many medical and biotechnological [15], alumina and silica colloidal particles were used as model substrate materials. CT was covalently immobilised using by amine coupling via reactive esters. This technique is relative straightforward and suitable for covalently linking biomolecules to a hydrophilic solid surfaces [15]. The immobilisation efficiency, the enzymatic activity and stability and the potential re-usability of immobilised CT were investigated was assessed at different operation and storage conditions by matrix-assisted laser desorption/ionisation time-of-flight mass spectrometry (MALDI-ToF MS) after lysozyme digestion. Our approach presents an analytical strategy that simultaneously enables the assessment of the enzyme immobilisation efficiency, the enzymatic activity, the stability and the potential re-usability and is a feasible tool for proteomic studies and diverse biotechnological applications.

5.2 Experimental

Materials. α-alumina colloidal particles (Al_2O_3-CP; >99.99 % wt, Taimei, TM-DAR, Lot. No. 8086) were purchased from Krahn Chemie GmbH (Germany). Silica colloidal particles (SiO_2-CP; > 99.9 % wt, Lot. No. 100618-02) were obtained from Fibre Optic Center (USA). Lyophilized α-CT type II from bovine pancreas (94.1 % wt, 65.622 units/mg protein, lyophilised, Lot. No. 60M7007V), lysozyme (LSZ; > 90 % wt, > 40000 units/mg protein, lyophilised, Lot. No. SLBG8654V, CAS 12650-88-3), (3-aminopropyl)triethoxysilane (APTES; ≥98 %, Lot. No. BCBH2173V, CAS 919-30-2), N-hydroxysuccinimide (NHS; ≥97 %, Lot. No. BCBB3130, CAS 6066-82-6) and □-Cyano-4-hydroxycinnamic acid (CHCA; ≥98 %, Lot. No. 81K3720, CAS 28166-41-8) were obtained from Sigma-Aldrich (Germany). 1-Ethyl-3-(3-

dimetylaminopropyl)carbodiimide (EDC; Lot. No. ML164683, CAS 25952-53-8) was purchased from Thermo Fisher Scientific Inc. (Germany).

Ammonium bicarbonate buffer (NH_4HCO_3; Lot. No. 171166396) was obtained from Carl Roth (Germany). Dithiotreitol (DTT; Lot. No. L1610611) and iodoacetamide (IAA; Lot. No. 398265A) were purchased from BioRad (Germany) and GE Healthcare (Germany), respectively. All other chemicals were obtained from Fluka (Switzerland) or Merck (Germany) at analytical grade. For all solutions double deionised water (ddH_2O) with a conductivity of 0.04 µS cm^{-1} produced by Synergy system (Synergy®, Millipore GmbH, Germany) was used.

Characterisation of Al_2O_3- and SiO_2- CP. In order to remove any organic residues, the Al_2O_3-and SiO_2-CPs were calcinated at 400°C for 4 h with a heating and cooling rate of 3°C/min (oven L3/11/S27, Nabertherm GmbH, Germany). The particle size was determined by dynamic light scattering (DLS, Microtrac UPA150, Grimm Labortechnik, Germany) and the specific surface area (BET) was measured by N_2 volumetric adsorption using a BELsorp-mini II device (BEL Japan, Japan). The ζ-potential measurements were performed in 1 vol % aqueous suspensions of Al_2O_3- or SiO_2-CP using the electroacoustic colloidal vibration current technique (Acoustic & Electroacoustic Spectrometer DT-1200, Dispersion Technology, USA) as described previously [16]. Al_2O_3- or SiO_2-CP suspensions were titrated using 1 M KOH or 1 M HCl to measure the ζ-potential as a function of pH and to determine the isoelectric point (IEP). The quantity of hydroxyl groups present on the surface of the CPs was determined by titrations according to Hidber using a titrator (TIM840, HACH LANGE GmbH, Germany) [17-18].

CT immobilisation onto Al_2O_3- and SiO_2-CP. Aqueous suspensions of Al_2O_3- and SiO_2-CPs were prepared by mixing 15 g of particles with 50 ml of ddH_2O, sterilised by autoclaving for 15 min at 121 °C and 2.05 bar (Systec 2540ELV, Systec, Germany) and afterwards ultrasonicated for 10 min using an ultrasound sonotrode Sonifier® 450 (output 150 W, pulse rate 0.5 s, Branson, USA) to break down particle agglomerates prior to precursor addition. Precursor solutions were prepared by mixing APTES with 50 ml of ddH_2O to a final concentration of 0.1 M (corresponding to a surface coverage of 26 µmol m^{-2} silane molecules normalized to the specific surface area of the unmodified Al_2O_3-CPs which is 12.8 m^2 g^{-1} from our measurements. At this precursor concentration, a maximal shift of the particle IEP and formation of 3.4 amino groups per nm² for Al_2O_3-CPs was found as shown in an own previous study [17]. Taking into account the BET specific surface area of SiO_2-CP (Table 5-1), APTES was added to a final amount of 0.3 M to generate an equal amount of amino groups on the SiO_2 surface. The precursor solutions were then added to the particle suspensions and stirred for 2 h at room temperature. Afterwards, the particles were centrifuged for 30 min at 1500g (Heraeus Megafuge 16, Fisher Scientific, Germany). The supernatant was discarded and the particles resuspended in 100 ml of ddH_2O. This washing procedure was repeated three times to remove any excess of precursors. The particles were subsequently dried at 70°C for 24 h by using a compartment dryer (UT6120, Heraeus Instruments, Germany).

For CT immobilisation, suspensions of functionalized α-alumina and silica CP were prepared at the concentrations of 80.40 mg ml^{-1} for alumina and 30.27 mg ml^{-1} for silica, which correspond to 2 vol% and 1.2 vol%, respectively and sonicated prior to CT addition. 310 µl CT solution (2.68 mg ml^{-1}) were mixed with 200 µl freshly prepared EDC solution using ddH_2O (10 mg ml^{-1}). 500 µl of α-alumina or silica suspension were added to this mixture and mixed. Afterwards, 100 µl NHS solution in ddH_2O (3 mg ml^{-1}) were added to the CP suspensions, stirred for 2 h at room temperature. CP with immobilised CT (CP-NH_2-CT) were centrifuged for 20 min at 21100g (Heraeus Fresco 21 centrifuge, Fisher Scientific, Germany). The supernatant was discarded and the particles were resuspended in 1 ml of ddH_2O. This washing procedure was repeated three times to remove any possible by-products. An overview of the preparation procedure is shown in figure 5-1.

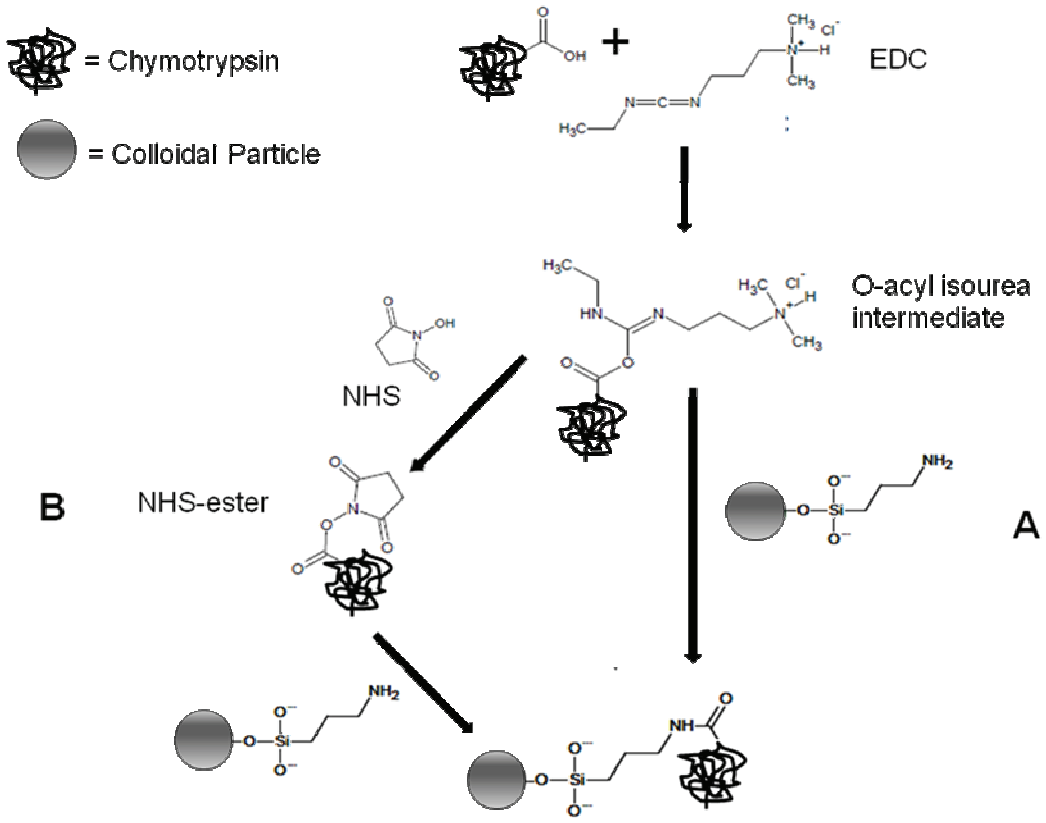

Figure 5-1: Detailed mechanism of CT activation with EDC and NHS. After EDC activation O-acyl-isourea is formed which is labile regarding hydrolysis by water. Due to this fact synthesis route B is unlikely because of regeneration of educts. Addition of NHS leads to the fast formation of NHS-ester and furthermore the reaction with amino-functionalized CP that makes synthesis route A more favoured.

.

Proteolysis test by MALDI ToF-MS measurements. LSZ was used as a substrate and digested by immobilised CT over night at 37°C in 400 mM NH_4HCO_3 buffer (pH 8), at a theoretical CT/LSZ (wt/wt) ratio of 1/13 using 10 µl of CP-NH_2-CT-suspensions assuming that 100% of used CT were immobilised. During incubation, all samples were shaken at 1400 RPM to avoid sedimentation of the CP and to assure an adequate mixing of substrate and enzyme. Before digestion, LSZ was reduced with 45 mM DTT at 50°C for 15 min and then alkylated with 100 mM iodoacetamide at room temperature for 15 min to improve accessibility of the LSZ cleavage sites [19]. The digestion was stopped by freezing the solution with liquid N_2. As positive controls for CP-NH_2-CT,

in-solution-digests of LSZ with CT were performed, while unmodified CP and LSZ were used as negative controls.

Samples from the digestion were taken at different times (5 minutes, 1 h, 2 h, 3.5 h, 5 h, 22 h, 23 h, 24 h, 25.5 h and 27 h) to probe the time dependency of the proteolysis. To test the re-usability of CP-NH_2-CT, samples for MALDI analysis were taken after 24 h, 48 h and 72 h. After each 24 h time interval, the digests were centrifuged for 5 min at 21,000g, the supernatant was removed, and the pellets were washed three times with NH_4HCO_3 buffer to extract weakly bound peptides. The pellets were finally dispersed in a freshly prepared LSZ solution for the next digestion period of 24 h. As a control, fresh CP-NH_2-CT samples were stored at room temperature (RT) for 24 h, 48 h and 72 h before starting the digestion assay. For long-term stability experiments, CP-NH_2-CT samples were stored for 7 weeks at RT and subsequently used for digestion as described above.

In order to obtain the activity equivalence of CP-NH_2-CT, a 0.75 mg ml^{-1} CT stock solution was prepared and diluted to be used in concentrations of 100%, 10%, 1%, 0.8%, 0.4% 0.2%, 0.1%, 0.01%, 0.001% and 0.0001%.

The MALDI ToF-MS analysis of peptides derived from proteolytic cleavage by CT was performed on a Voyager-DETM PRO Biospectrometry Workstation from Applied Biosciences controlled by the Voyager Control Panel Software (USA). All measurements were carried out on polished steel targets coated with a CHCA thin-film matrix. The latter was freshly prepared with a saturated CHCA solution in 100 % acetone, which was allowed to dry before starting the MALDI experiments.

Data analysis. The MALDI spectra were analysed concerning the peak positions (m/z values) and the peak areas of individual peptides after the digestion of LSZ. Measurements were repeated five times to achieve statistically relevant results. The standard deviations are reported as error bars in the figures. The peptides were identified by comparing the experimental peak data with in-silico-digests data using the FindPept tool from ExPASy Bioinformatics Resource Portal (Swiss Institute of Bioinformatics) with a tolerance of 0.8 Da. The LSZ sequence from *Gallus gallus* was used as the input for the in-silico-digest analysis (Accession code AAA48943, NCBI, 147 amino acids).

The experimental peak areas were analysed with the Data Explorer 4.0 software (Applied Biosystems) after performing an automated baseline correction of the spectra.

The kinetic data were fitted using the PRISM software (v. 5.01, GraphPad Software Inc., USA) with the equation

$$Y = Y_0 + (Y_{max} - Y_0) * (1 - e^{K*t}) , \qquad (5\text{-}1)$$

where Y is the MALDI peak area of a selected peptide, t is the time, Y_0 and Y_{max} are the fitted values of peak areas at t = 0 and t = ∞, and K is a characteristic rate constant.

5.3 Results and Discussion

Results. Due to their use in many biotechnological applications, alumina and silica CP with a comparable size were selected as material support for CT immobilisation. Since alumina and silica CPs have a comparable particle size but different exchange capacities and specific surface areas (Table 5-1), different precursor concentrations were used in order to create the same NH_2-density on both materials. The amount of APTES was calculated by taking into account the different BET as reported [17].

The immobilisation of CT on the CP was achieved by amine coupling via reactive esters using the EDC/NHS method [20], as EDC is water-soluble and it can be directly added to CT-solutions and CP aqueous suspensions without using organic solvents. To directly compare the immobilisation efficiency for both materials, an identical concentration of CT was used for the immobilisation to alumina and silica. Nevertheless, it was not possible to determine the amount of the immobilized protein. Due to the presence of EDC, NHS and their by-products, conventional protein quantification [21-24] and enzymatic activity assays [25-26] could not be employed to quantify the CT remaining in solution after the immobilisation step, as these assays were strongly disturbed by the presence of the reactants (data not shown). Therefore, CT activity was directly analysed by MALDI ToF-MS by monitoring the generation of proteolytic peptides formed by the digestion of LSZ by immobilised CT.

Proteolytic digests were performed by incubation of CP-NH_2-CT with LSZ and subsequently the supernatant of the solution was investigated for LSZ-derived peptides with MALDI ToF-MS (Fig. 5-2).

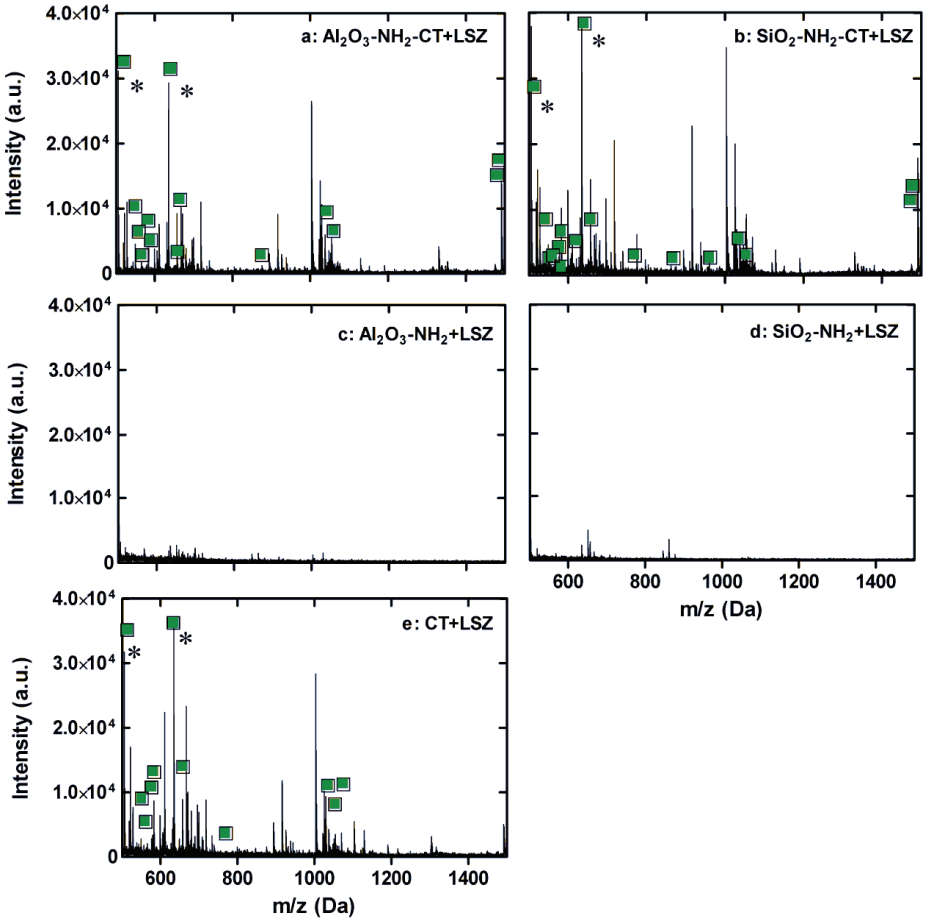

Figure 5-2. a, b: Mass spectra of CT immobilized to Al_2O_3-NH_2 and SiO_2-NH_2 measured by MALDI ToF-MS using LSZ as substrate. c, d: Al_2O_3-NH_2 and SiO_2-NH_2 with LSZ as negative controls. e: *In-solution-digest* of LSZ using free CT as positive control. Incubation time was 24 h for all experiments. Green markers indicate peaks which can be identified by data base as LSZ fragments (see tab. 5-2). Asterisks indicate peaks used for further analysis representing peptides MRSL and GRCEL, respectively.

When LSZ was exposed to either SiO_2- or Al_2-O_3-CP-NH_2-CT, distinct peptide pattern were observed in the MALDI spectra (Fig. 5-2a and 5-2b). On the contrary peptide peaks in the same spectral region were not found after incubation of LSZ with non-functionalized CPs (Fig. 5-2c and 5-2d). Peptide sequence analysis with the FindPept tool (in-silico-digest) revealed that the peptides identified covered 44 % of the LSZ

sequence Fig. 5-2a and 5-2b. For comparison, a digest of LSZ with unbound CT was performed. An almost identical peptide pattern with a sequence coverage of 40 % was observed (Fig. 5-2e) as for LSZ digestion with CP-bound CT (Fig. 5-2a and b). A similar protein sequence coverage were recently reported by Xiao *et al* [27]. Furthermore Xu *et al.* and Lin et al. reported coverage values ranging from 40-90 % for the used proteins [12-13]. All identified peptides and their sequence are listed in Table 5-1.

Table 5-1: Peptides identified by *in-silico-digest* of LSZ cleaved by CT using FindPept-tool from EXPASY.org. All peptides can be found in figure 2 indicated by green markers. Only peptides with less than 2 missed cleavage sites were considered.

Measured Mass (Da)	Sequence	Position	Missed Cleavages
505.925	MRSL	1-4	1
537.895	VLCF	8-11	1
570.876	LILVL	5-9	2
576.021	SLGNW	42-46	1
595.150	RGYSL	39-43	1
596.998	LPLAAL	12-17	1
610.211	KRHGL	31-35	0
634.151	GRCEL	22-26	0
649.028	CFLPL	10-14	1
787.185	DNYRGY	36-41	1
861.759	VLCFLPL	8-14	2
954.045	AAAMKRHGL	27-35	1
1028.306	LPLAALGKVF	12-21	2
1047.313	CNIPCSALL	94-102	1
1052.262	GNWVCAAKF	44-52	1
1529.586	GNWVCAAKFESNF	44-56	2
1532.610	WCNDGRTPGSRNL	81-93	1

For further digestion studies, the LSZ-derived peptides MRSL (506 Da) and GRCEL (634 Da), marked with asterisks in Fig. 5-2, were selected as these two peptides were present in all obtained spectra and showed consistently high intensities.

In order to compare the enzymatic activity of the immobilised with the activity of the unbound CT, a series of in-solution-digests were performed with constant concentration of LSZ and stepwise decreasing the concentrations of unbound CT (Fig. 5-3).

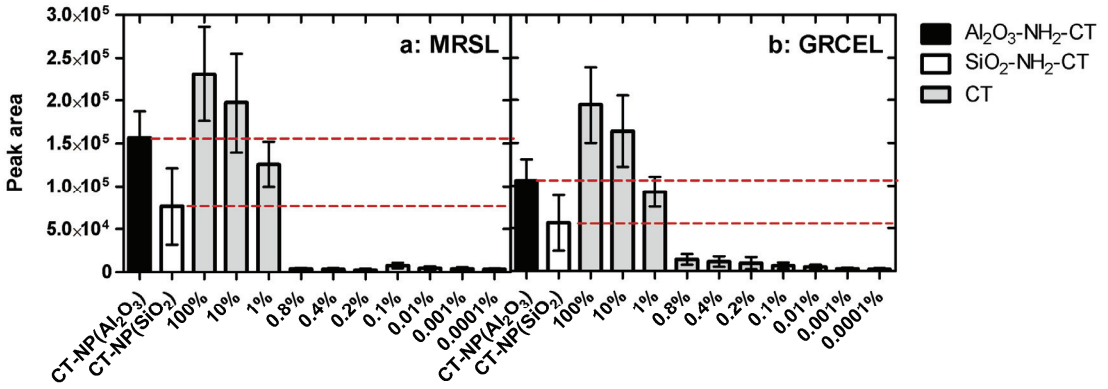

Figure 5-3. Analysis of peak areas as a function of different CT concentration of LSZ peptides MRSL (505.9 Da, a) and GRCEL (634.9 Da, b) after LSZ digestion after 24h digestion by CT immobilized on Al_2O_3-NH_2 or SiO_2-NH_2 compared to *in-solution-digests* with equivalent concentrations of pure CT. 100% corresponds to the initial concentration used for immobilization synthesis.

The 100% value represents the activity determined for the concentration of CT that was initially used for the immobilisation procedure which corresponds to 0.75µg ml^{-1}. Under the assumption that the MALDI peak areas of the LSZ-derived peptides MRSL and GRCEL are proportional to the concentrations of these peptides after digest, we used those as a semi-quantitative estimate of the enzymatic activities of the CT present in the digest. Indeed, both the MRSL (Fig. 5-3a) and GRCEL (Fig. 5-3b) peak areas measured after 24 h in-solution digests were lowered with decreasing concentration of unbound CT. Comparison of the peak areas determined for the CP-NH_2-CT samples (black and white bars for alumina and silica CP, respectively) with those of in-solution-digests containing different concentrations of CT (Fig. 5-3, grey bars) revealed that more active CT (corresponding to between 1% and 10% of the CT applied for the immobilisation process) was present in Al_2O_3-NH_2-CT than in SiO_2-NH_2-CT (less than 1%).

MALDI ToF-MS was used further to compare the time-dependence of the LSZ digestion by unbound and immobilised CT. The average peak areas of the peptides GRCEL and MRSL in the spectra of the digests were determined and plotted as a function of the incubation time (Fig. 5-4).

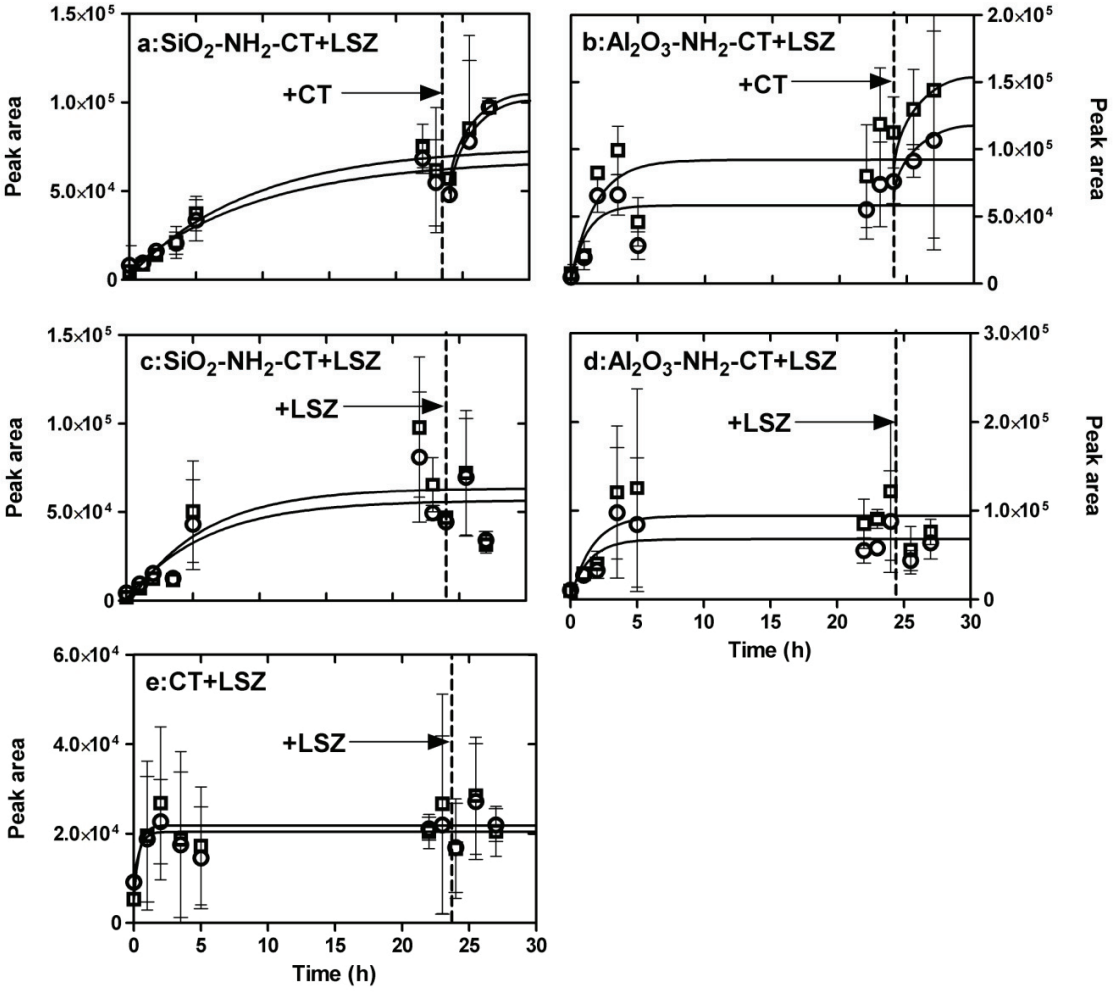

Figure 5-4. Peak detection as a function of digestion time. CT immobilized on Al_2O_3-NH_2 (a) and SiO_2-NH_2 (b) using LSZ as substrate. Two distinguished peaks occurring in all spectra were chosen to assess kinetics referring to the peptides MRSL (505.9 Da, assigned **O**) and GRCEL (634.9 Da, assigned □). Positive controls (c, d) were pure CT and LSZ in solution.

Comparison of the generation of the two peptides in the digests containing SiO_2-NH_2-CT (Fig. 5-4a and c), Al_2O_3-NH_2-CT (Fig. 5-4b and d) or unbound CT (Fig. 5-4e) revealed that the peptides were generated more rapidly in presence of the excess of unbound CT. The fast increase in the peak areas in the digests with unbound CT

reached a plateau within 2.5 h, while the generation of peptides was slower in the digests containing CP-NH_2-CT and maximal peptide levels were observed after more than 5 h (Fig. 5-4a-d). The data were fitted with an exponential function (see Materials and Methods, equation 1) where the peak areas at t = 0 were constraining to 0 (Y_0 value in eq. 1). The fitted values of the maximum peak area Y_{max} and of the characteristic rate constant K are shown in Table 5-2. Interestingly, the maximum peak area of the two peptides generated in digests with unbound CT was remarkably smaller than of that determined for digests containing CP-NH_2-CT (Table 5-2).

Table 5-2: Fitting parameters of peak detection as a function of time (see Fig. 5-4). Y_0 was constrained to zero. Y_{max} and K were automatically calculated by PRISM software.

CP	**SiO_2-NH_2-CT**		**Al_2O_3-NH_2-CT**		**Control 1**		**Control 2**	
Peptide	**GRCEL**	**MRSL**	**GRCEL**	**MRSL**	**GRCEL**	**MRSL**	**GRCEL**	**MRSL**
K	0.2764	0.2438	0.3151	0.3031	1.488	1.154	2.186	2.028
Y_{max}	145826	90385	168659	90218	256080	141508	257261	136268

The addition of extra CT after 23 h caused a further increase of the peak areas for the case of CP-NH_2-CT (Fig. 5-4 a, b) whereas additional LSZ produced no variation (Fig. 5-4 c and d). Notably, the addition of LSZ to unbound CT also revealed no changes in the measured peak areas (Fig. 5-4 e).

To probe the re-usability of the immobilised enzymes we tested the proteolytic activity of the CP-NH_2-CT materials in three consecutive LSZ digestion steps, each lasting 24 h. After each step, the samples were rinsed, MALDI-ToF-MS spectra of the supernatant solutions were collected, and new 24 h digestions were started. The resulting peptide peaks in the MALDI spectra were used to assess the enzymatic activity at a semi-quantitative level, as in the previous experiments (Fig. 5-5).

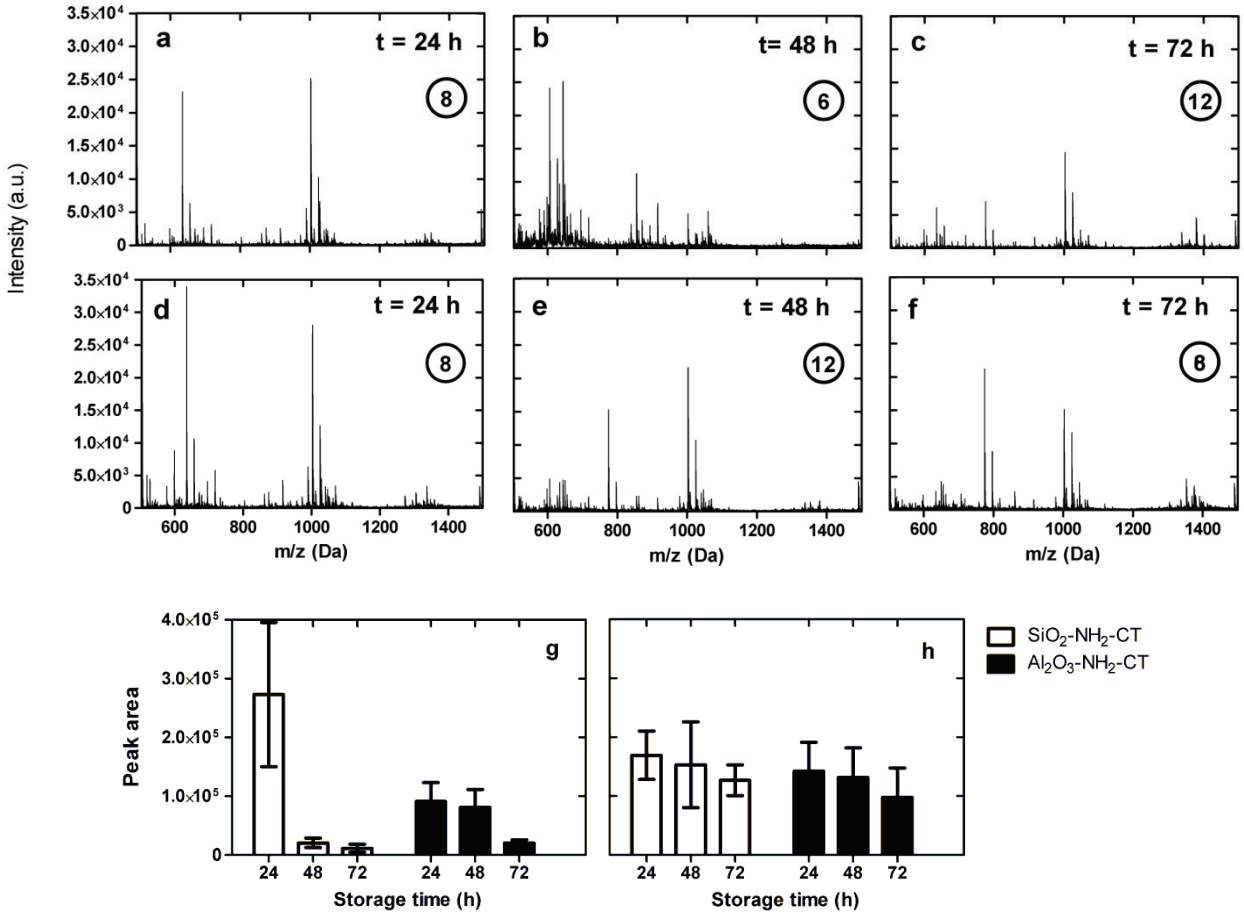

Figure 5-5. Mass spectra of CT immobilized on alumina (a-c) and silica (d-f) using LSZ as substrate performed after 24, 48 and 72 hours using fresh LSZ solution for every time point but the same immobilized CT, respectively. As a marker for digest performance the number of identified peptides is shown in circled values (images a-f). Furthermore average peak areas of exemplary peptides MRSL and GRCEL are shown in figures g & h. Reusability experiments including washing steps are shown in figure g while in figure h the same experiment was performed with unused CP-NH_2-CT which were stored for 24, 48 and 72 hours before digestion, respectively .

Both Al_2O_3-NH_2-CT and SiO_2-NH_2-CT were able to digest LSZ within each of the three consecutive steps as demonstrated by the generation of a high number of peptides clearly identified as part of the LSZ sequence (Fig. 5-5). However, the averaged peak areas of the MRSL and GRCEL peptides strongly decreased after the first 24 h digest period, especially in the case of SiO_2-NH_2-CT, while a less pronounced effect was observed for Al_2O_3-NH_2-CT (Fig. 5-5g).

Storage of Al_2O_3-NH_2-CT and SiO_2-NH_2-CT for 24 h, 48 h and 72 h at RT before incubation with LSZ revealed substantial peptide formation after all storage periods and only a slight decrease of the peak areas for both CP materials (Fig. 5-5h).

In addition, fresh samples of Al_2O_3-NH_2-CT and SiO_2-NH_2-CT that had been stored at RT for 7 weeks generated characteristic LSZ peptide peaks in a 24 h digest although the overall peak intensity was rather low (Fig. 5-6).

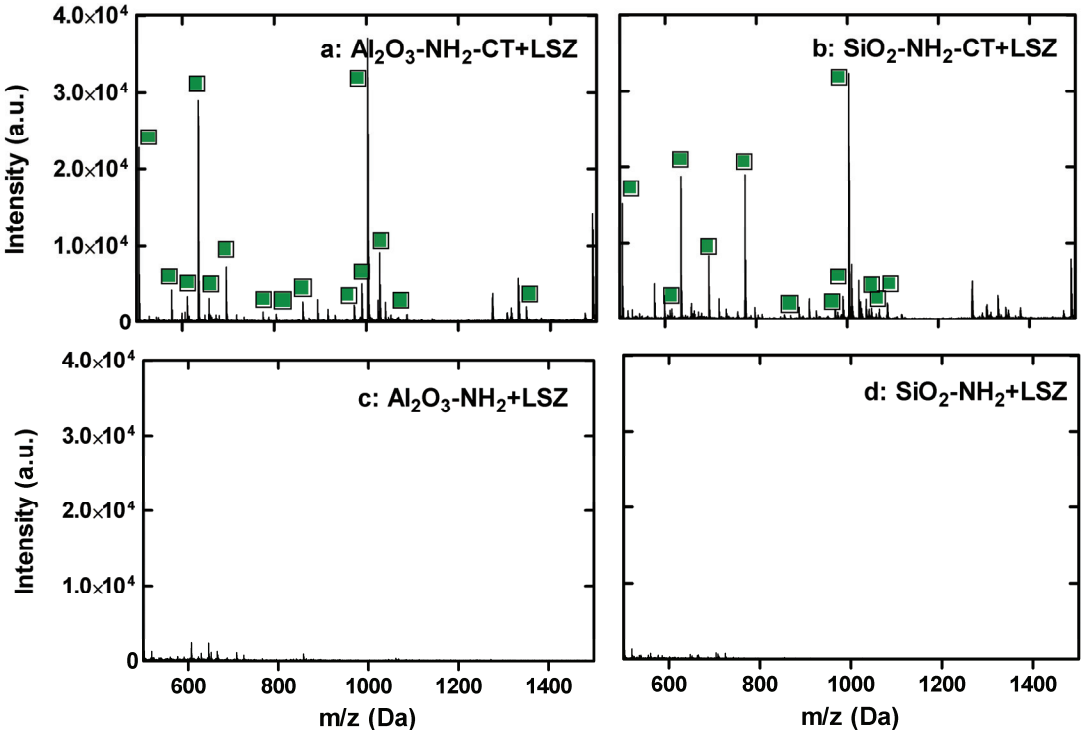

Figure 5-6. a, b: Enzymatic activity of CT immobilized to AL_2O_3-NH_2 and SiO_2-NH_2 measured by MALDI ToF-MS using LSZ as substrate. c ,d: Amino group functionalized Al_2O_3 and SiO_2 with LSZ as negative controls. Green markers indicate peaks that can be identified by data base as corresponding to LSZ. Measurements were performed after 7 weeks of storage at room temperature.

Discussion. In our study the popular and simple immobilisation approach based on amine coupling with EDC and NHS was found to be suitable to covalently bound CT to the amine-functionalized alumina and silica CP and maintain CT activity. This is in agreement with Hong *et al.* [29] which employed a similar approach to covalently immobilise and stabilise CT on the amine-functionalized superparamagnetic nanogels.

Furthermore, this immobilisation approach did not completely suppress CT activity as multiple LSZ-derived peptides formed after proteolytic digestion (Fig. 5-2) similar to the spectra obtained after CT in-solution-digests. LSZ-derived peptides formation is clearly induced by the presence of CT on particle surface as no LSZ digestion peaks were observed by using amino-functionalized CP suspensions and LSZ. Taking into

account the number of identified peptides as an attribute for our digestion experiments, previously studies using trypsin and CT revealed comparable results. Similar to our study, the efficiency of digestion by immobilised enzymes was evaluated by analyzing the sequence coverage. [8-10].

Bound CT maintained its activity as demonstrated by the generation of LSZ-derived peptides. The covalent linking of the enzyme at the particles may have occurred via two parallel pathways that result in the same product (see Fig. 5-1). EDC as a carbodiimide in combination with NHS was chosen for the immobilisation synthesis employed for the efficient conjugation of proteins containing carboxylates to amino-functionalized mineral surfaces [20]. As a disadvantage, the reaction may also involve amino groups of other CT molecules, leading to protein-protein cross-linking and agglomeration. This process cannot be completely prevented, although it can be reduced using a low protein/surface ratio as done in our study. Moreover, the formation of loosely bound protein coronas surrounding the particles as well as non-specific adsorption of proteins can take place [11]. However, only a minor fraction of non-covalently bound proteins is expected to be present after the thorough washing steps which follow covalent binding (see Material and Methods section).

Although, by MALDI-ToF no direct information about the total amount of immobilised CT could be obtained, an analysis of the peak areas of the peptides MRSL and GRCEL, resulting from the digestion of LSZ, allowed at comparison between the enzymatic activities of the immobilised CT with that of the CT applied for the immobilisation. This comparison was done assuming that the amount of non-immobilised CT in solution after several thorough washing steps is insignificant as noted above. Additionally, the amount of CT autolysis peaks is negligible (see Figure 5-7) hence the influence of these factors is marginal.

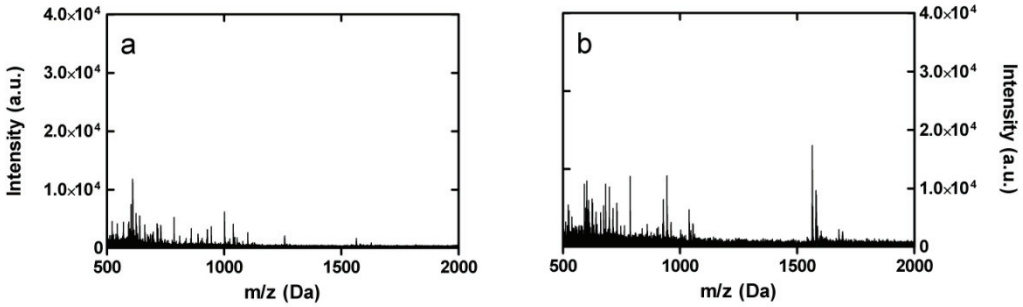

Figure 5-7. Check for autolysis peaks from non-immobilized CT after 24 (A) and 48 (B) hours incubation in 400 mM NH_4HCO_3 buffer.

The results presented in Fig. 5-3 show that, for the peptides MRSL and GRCEL, smaller peak values could be detected from digested LSZ using CT immobilised to SiO_2-CP than to Al_2O_3- CP. This can be possibly related to two different reasons. Either a lower amount of CT was immobilised onto silica than on alumina, or by different linking modes of CT on the different surfaces, leading to different activities. The second reason seems to be more likely due to the fact that we performed the synthesis in the way expecting the same amount of the amino group on the surface of colloidal particles and accordingly the same amount of immobilised CT in the second synthesis step. In general, the lower activity observed for CT immobilised onto CP may results from suboptimal immobilisation and/or from an reduced intrinsic activity of the immobilised CT. Currently we cannot experimentally discriminate between these two options. Possible reasons for a low CT activity despite of a maximal immobilisation of CT to the particles may include: (i) hindered accessibility of the substrate to the active site of CT caused by the tethering of the CT to the CP surface, which addresses all exposed carboxyl groups rather than selected anchoring points far from the active site; (ii) conformational changes of CT in the immobilised state; (iii) CT-CT agglomeration by cross-linking induced by the linking protocol and (iv) an increased (material-dependent) tendency for CT oxidation affecting the enzyme activity as described in earlier studies [30]. These factors are also expected to be responsible for the slower digestion kinetics of immobilised CT with respect to free CT in solution. For a better comparison, kinetic experiments were conducted by adjusting the concentration of unbound CT to 10% (Fig. 5-3). The kinetic analysis over 27 h showed a plateau that was reached within 2.5 h for unbound CT and more than 5 h for CT immobilised onto both materials. This plateau is probably due to an occlusion of the active site by the proteolysis products, since the addition of extra substrate (+LSZ) leads to no obvious changes in the kinetic curves. In contrast, after addition of extra enzymes (+CT) to the reaction, an increase of the reaction products (in this case peptides MRSL and GRCEL) was observed. A reduction of enzymatic activity and slower digestion kinetics after immobilisation to solid supports has been already observed for other enzymes such as glucose oxidase [16] or trypsin [17].

Compared to unbound CT, the initial generation of proteolytic peptides by CP-bound CT was slower, even though the maximal amount of peptide determined after 23 h was twice as much. In addition, both unbound CT as well as CP-bound CT became inactive after 23 h of incubation, as the addition of fresh LSZ did not lead to an additional

increase in the amounts of proteolytic peptides. These findings may suggest that CP-bound CT, remained longer active than unbound CT. Although, an inactivation of the enzyme due to autolysis is quite unlikely, it cannot be excluded for the CP-NH_2-CT materials. In fact, low intensity peaks from autolysed CT were detectable. Furthermore, a pre-incubation of CT (to provoke CT autolysis) followed by LSZ in-solution-digest without CP revealed negligible changes in observed peak pattern compared to digest using fresh CT (see Figure 5-8).

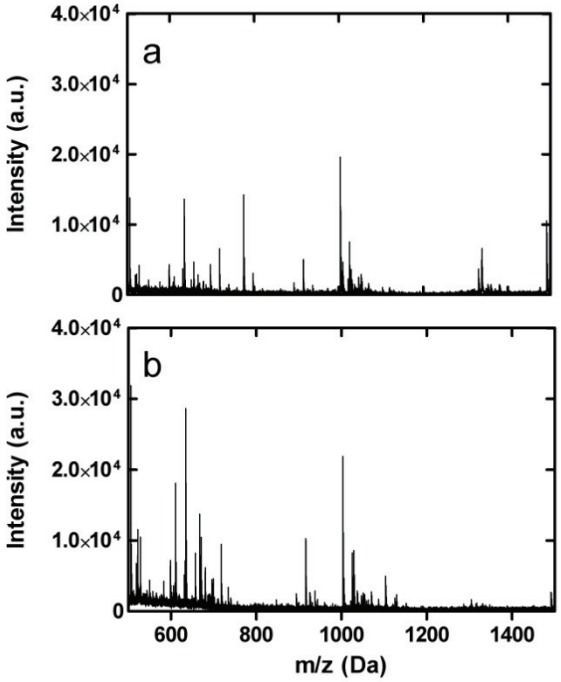

Figure 5-8. Influence of CT autolysis on protease activity. Spectra comparison between LSZ in-solution-digest using (A) CT that was incubated for 24 hours before starting digest (to provoke CT autolysis) and (B) in-solution-digest without pre-incubation of CT.

For technical applications, an important parameter to assess the efficacy of enzyme-functionalised materials is their cyclic re-usability. Our cyclic re-usability experiments (see Fig. 5-5) showed that after each digestion roughly the same number of LSZ peptides could be identified, as consequence of the active LSZ cleavage by CT. These results are in agreement with previous investigations with CT immobilised on epoxy-modified silica monolithic support [8-9]. However, we found that the MALDI peak areas associated to the cleaved peptides MRSL and GRCEL decreased, indicating a loss of enzymatic activity. This loss appears to be more pronounced for silica than for alumina, suggesting that the type of support material has an influence on the re-usability

efficacy. Interestingly, a very limited loss of enzymatic activity was observed when the immobilised enzymes were stored at room temperature and freshly used after 24 h, 48 h and 72 h (Fig. 5-5h). In fact, the materials were found to be active towards LSZ digestion even after 7 weeks of storage at room temperature, comparable to studies with CT immobilised onto chitosan grafted with polymethyl methacrylate [31]. Therefore, the activity loss in the re-usability tests is not expected to originate from slow conformational changes of the enzyme in the immobilised state which would also take place during long-term storage, but connected with the digestion reaction. For instance, occlusion of the active site by reaction intermediates that remain trapped due to steric hindrances caused by the tethering to the ceramic particles, or that remain adsorbed to the particle surfaces, could lead to a progressive "poisoning" of the immobilised enzyme. Future studies shall be devoted to optimizing the immobilisation procedure in order to maximize the efficiency and improve the re-usability of immobilised enzyme on the colloidal ceramic particles.

5.4 Conclusions

This study investigated the coupling efficiency, enzymatic activity and enzyme kinetics of CT immobilised onto SiO_2- and Al_2O_3-NH_2-CP using MALDI-ToF MS. Although this analysis does not allow an exact quantification of the amount immobilized onto CPs it was possible to obtain a semi-quantitative information on the activity of enzymes immobilized to CP by comparison with data from in-solution-digests with different protease concentrations. Investigations of long-time-storages and kinetics helped to understand influences of colloidal particles on digests. The usage of MALDI ToF-MS was successfully applied for the performance of these analyses. By using this method it was possible to measure "real" products of enzymatic activity without any artificial protease substrates or intermediate chemicals that have to be used for other methods [25-26, 32-33]. It was possible to get an easy and fast visual overall-information of the amount of enzymatic products as well as detailed information about many single peptides in *one* experiment. Beside this, the detection limit of MALDI ToF-MS, up to femtomol range [34] is substantially lower than for many other colorimetric or fluorescence used for enzyme activity measurements [35-36]. The results from this study will help to advance the knowledge about immobilisation of proteins to inorganic substrates. In proteomic research, especially in the field of bioengineering (e.g. in batch

processes, bio-reactors etc.) it is of prime importance to control enzymatic processes or, if needed, to isolate enzymes from reactions fast and easy by the usage of CP bound enzymes. In future works, the technique described here could even be used to obtain data about the immobilisation efficiency of several enzymes in parallel without big effort.

5.5 References

[1] Barquero-Quiros M, Dominguez-Renedo O, Alonso-Lomillo MA, Arcos-Martinez MJ. Biosensor for aluminium(III) based on its inhibition of alpha-chymotrypsin immobilized on a screen-printed carbon electrode modified with gold nanoparticles. Microchim Acta 2012;179(1-2):65-70.

[2] Bhat MK. Cellulases and related enzymes in biotechnology. Biotechnol Adv 2000;18(5):355-383.

[3] Meyer AS, Isaksen A. Application of Enzymes as Food Antioxidants. Trends Food Sci Tech 1995;6(9):300-304.

[4] Vellard M. The enzyme as drug: application of enzymes as pharmaceuticals. Curr Opin Biotech 2003;14(4):444-450.

[5] Ansari SA, Husain Q. Potential applications of enzymes immobilized on/in nano materials: A review. Biotechnol Adv 2012;30(3):512-523.

[6] Sheldon RA. Enzyme immobilization: The quest for optimum performance. Adv Synth Catal 2007;349(8-9):1289-1307.

[7] Rivera JG, Messersmith PB. Polydopamine-assisted immobilization of trypsin onto monolithic structures for protein digestion. Journal of Separation Science 2012;35(12):1514-1520.

[8] Yamaguchi H, Miyazaki M, Honda T, Briones-Nagata MP, Arima K, Maeda H. Rapid and efficient proteolysis for proteomic analysis by protease-immobilized microreactor. Electrophoresis 2009;30(18):3257-3264.

[9] Li J, Wang JQ, Gavalas VG, Atwood DA, Bachas LG. Alumina-pepsin hybrid nanoparticles with orientation-specific enzyme coupling. Nano Lett 2003;3(1):55-58.

[10] Guisan JM, Bastida A, Cuesta C, Fernandezlafuente R, Rosell CM. Immobilization Stabilization of Alpha-Chymotrypsin by Covalent Attachment to Aldehyde Agarose Gels. Biotechnol Bioeng 1991;38(10):1144-1152.

[11] Prikryl P, Lenfeld J, Horak D, Ticha M, Kucerova Z. Magnetic Bead Cellulose as a Suitable Support for Immobilization of alpha-Chymotrypsin. Appl Biochem Biotech 2012;168(2):295-305.

[12] Xu XQ, Deng CH, Yang PY, Zhang XM. Immobilization of trypsin on superparamagnetic nanoparticles for rapid and effective proteolysis. J Proteome Res 2007;6(9):3849-3855.

[13] Lin S, Yun DJ, Qi D, Deng C, Li Y, Zhang X. Novel Microwave-Assisted Digestion by Trypsin-Immobilized Magnetic Nanoparticles for Proteome Ananlysis. Journal of Proteome Research 2007;7:1297-1307.

[14] Jeng JY, Lin MF, Cheng FY, Yeh CS, Shiea JT. Using high-concentration trypsin-immobilized magnetic nanoparticles for rapid in situ protein digestion at elevated temperature. Rapid Commun Mass Sp 2007;21(18):3060-3068.

[15] Treccani L, Klein TY, Meder F, Pardun K, Rezwan K. Functionalized ceramics for biomedical, biotechnological and environmental applications. Acta Biomater 2013;9(7):7115-7150.

[16] Dukhin AS, Goetz PJ, editors. Studies in Interface Science. Amsterdam: Elsevier, 2002.

[17] Meder F, Daberkow T, Treccani L, Wilhelm M, Schowalter M, Rosenauer A, et al. Protein adsorption on colloidal alumina particles functionalized with amino, carboxyl, sulfonate and phosphate groups. Acta Biomater 2012;8(3):1221-1229.

[18] Hidber PC. Zusammenhang von Struktur und Wirkung von Carbonsäuren als Verflüssiger für wässrige α-Aluminiumoxidsuspensionen. Zurich: ETH Zurich Switzerland; 1993.

[19] Walker JM. The protein protocols handbook. 2nd ed. Totowa, N.J.: Humana Press, 2002.

[20] Hermanson GT, editor. Bioconjugate Techniques. 2nd edition ed: Elsevier, 2008.

[21] Reisner AH, Nemes P, Bucholtz C. Use of Coomassie Brilliant Blue G250 Perchloric-Acid Solution for Staining in Electrophoresis and Isoelectric Focusing on Polyacrylamide Gels. Anal Biochem 1975;64(2):509-516.

[22] Compton SJ, Jones CG. Mechanism of Dye Response and Interference in the Bradford Protein Assay. Anal Biochem 1985;151(2):369-374.

[23] Smith PK, Krohn RI, Hermanson GT, Mallia AK, Gartner FH, Provenzano MD, et al. Measurement of Protein Using Bicinchoninic Acid. Anal Biochem 1985;150(1):76-85.

[24] Wiechelman KJ, Braun RD, Fitzpatrick JD. Investigation of the Bicinchoninic Acid Protein Assay - Identification of the Groups Responsible for Color Formation. Anal Biochem 1988;175(1):231-237.

[25] Ghosh KK, Verma SK. Kinetics of alpha-chymotrypsin catalyzed hydrolysis of 4-nitrophenyl acetate in ethanolamine surfactants. Indian J Biochem Bio 2008;45(5):350-353.

[26] Mekras CI, George MH, Barrie JA. Immobilization of Alpha-Chymotrypsin on Poly(Urethane-Graft-Acrylic Acid). Int J Biol Macromol 1989;11(2):113-118.

[27] Xiao P, Lv XF, Man Y, Qing H, Li Q, Deng YL. Rapid and Efficient Proteolysis for Protein Analysis by an Aptamer-Based Immobilized Chymotrypsin Microreactor. Anal Lett 2013;46(5):868-878.

[28] Sustrova B, Novotna L, Kucerova Z, Ticha M. Immobilization of alpha-chymotrypsin to magnetic particles and their use for proteolytic cleavage of porcine pepsin A. J Mol Catal B-Enzym 2009;60(1-2):22-28.

[29] Hong J, Gong PJ, Xu DM, Dong L, Yao SD. Stabilization of alpha-chymotrypsin by covalent immobilization on amine-functionalized superparamagnetic nanogel. J Biotechnol 2007;128(3):597-605.

[30] Silva AMN, Marcal SL, Vitorino R, Domingues MRM, Domingues P. Characterization of in vitro protein oxidation using mass spectrometry: A time course study of oxidized alpha-amylase. Archives of Biochemistry and Biophysics 2013;530(1):23-31.

[31] Abd El-Ghaffar MA, Hashem MS. Calcium alginate beads encapsulated PMMA-g-CS nano-particles for alpha-chymotrypsin immobilization. Carbohyd Polym 2013;92(2):2095-2102.

[32] Farmer DA, Hageman JH. Use of N-Benzoyl-L-Tyrosine Thiobenzyl Ester as a Protease Substrate - Hydrolysis by Alpha-Chymotrypsin and Subtilisin Bpn'. J Biol Chem 1975;250(18):7366-7371.

[33] Bizzozero SA, Baumann WK, Dutler H. Kinetic investigation of the alpha-chymotrypsin-catalyzed hydrolysis of peptide-ester substrates. The relationship between the structure of the peptide moiety and reactivity. Eur J Biochem 1975;58(1):167-176.

[34] High Mass Linear Analysis of intact Proteins on the 4800 MALDI ToF/ToFTM Analyzer: Technical Note Applied Biosystems 2005.

[35] Fan HL, Jiang XH, Zhang T, Jin QH. Peptide-induced fluorescence quenching of conjugated polyelectrolyte for label-free, ultrasensitive and selective assay of protease activity. Biosens Bioelectron 2012;34(1):221-226.

[36] Anderson E, Sze KWC, Sathe SK. New Colorimetric Method for the Detection and Quantitation of Proteolytic-Enzyme Activity. J Agr Food Chem 1995;43(6):1530-1534.

6 Influence of surface treatment on protein adsorption

The experiments and results within chapter were generated in collaboration with SCHOTT Company for the European ADGLASS project (*www.adglass.eu*).

6.1 Introduction

Generally spoken, the treatment of surfaces can be performed to either improve or prevent adhesion of molecules. To enhance the surface coverage with molecules like proteins, classically linker chemistry is applied. Peptides or proteins can be coupled to inorganic surfaces by usage of surface silanization followed by chemical attachment of linkers that can bind via reactive groups (see also chapter 5). This procedure was successfully used in several experiments and has therefore become a *standard* technique [1-4]. Furthermore, it was shown that micro- or nano-structuring of surfaces is an appropriate method to improve the adhesion of proteins or cells [5,6].

To control protein adhesion, self-assembled monolayers (SAMs) applied to inorganic surfaces have shown a great application potential [7-11]. As a classical SAM, polyethylene glycol (PEG) has lead to promising results considering adhesion prevention [12] and was therefore used to control adsorption [13,14]. Even the spreading of foreign proteins as a "non-adhesion-coating" was successfully tested [15].

Beside the application of molecules onto surfaces other treatments using chemicals or procedural applications (i.e. plasma treatment) was used to investigate molecular adhesion [16].

The prevention of molecular adhesion has become an extended field of research, not only because of understanding the molecular adhesion mechanisms but also because of economical and medical reasons. It can help to save money and increase medical care. Medical equipment like catheters or pharmaceutical glass vials can be improved considering their adhesion behaviour.

In this chapter the influence of surface treatment using acids, bases and plasma impulse chemical vapor deposition (PICVD [17]) is investigated by BCA assay, FITC fluorescence labelling and MALDI ToF-MS in relation to protein adsorption onto silica surfaces.

6.2 Experimental

BCA-Assays. The used BCA assay was purchased from Pierce. To validate the assay considering the linear context between protein concentration and measured OD, two experiments were performed. First, bovine serum albumin (BSA, purchased from Sigma Aldrich) in differing concentrations was incubated in borosilicate glass bottles from Schott company for 2 h at 37 °C. Samples from supernatant were then tested for their protein content at a wavelength of 560 nm using a fluorescence reader. The serial dilution of this protein solution was performed using concentrations ranging from 0.25 µg/mL to 80 µg/mL. Second, repetition experiments were performed to validate the accuracy of this assay. Separated BCA assays were performed as described above using equal parameters and chemicals. To test the influence of chemical treatment of glass surfaces, PICVD glass bottles purchased from Schott company were incubated with NaOH (40%), HCl (37%) or no chemicals (control surface) for 30 minutes. All surfaces were rinsed thoroughly after incubation with bidest. H_2O and dried in N_2 flow. Afterwards a BSA protein solution with a concentration of 4 µg/mL was added with a subsequent incubation on the surfaces at a temperature of 37 °C. Samples from supernatant were taken immediately after addition of solution (0 minutes) and then in time steps of 10 minutes each. The last sample was taken at t=120 minutes.

MALDI ToF-MS. First, a protein standard curve was measured with MALDI comprising five different concentrations (0.036, 0.36, 3.6, 36, 360 µg/mL). The used protein was lysozyme, purchased from Sigma Aldrich. Lysozyme solutions were prepared in PICVD glass bottles from Schott and directly prepared for measurements on steel targets using a saturated CHCA (Sigma Aldrich) solution in 100% Acetone, which was allowed to dry immediately before starting the MALDI experiments. For statistical reasons 10 spectra were collected for each concentration, comprising 200 laser shot per spectrum.

To identify the influence of surface materials a lyszoyme protein solution (100µg/mL in H_2O) was prepared and immediately transferred to a polypropylene tube, and two different glass bottles from Schott company. One bottle consisted of borosilicate glass, the other was a special plasma treated (PICVD) silica glass bottle to minimize or prevent adhesion, respectively. Sample vessels were then covered with parafilm, incubated at RT and shaken at 100 RPM between sampling. Samples were then taken after 19, 43 and 91 hours and immediately after surface contact (0 hours). Ten sample

spots (á 5 spectra with 200 shots) were prepared for each surface and time step. Samples were transferred onto a freshly prepared CHCA matrix spot (saturated in 100 % Acetone) in measured without delay.

Fluorescence Measurements (FITC). Fluorescein isothiocyanate labeled BSA (FITC-BSA) was purchased from Sigma Aldrich to test the adhesion on borosilicate and plasma treated (PICVD) glass bottles from Schott company. Bottoms of these bottles were cut mechanically, cleaned with isopropanol, rinsed thoroughly with bidest. H_2O and transferred directly to 12-well-plates. A FITC-BSA protein solution with a concentration of 20µg/mL (2mL) was added and surfaces were then incubated at RT on an orbital shaker at 200 RPM. Samples were always covered with aluminium foil to prevent a fading of fluorescence activity. After 24, 48, 120 and 144 hours glass samples were taken out of protein solution, rinsed with H_2O and fluorescence emitting light was measured at a wavelength of 518 nm. As control, one surface was incubated with bidest. H_2O but handled in the same way as all other samples. An overview of the experimental setup prior to the described analyses is shown in figure 6-1.

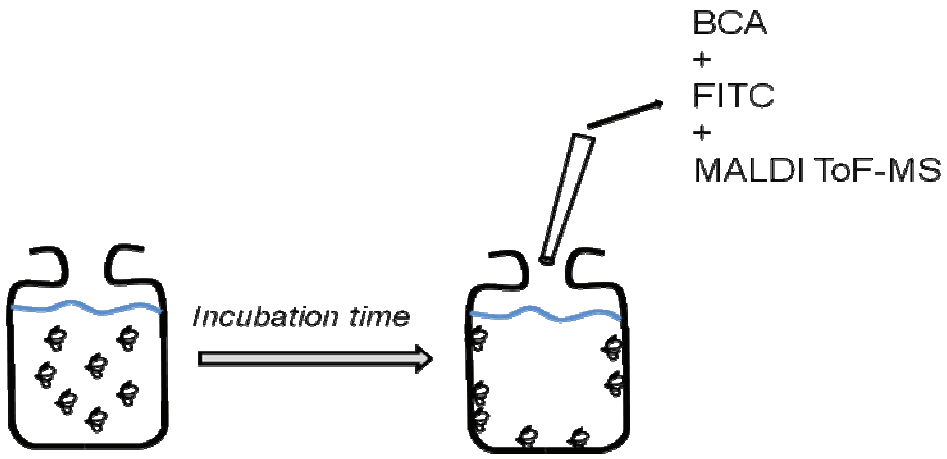

Figure 6-1. Scheme of experimental setup for depletion measurements. Protein / peptide solution is filled into glass bottles provided from SCHOTT. After an incubation time samples from the solution are taken and used for analyses, e.g. BAC assays, FITC measurements or MALDI ToF-MS analysis. The adhesion of molecules onto the inner bottle surface is accompanied by a decrease of free molecules in solution.

6.3 Results and Discussion

To describe the influence of surface treatments on the adsorption behavior of proteins three different techniques were used. First, the adsorption was measured indirectly by determination of the amount of proteins in the supernatant of solutions with the BCA assay. Before starting the adsorption experiment the sensitivity of the assay was tested (Figure 6-2). It can be found that this assay reveals a linear context between protein amount and measured light adsorption over a range of 1 to 80 µg/mL. In the range of 0.25 to 1 µg/mL the results obey a non-linear function and should not be used for any quantitation of protein amounts. Also the repetition experiments shown in figure 6-3 reveal a very high accuracy with no obvious deviations.

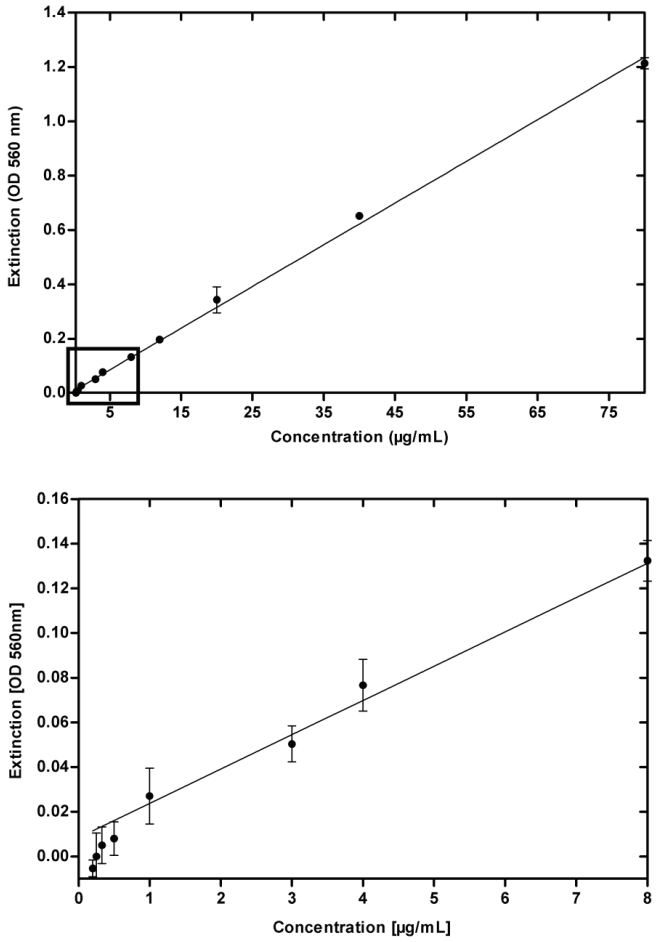

Figure 6-2. Standard curves for BCA assays. BSA protein was used to generate calibration curves for determination of unknown concentrations in supernatants of depletion experiments. Lower image is a magnification of upper image in the range between 0 and 8µg/mL.

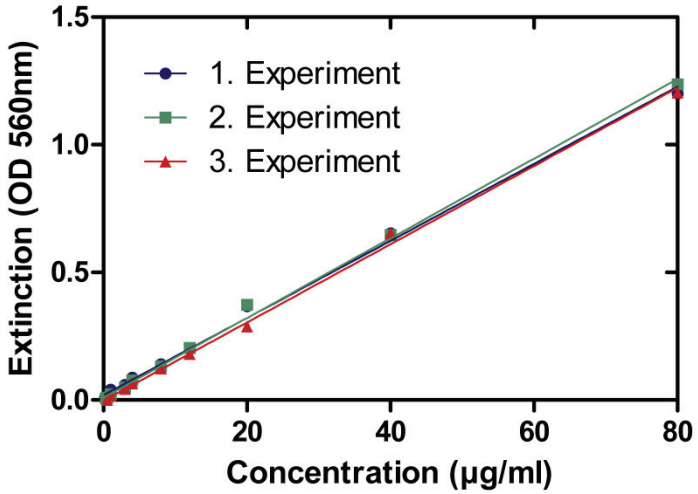

Figure 6-3. Reproducibility measurement of BCA assay. The same assay was used for three separated experiments to investigate the response at 560 nm for different BSA concentrations.

Borosilicate glass surfaces were measured after treatment with NaOH and HCl in contrast to non-treated surfaces. Because of the rinsing with H_2O after acid / base treatment, changes in surface charge are excluded. Any proton transfers were thereby removed so that only surface structural changes could influence adsorption. The results in figure 6-4 show that the slopes of the linear regression fits are equal. Any influence on the treatments should result in a shift of slopes due to increased or decreased adsorption kinetics. It should be mentioned that high oscillations occur within each time series. It is obvious that these oscillations are high compared to the final decrease of values compared to starting values. Therefore this method seems to be not sensitive enough to make precise statements about adsorbed protein amounts and surface treatments, respectively. Nevertheless, a decrease of protein amounts is clearly observable for all three surfaces. Finally, it can be concluded that the treatments with acids or bases has no influence or that this assay is not sensitive enough to detect possibly small changes in adsorption behavior changes.

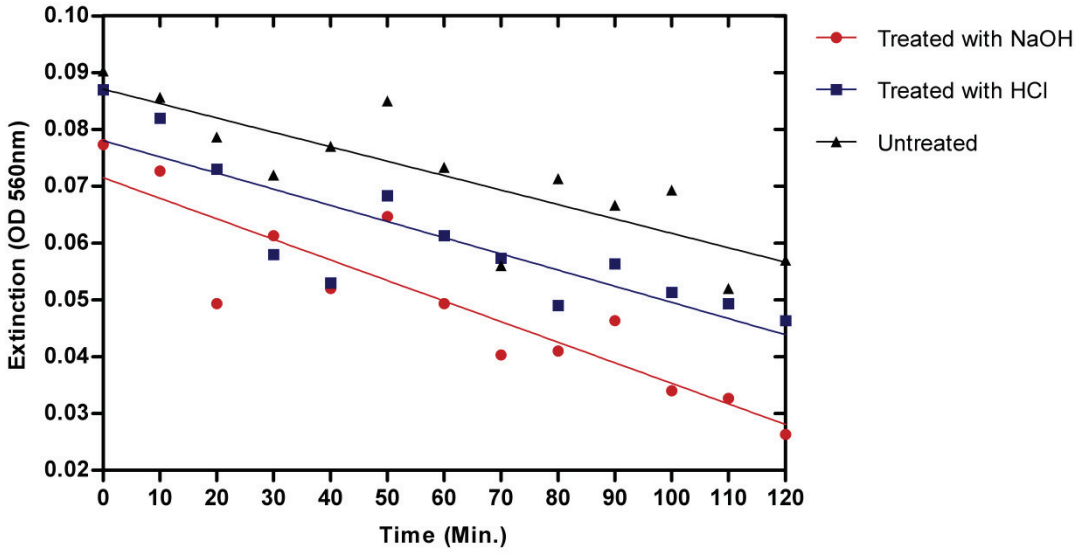

Figure 6-4. BCA assay kinetic for determination of relative amounts of BSA proteins. Proteins in supernatant in depletion experiments were measured after contact with glass surfaces that were treated in different ways.

Another treatment to prevent the adsorption of proteins, which was also investigated in chapter 3, is the use of plasma induced chemical vapor deposition (PICVD). This plasma technique, which was originally described from Spallek et al., produces a SiO_2 surface without any impurities, unlike e.g. in borosilicate glasses. To analyze the influence of the PICVD treatment on protein adsorption, our MALDI depletion technique was used (see chapter 3). As described in chapter 3 in detail, it is not possible to make quantitative statements about protein concentrations in solutions with this technique, although a context between protein amounts and MALDI peak areas can be found (see Figure 6-5). An observed increase of standard deviations can here explained by the increasing amount of proteins in solution and therefore a higher statistical possibility of multiple charge transfers to the proteins. This result in a broader distribution of charges carried by the proteins so that the molecule acceleration is also wider distributed (different flight velocities). More proteins carrying very high or low amounts of charges will reach the detector and increase the statistical values e.g. the standard deviation.

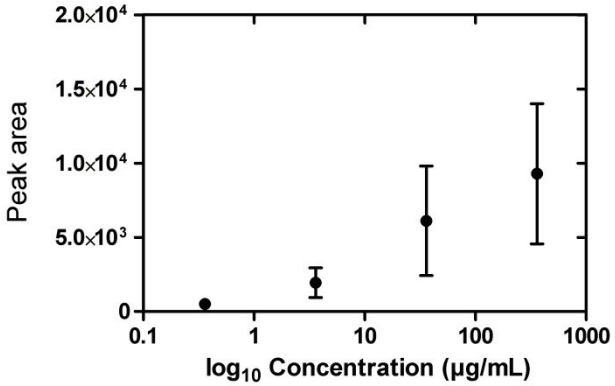

Figure 6-5. „Calibration curve“ of LSZ using differing protein concentrations. Although a determination of absolute amounts is hardly or not possible, a connection between applied protein amount and peak areas from MALDI ToF-MS measurements is obvious.

However, standard curves obtained from MALDI peak signals related to given protein concentrations were previously used [18-20].The analysis of the relative amount of proteins in the supernatant of protein solutions that were in contact with differently treated surface indicates an obvious difference in adsorbed amounts (Figure 6-6). As expected, the amount of protein in solutions that were incubated on borosilicate surfaces reveal a higher adsorption depicted through a higher decrease of MALDI peak areas than samples that were in contact to PICVD treated surfaces. In comparison a third surface (polypropylene) was tested. Here it can be found that after a first decrease of protein peak values the adsorption curve increases again. In previous experiments it was found that polystyrene has higher maximum protein adsorption densities and higher adsorption capacities than silica [21]. Although another polymer surface was used, the tendency for higher adsorption concerning proteins was comparable. Other studies revealed an influence of the chemical compositions of glass-ceramics on protein adsorption [22]. This shows the high impact of chemical dopants in biomedical glasses.

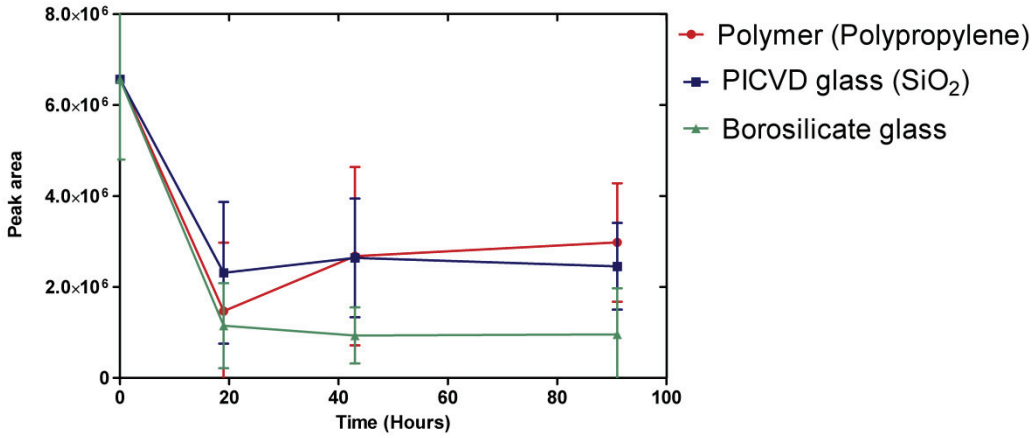

Figure 6-6. Depletion experiment with LSZ over a time range of 90 minutes. MALDI ToF-MS peak areas indicate that a depletion of protein is detectable with this method. Even adsorption differences due to surface treatments or materials can be distinguished.

After these findings, the effect of adsorption minimization through plasma treatment was tested using BSA that was labeled with a fluophore (FITC). In contrast to other measurements described in this chapter, the detection of BSA-FITC is a direct detection method. The results in figure 6-7 show that over a time range of 144 hours a clear difference between the adsorbed amounts of proteins considering different glassy surfaces is observable.

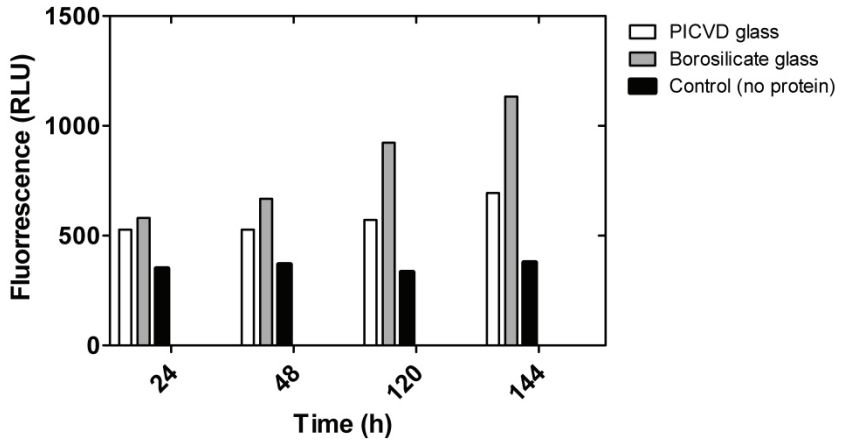

Figure 6-7. Fluorescence measurements of labeled bovine serum albumine (BSA-FITC). An obvious increase of fluorescence, and protein amount respectively, on the borosilicate glass surfaces is detectable. In contrast, plasma treated glass (PICVD) appears to be more adhesion resistant which is apparent through a slighter increase in fluorescence.

Again, the plasma treated surface shows a slower increase of protein amounts measured directly on the surface. This adsorption preventing effect of PICVD glass was also found before (see chapter 3, Fig. 3-5). It should be remarked that within this experiment the fading of fluophore activity caused by sun light during the measurements cannot be eliminated totally. It was possible anyway to show that the chemical composition and surface material itself has a strong influence on protein adsorption in drug storage devices as it was discussed before [23]. Finally, in the here presented study it cannot totally excluded that surfactants influenced the protein adsorption due to hydrophobic competition effects on the surfaces. This effect was described earlier by experiments using anionic, cationic and non-ionic surfactants in adsorption studies [24,25].

6.4 References

[1] T. N. Krogh, T. Berg, P. Hojrup. Protein analysis using enzymes immobilized to paramagnetic beads. Anal. Biochem. 274:153-162, 1999

[2] Y. Li, X. Xu, C. Deng, P. Yang, X. Zhang. Immobilization of trypsin on superparamagnetic nanoparticles for rapid and effective proteolysis. J. Proteome Res. 6: 3849-3855, 2007

[3] S. Lin, D. Yun, D. Qi, C. Deng, Y. Li, X. Zhang. Novel microwave-assisted digestion by trypsin-immobilized magnetic nanoparticles for proteomic analysis. J. Proteome Res. 7: 1297-1307, 2008

[4] J. R. Freije, P. P. M. F. A. Mulder, W. Werkman, L. Rieux, H. A. G. Niederlander, E. Verpoorte, R. Bischoff. Chemically modified, immobilized trypsin reactor with improved digestion efficiency. J. Proteome Res. 4: 1805-1813, 2005

[5] C. Gonzales-Garcia, S. R. Sousa, D. Moratal, P. Rico, M. Salmeron-Sanchez. Effect of nanoscale topography on fibronectin adsorption, focal adhesion size and matrix organization. Colloid. Surface B 77: 181-190, 2010

[6] M. Yaseen, X. Zhao, A. Freund, A. M. Seifalian, J. R. Lu. Surface structural conformations of fibrinogen polypeptides for improved biocompatibility. Biomaterials 31: 3781-3792, 2010

[7] E. Ostuni, B. A. Grzybowski, M. Mrksich, C. S. Roberts, G. M. Whitesides. Adsorption of proteins to hydrophobic sites on mixed self-assembled monolayers. Langmuir 19:1861-1872, 2003

[8] E. Ostuni, R. G. Chapman, M. N. Liang, G. Meluleni, G. Pier, D. E. Ingber, G. M. Whitesides. Self-assembled monolayers that resist the adsorption of proteins and the adhesion of bacterial and mammalian cells. Langmuir 17: 6336-6343, 2001

[9] L. Li, S. Chen, S. Jiang. Protein adsorption on alkanethiolate self-assembled monolayers: Nanoscale surface structural and chemical effects. Langmuir 19: 2974-2982, 2003

[10] S. Margel, E. A. Vogler, L. Firment, T. Watt, S. Haynie, D. Y. Sogah. Peptide, protein, and cellular interactions with self-assembled monolayer model surfaces. J. Biomed. Mater. Res. A 27: 1463-1476, 1993

[11] E. Ostuni, R. G. Chapman, R. E. HolmLin, S. Takayama, G. M. Whitesides. A survey of structure-property relationships of surfaces that resist the adsorption of protein. Langmuir 17: 5605-5620, 2001

[12] X. Khoo, P. Hamilton, G. A. O´Toole, B. D. Snyder, D. J. Kenan, M. W. Grinstaff. Directed assembly of PEGylated-peptide coatings for infection-resistant titanium metal. J. Am. Chem. Soc. 131: 10992-10997, 2009

[13] N. Xia, Y. Hu, D. W. Graininger, D. G. Castner. Functionalized poly(ethylene glycol)-grafted polysiloxane monolayers for control of protein binding. Langmuir 18: 3255-3262, 2002

[14] S. Bozzini, P. Petrini, M. C. Tanzi, S. Zürcher, S. Tosatti. Poly(ethylene glycol) and hydroxy functionalized alkane phosphate mixed self-assembled monolayers to control nonspecific adsorption of proteins on titanium oxide surfaces. Langmuir 26: 6529-6534, 2010

[15] S. Pillai, A. Arpanaei, R. L. Meyer, V. Birkedal, L. Gram, F. Besenbacher, P. Kingshott. Preventing protein adsorption from a range of surfaces using aqueous fisch protein extract. Biomacromolecules 10: 2759-2766, 2009

[16] Y. Hu, Y. Peng, L. Brousseau, A. Bouamrani, X. Liu, M. Ferrari. Nanotexture optimization by oxygen plasma of mesoporous silica thin film for enrichment of low molecular weight peptides captured from human serum. Sci. China Chem. 53: 2257-2264, 2010

[17] M. Walther, M. Heming, M. Spallek. Multilayer barrier coating system produced by plasma-impulse chemical vapor deposition (PICVD). Surf. Coat. Technol. 80:200-202, 1996

[18] J. Zhang, G. R. Kinsel. Quantification of protein-polymer interactions by matrix-assisted laser desorption/ionization mass specrtometry. Langmuir 18: 4444-4448, 2002

[19] H. J. Griesser, P. Kingshott, S. L. McArthur, K. M. McLean, G. R. Kinsel, R. B. Timmons. Surface-MALDI mass spectrometry in biomaterials research. Biomaterials 25: 4861-4875, 2004

[20] A. K. Walker, Y. Wu, R. B. Timmons, G. R. Kinsel. Effects of protein-surface interactions on protein ion signals in MALDI mass spectrometry. Anal. Chem. 71: 268-272, 1999

[21] F. K. Onwu, S. P. I. Ogah. Adsorption of lysozyme unto silica and polystyrene surfaces in aqueous medium. Afr. J. Biotechnol. 10: 3014-3021, 2011

[22] A. Rosengren, S. Oscarsson, M. Mazzocchi, A. Krajewski, A. Ravaglioli. Protein adsorption onto two bioactive glass-ceramics. Biomaterials 24: 147-155, 2003

[23] M. Goebel-Stengel, A. Stengel, Y. Tache, J. R. Reeve Jr. The importance of using the optimal plasticware and glassware in studies involving peptide. Anal. Biochem. 414: 38-46, 2001

[24] M. R. Duncan, J. M. Lee, M. P. Warchol. Influence of surfactants upon protein/peptide adsorption to glass and polypropylene. Int. J. Pharm. 120:179-188, 1995

[25] O. Joshi, J. McGuire. Adsorption behavior of lysozyme and Tween 80 at hydrophilic and hydrophobic silica-water interfaces. Apll. Biochem. Biotechnol. 152: 235-248, 2009

7 Conclusions

Protein adhesion onto inorganic surfaces represents a major problem and is therefore an interesting field for research, industrial solutions or medical devices. Even the adhesion of cells that can end in the formation of biofilms starts with protein / peptide interactions with inorganic surfaces. The removal of this biofilms is time-consuming and expensive. Within this work a new MALDI ToF-MS supported depletion technique was used to identify peptides that bind either good or weak to SiO_2 surfaces. The results were confirmed using SMFS experiments. Beside this, undigested proteins were additionally tested for their adsorption by SMFS. It was found that TPGSR peptide can be regarded as a good SiO_2-binding peptide. Although this method comprises limitations, first results indicate that this method is a fast and easy technique in comparison to standard identification methods (e.g. phage display). Results were partially confirmed by QCM-D, AFM and MD simulations. Furthermore, SMFS experiments of the newly identified peptides revealed average desorption forces of 249 pN and 309 pN for peptides GCRL and WWCNDGR, respectively, and confirmed the slight differences between these peptides. Protein SMFS experiments showed that the used immobilization technique for AFM tips was successful. Tip-sample-sepration-distributions (max. at 30 nm), measured at desorption events, fit well to theoretical protein contour lengths for chymtotrypsin (max. at 25 nm). Using lysozyme force pattern, it can proposed that peaks within SMFS curves are induced by breaking disulfide bonds, although effects of multiple-bound proteins to AFM tips, linker-surface interactions or surface impurities cannot be excluded.

Many biotechnological applications try to link proteins to inorganic surfaces with respect to their distinct properties e.g. enzymatic functions. The processed surfaces can be flat (medical devices like catheters) or spherical (nano particles / colloidal particles). Hence, in this work enzymes (chymotrypsin) were linked chemically to colloidal particles. By analysing the so-produced protein covered particles, it was found that the activity as well as the storage stability is conserved (at RT) for at least seven weeks is assured. In addition, it was possible to identify the relative enzymatic product amount over time (kinetics). From this kinetics it can be seen that the linkage to colloidal particles decreases the enzymatic activity compared to free, unbound chymotrypsin and increases the time for reaching a constant plateau from 4 hours to 15 hours. *In-solution-*

digests with a decreasing amount of chymotrypsin but constant substrate concentration, made it possible to compare total enzymatic activities. 1% to 10% of free chymotrypsin led to the same product concentration as it was found for immobilized chymotrypsin.

In contrast to biotechnological solutions, were protein adhesion is volitional, the field of research considering protein adhesion prevention has expanded strongly. Technical, chemical or biological surface treatments have been introduced and analyzed to prevent the adhesion of proteins, peptides or cells. As a simple starting point, surface treatments using acids and bases were tested in this work. These showed no statistical improvement in adsorption prevention. Furthermore a plasma treated glass from Schott was tested for adhesion properties in contrast to borosilicate glass. Using fluorescence labelled bovine serum albumin it was possible to confirm the adhesion minimization as proposed by Schott. Finally, MALDI was successfully used to verify this finding.

The here presented results on protein and peptide adsorption will hopefully support and expedite the knowledge of underlying adhesion mechanisms that can be found in various technical and scientific questions.

8 Outlook

The results that were presented within this thesis can be seen as basic work with the potential for further analyses. The binding of proteins or peptides to inorganic surfaces is an immense field that still contains many open questions. Further projects / work could focus on the identification of material recognizing peptide sequences and the underlying adhesion mechanisms. A systematic investigation of many synthetic peptides with fixed amino acid compositions on different technical relevant surfaces could give insight into the role of single amino acids and their side chains. These analyses could be done, like it was started here, using Atomic Force Microscopy (AFM). Desorption forces will hopefully give information about the strength of surface interactions. Beside peptides, proteins should be further tested for their adhesion onto surfaces by AFM. Especially the deeper analysis of force-distance-curves and their peak pattern could reveal protein unfold mechanisms and uncover the role of disulfide bonds. In this context an accompanying and extensive computer-assisted pattern recognition analysis would be necessary. Due to the high sensitivity of AFM many unwanted side effects (e.g. like impurities, multiple protein binding to the tip) must be eliminated. Therefore, a lot of preparation parameters must be tested to identify the most appropriate method.

As another promising method matrix assisted laser desorption/ionization time-of-flight mass spectrometry (MALDI ToF-MS) could be used for the analysis of protein orientation after adsorption to surfaces. Peptides in solution from a digested model protein can be allowed to adsorb to surfaces by depletion. The analysis of the peptide solution after incubation will gain insight into peptides that remain in solution and peptides that adhere to the surface (and are therefore less abundant in solution). The computational analysis of the position of the adhering peptides inside the protein could reveal information about the preferred protein orientation over the surface.

Further, the coupling of single molecules with fluorophores (e.g. for Fluorescence Resonance Energy Transfer (FRET) measurements) is another promising branch of research. In general, the analysis of adsorption modes of proteins or peptides by AFM or MALDI ToF-MS can then be combined with the entire activity provided by the conservation of the three dimensional structure.

Another aspect to be investigated by MALDI ToF-MS is the determination of the free energy of protein adsorption process. By measuring the adsorbed amount of proteins after a specific incubation time for different molar concentrations of molecules, an isothermal function should be predictable.

As a last and general point, all here described ideas for future works can/should be associated with computational modelling of molecule-surface interactions. Although the modelling and analysis of realistic circumstances can be difficult due to limited models, computational support is an essential part for understanding adsorption phenomena.

Acknowledgements

I would like to thank Prof. Lucio Colombi Ciacchi who gave me the possibility to make my Phd in his working group. He always had an open door for any kind of questions and helped me with fruitful discussions.

Thanks for the stimulating cooperation to the working group of Prof. Kurosch Rezwan, especially to Ludmilla Derr and Laura Treccani. Also Ralf Dringens professional support in our discussions helped a lot. Thank you.

I must thank Dr. Ingo Grunwald and his group for the helpful support in laboratory related questions, the possibility to use the IFAM equipment and last but not least for some diverting discussions about children……

Many thanks are given to the the HMI working group consisting of Nils, Jens, Gang, Julen, Steffen, Stefan, Tatjana, Monika, Susi, Julian B., Qing, Qingfeng, Julian S. and Mohammad for a relaxed and pleasant working atmosphere.

Meike I have to thank in particular for listening to upcoming problems. She always found time for discussions or cheering me up when I was in a bad mood.

Sebastian Potthoff supported me at some computational and analytical problems. His python script helped me a lot. Thank you.

Thanks to Linda who helped and supported me concerning QCM measurements as well as Klaus for the possibility to use the MALDI ToF-MS at the IFAM.

Finally, I am deeply grateful to my mother, Gabi, and my grandparents Eva and Helmut although my grandfather was not able to witness the termination of my Phd time. I will never forget you.

Michaela and Sebastian were always there for me and without their support during the last years this work wouldn´t be possible. I am deeply grateful to you.

Publications

Papers

[1] Biomimetic graphene-FePt nanohybrids with high solubility, ferromagnetism, fluorescence, and enhanced electrocatalytic activity

Gang Wei, Yue Zhang, Sascha Steckbeck, Zhiqiang Su, and Zhuang Li

Journal of Materials Chemistry, 2012, 22, 17190-17195

[2] Identification of Materials Binding Peptide Sequences guided by a MALDI ToF-MS depletion assay

Sascha Steckbeck, Julian Schneider, Linda Wittig, Klaus Rischka, Ingo Grunwald, Lucio Colombi Ciacchi

Analytical Methods, DOI 10.1039/c3ay42042f, 2014

[3] Assessment of the proteolytic activity of chymotrypsin immobilized onto colloidal particles

Ludmilla Derr*, Sascha Steckbeck*, Ralf Dringen, Lucio Colombi Ciacchi, Kurosch Rezwan, Laura Treccani

*shared first authorship, *submitted manuscript*

[4] Label-Free Biosensing with Single-Molecule Force Spectroscopy

Gang Wei, Sascha Steckbeck, Susan Köppen, Lucio Colombi Ciacchi

Chemical Communications, 2013, 49, 3239-3241

[5] Direct force measurements on peeling heteropolymer ssDNA from a graphite surface using single-molecule force spectroscopy

Gang Wei, Qing Li, Sascha Steckbeck, Lucio Colombi Ciacchi

Physical Chemistry Chemical Physics, DOI 10.1039/c3cp54121e, 2014

Patents

[1] Verfahren zur Identifizierung von oberflächen-adhesiven Peptidsequenzen

Ingo Grunwald, Sascha Steckbeck, Lucio Colombi Ciacchi

German Patent Application: DE 102012214202.9 (2012)

Proceedings

[1] Contribution in "Bionik und Nachhaltigkeit - Lernen von der Natur"

12. International Summer-Academy St. Marienthal, Germany, Erich-Schmidt-Verlag (2007)

S. Steckbeck

Talks and Posters

[1] ICPL 4-plex: Isotopic Protein Labeling for Quantitative Protein Analysis by nano-LC MALDI-TOF/TOF (poster)
ABRF Meeting, Memphis, Tennessee, USA, February 2009

S. Hahner, S. Steckbeck, W. Evers, A. Resemann, D. Suckau

[2] Analyse der Proteinadsorption an pharma-relevanten Glasoberflächen (talk)

Sitzung des DGM Querschittarbeitskreises „Grenzflächen“, 6.10.2011, Charité Berlin

S. Steckbeck, L. Gätjen, I. Grunwald

[3] Identification of Strong and Weak Binding Peptides at the Amorphous SiO2/Water Interface by MALDI ToF-Mass Spectrometry (poster)

DGBM-Kongress 2012 (Deutsche Gesellschaft für Biomaterialien), Hamburg, Germany

S. Steckbeck, J. Schneider, K. Rischka, I. Grunwald, L. Colombi Ciacchi

[4] Chemical and structural analysis of adhesive proteins (talk)

COST Action TD0906, 6. & 7.9.2012, University of Newcastle (UK)

S. Steckbeck, L. Gätjen, K. Richter, K. Rischka, L. C. Ciacchi, I. Grunwald

Declaration / Erklärung

Ich erkläre hiermit, daß ich die vorliegende Arbeit ohne unerlaubte fremde Hilfe angefertigt und keine anderen als die von mir angegebenen Quellen und Hilfsmittel benutzt habe. Alle wörtlich und inhaltlich entnommenen Stellen der benutzten Werke sind als solche kenntlich gemacht.

_____

Sascha Steckbeck